

UNCLASSIFIED

AD 295 897

*Reproduced
by the*

**ARMED SERVICES TECHNICAL INFORMATION AGENCY
ARLINGTON HALL STATION
ARLINGTON 12, VIRGINIA**



UNCLASSIFIED

NOTICE: When government or other drawings, specifications or other data are used for any purpose other than in connection with a definitely related government procurement operation, the U. S. Government thereby incurs no responsibility, nor any obligation whatsoever; and the fact that the Government may have formulated, furnished, or in any way supplied the said drawings, specifications, or other data is not to be regarded by implication or otherwise as in any manner licensing the holder or any other person or corporation, or conveying any rights or permission to manufacture, use or sell any patented invention that may in any way be related thereto.

63-2-3

CATALOGED BY ASTIA 295897
AD AD NO. _____

Office of Naval Research

Contract Nonr-1866 (16)

NR-372-012

PARAMAGNETIC RESONANCE LINESHAPES
AT LOW TEMPERATURE



By

Ivar Svare and George M. Seidel

September 5, 1962

Technical Report No. 378

Cruft Laboratory
Harvard University
Cambridge, Massachusetts

RECEIVED
JUL 10 1962
JSL

Office of Naval Research

Contract Nonr-1866(16)

NR - 372 - 012

Technical Report

on

PARAMAGNETIC RESONANCE LINES

AT LOW TEMPERATURE

by

Ivar Svare and George M. Seidel

September 5, 1962

The research reported in this document was made possible through support extended Cruft Laboratory, Harvard University, jointly by the Navy Department (Office of Naval Research), the Signal Corps of the U. S. Army, and the U. S. Air Force, under ONR Contract Nonr-1866 (16). Reproduction in whole or in part is permitted for any purpose of the United States Government.

Technical Report No. 378

**Cruft Laboratory
Harvard University
Cambridge, Massachusetts**

ERRATA

Technical Report No. 378

Contract Nonr-1866(16)

September 5, 1962

"Paramagnetic Resonance Lineshapes at Low Temperature."

By George Seidel and Ivar Svarre

Page

- 2, line 17, for $d\nu/n$ read $h d\nu$
- 2, line 18, for ν/n read $h\nu$
- 9, Eq. 1-12, the denominator should read: $\text{Trace} \left(b \overline{\mathcal{K}} [\hat{M}_-, \hat{M}_+] \right)$
- 19, line 2, for $S_{+i} S_{-i}$ read $S_{+i} S_{-j}$
- 19, Eq. 1-37, first term on second line should read: $\sum_{i, k'}' \overline{\mathcal{K}}_{ik'}^{(1)}$
- 21, Eq. 1-40, the k subscript on $\overline{\mathcal{K}}_{ik}^{(1)}$ should read: $\overline{\mathcal{K}}_{ik'}^{(1)}$ on line 4
- 24, Eq. 1-48 should read:

$$\sum_{\substack{j \\ r_{ij} > \xi}}' \frac{(3 \cos^2 \theta_{ij} - 1)}{r_{ij}^3} = \dots$$

- 34, Eq. 1-64, limits of integration in denominator should be: $-\infty$ to $+\infty$.
- 48, line 18, for 1 mm^2 read 1 mm^3
- 52, in denominator of Eqs. 2-12 and 2-13, a should be: a_0
- 67, Eq. 2-32, the left side should read simply:

$$\left(\frac{Q_{\text{ex}}}{Q_0} - 1 \right) > >$$

- 69, Eq. 2-39, the last term should read: $+\frac{1}{4}(2 - \sqrt{6}) a^2 \chi''^2 + \dots]$
- 70, line 1, for $b = \frac{1}{2}$ read $b = 1$

Figure 2 (after page 45): next to P_3 designation should be ^4He , instead of ^3He

CONTENTS

TABLE OF CONTENTS.....	i
LIST OF FIGURES.....	iii
TABLE	iv
ABSTRACT.....	v
CHAPTER 1 THE THEORY OF PARAMAGNETIC RESONANCE LINE- SHAPES IN SOLIDS AT VERY LOW TEMPERATURES	
1.1 Introduction	1
1.2 Outline of moment calculation when $h\nu \geq kT$	4
1.3 Application of the moment formulas to interaction between like neighbors	12
1.4 Line moments from interaction between unlike spins	18
1.5 Discussion of demagnetizing effects	24
1.6 Comment on the fourth moment and the effect of exchange .	28
1.7 Comment on McMillan and Opechowski's second approximation	32
1.8 Comment on the possibility of magnetostatic modes in paramagnetic crystals at low temperature	35
CHAPTER 2 DISCUSSION OF EXPERIMENTAL APPARATUS AND TECHNIQUE	
2.1 Description of microwave and low temperature systems ⁴¹ ..	41
2.2 Discussion of possible microwave saturation	49
2.3 Discussion of heat contact between sample and ³ He system	53
2.4 Heat leak through capillary	61
2.5 Discussion of spectrometer linearity and large-signal corrections	64
CHAPTER 3 MEASUREMENTS ON NEODYMIUM ETHYL SULFATE	
3.1 Description of neodymium ethyl sulfate	71
3.2 Measurements of line areas	74
3.3 First moment changes	77
3.4 Second moment changes	82
3.5 Discussion of possible antiferromagnetic coupling in neodymium ethyl sulfate	86
CHAPTER 4 MEASUREMENTS ON NICKEL FLUOSILICATE	
4.1 Description of nickel fluosilicate	93
4.2 First moment changes	97
4.3 Second moment changes	101
4.4 Discussion of nickel fluosilicate results	105

CHAPTER 5 MEASUREMENTS ON COPPER POTASSIUM SULFATE AND COPPER SULFATE

5.1	Description of copper potassium sulfate	108
5.2	First moment changes	111
5.3	Discussion of exchange in $K_2Cu(SO_4)_2 \cdot 6H_2O$	117
5.4	Description of copper sulfate	120
5.5	Measurements on copper sulfate and discussion of observed magnetostatic modes	123

CHAPTER 6 RESONANCE LINE BROADENING FROM VARIATION IN CRYSTALLINE FIELD

6.1	Introduction	129
6.2	Measurements	132
6.3	Discussion	136
CONCLUSION		140
ACKNOWLEDGMENTS		141
APPENDIX I		A1
APPENDIX II		A7
REFERENCES		R1

LIST OF FIGURES

Figure Number

1	Block diagram of waveguide spectrometer	44a
2	Schematic drawing of ^3He cryostat	45a
3	Detail showing sample mounted inside microwave cavity and in heat contact with ^3He reservoir.....	46a
4	Reflected power from cavity as function of absorption in sample ..	68a
5a	Unit cell of $\text{Nd}(\text{C}_2\text{H}_5\text{SO}_4)_3 \cdot 9\text{H}_2\text{O}$ showing string of nearest neighbors	71a
5b	Probable arrangement of water molecules around the neodymium ion	71a
6	Resonance lineshape in $\text{Nd}(\text{C}_2\text{H}_5\text{SO}_4)_3 \cdot 9\text{H}_2\text{O}$ as function of temperature	74a
7	Measured areas of the three resonance lines in $\text{Nd}(\text{C}_2\text{H}_5\text{SO}_4)_3 \cdot 9\text{H}_2\text{O}$ compared to the theoretical absorption ratios	76a
8	Peak position of lines in $\text{Nd}(\text{C}_2\text{H}_5\text{SO}_4)_3 \cdot 9\text{H}_2\text{O}$ compared to calculated first moment shifts	77a
9	Schematic representation of various neighbor arrangement in $\text{Nd}(\text{C}_2\text{H}_5\text{SO}_4)_3 \cdot 9\text{H}_2\text{O}$ showing how the possibility for spin-flips will influence the energy levels of a spin	78a
10	Calculated square roots of second moments as function of temperature in $\text{Nd}(\text{C}_2\text{H}_5\text{SO}_4)_3 \cdot 9\text{H}_2\text{O}$ compared to some measured values	84a
11	Rhombohedral unit cell of $\text{NiSiF}_6 \cdot 6\text{H}_2\text{O}$	93a
12	Measured resonance lineshape in $\text{NiSiF}_6 \cdot 6\text{H}_2\text{O}$ as function of temperature	97a
13	Measured peak positions of resonance lines in $\text{NiSiF}_6 \cdot 6\text{H}_2\text{O}$ compared to calculated first moments	98a
	Figure 13a Lower, strong line	98a
	Figure 13b Upper, weak line	98a

Figure Number

14	Measured and calculated square root of second moment of lower line in $\text{NiSiF}_6 \cdot 6\text{H}_2\text{O}$ when $H_0 \parallel z$	102a
15	Measured and calculated square root of second moment in $\text{NiSiF}_6 \cdot 6\text{H}_2\text{O}$ when the magnetic field is in a direction where the two resonances overlap	104a
16	Shape of resonance line I in $\text{K}_2\text{Cu}(\text{SO}_4)_2 \cdot 6\text{H}_2\text{O}$ as function of temperature	112a
17	First moment shift of resonance in $\text{K}_2\text{Cu}(\text{SO}_4)_2 \cdot 6\text{H}_2\text{O}$	112b
	Figure 17a Field Angle 45° with respect to crystal axes a and b	112b
	Figure 17b Field parallel to b-axis	112b
18	Shape of resonance line in $\text{CuSO}_4 \cdot 5\text{H}_2\text{O}$ as function of temperature	125a
19a	Direction of magnetic axes in $\text{Ni}(\text{NH}_4)_2(\text{SO}_4)_2 \cdot 6\text{H}_2\text{O}$	130a
19b	Energy levels in $\text{Ni}(\text{NH}_4)_2(\text{SO}_4)_2 \cdot 6\text{H}_2\text{O}$ when $H_0 \parallel z$	130a

TABLE

Table 6-1	Measured linewidths and spin-Hamiltonian parameters in nickel Tutton salt	135
-----------	---	-----

ABSTRACT

The main part of this report is concerned with the shape of paramagnetic resonance lines under conditions where $h\nu \geq kT$. In such a case the spin levels are not equally populated and the line moments resulting from spin-spin interactions change. From the temperature dependence of the lineshape it is possible to determine the strength and nature of the coupling between the ions.

The condition $h\nu \geq kT$ was obtained experimentally by cooling the sample in a He^3 cryostat to 0.3°K .

The extension of the Van Vleck line moment theory to low temperature by weighting the population of each spin level by the proper Boltzmann factor has been considered by a number of authors, and this theory is reviewed in Chapter 1. The moment changes depend upon whether the interacting spins are identical or not. In the interpretation of the experiments, it is found that two spins may be alike or unlike, depending upon the local field due to their neighbors or to their magnetic nuclei. Particular consideration is also given to the consequences of the large magnetization of paramagnetic salts at low temperatures. Demagnetizing effects and the excitation of magnetostatic modes are discussed.

In Chapter 2 the microwave spectrometer and low temperature system are described. The problem of heat-contact between the sample and the He^3 reservoir is discussed in detail. Approximate correction formulas for the spectrometer response are given in the case of strong absorption in the sample.

Measurements on neodymium ethyl sulfate are discussed in Chapter 3. The temperature dependence of the absorption lineshape of this salt can be almost completely explained on the basis of dipolar interactions alone. However,

TR378

there seems to be evidence for some additional, weak, antiferromagnetic exchange coupling. Chapter 4 is concerned with measurements of nickel fluosilicate. The exchange interaction has been found to be isotropic, ferromagnetic, and of magnitude $3.9 \cdot 10^{-18}$ ergs.

Because of the hyperfine interaction in $\text{CuK}_2(\text{SO}_4)_2 \cdot 6\text{H}_2\text{O}$, it has been possible to obtain rough estimates of two different exchange constants in this salt. This problem and a discussion of the observation of magnetostatic modes are presented in Chapter 5.

Chapter 6 is not directly related to the rest of this report. In it are reported measurements on diluted nickel double sulfates undertaken in an effort to obtain a suitable salt for a zero field maser. However, the linewidths observed were much too large for such a device, the broadening being the result of crystalline field variations.

CHAPTER 1

THE THEORY OF PARAMAGNETIC RESONANCE LINESHAPES IN SOLIDS AT VERY LOW TEMPERATURE

1.1. Introduction.

Electron and nuclear spins are quantized in a magnetic field. In resonance experiments we induce transitions between the energy levels of the spins by a suitable microwave or radio-frequency field and observe the power absorbed. In a constant field a single, non-interacting spin would have infinitely sharp energy levels (except for the broadening due to the very small, but finite probability of spontaneous emission), and if we could observe this spin alone, the resonance line would look like a δ -function. The actual lines observed in solids are always somewhat broadened, and there are several reasons for this :

a) The $N \approx 10^{20}$ or so spins in the sample may not be identical.

The electric crystalline field each spin sees from its neighboring ions may vary somewhat since the interionic distances can change slightly because of distortions, impurity stresses and microscopic cracks in the solid. Through the spin-orbit coupling, this will give a spread of the g -value and of any crystalline field splitting of the spin ground state. Some measurements on the variation of the zero field splitting will be reported in Chapter 6 .

b) The spins will interact among themselves through dipolar and exchange forces. Each spin sees an additional, varying field from the random orientation of all its magnetic dipole neighbors, and this will

broaden the resonance lines. It is then immediately recognized that if we do the resonance experiment at a temperature where all spins will be frozen in their lowest state, all spins will see the same ordering of their neighbors, and there will be no line broadening from this cause. In the next sections we will review the theory of the temperature dependence of resonance lineshapes caused by spin-spin interaction. In Chapters 3-5 the results of some experiments made at 30 kMc/s and down to 0.4°K will be compared to the theory.

c) The spins may interact so strongly with the lattice that this causes broadening of the resonance. The spin-phonon interaction is a strong function of temperature, and it is usually not difficult by cooling to make the spin-lattice relaxation time T_1 so long that this type of broadening is not important.

The shape of a resonance line can be given by a normalized absorption amplitude $f(\nu)$ at each frequency ν so that $\int_0^{\infty} f(\nu) d\nu = 1$. To calculate $f(\nu)$ we would have to find the eigenvalues of the $(2S+1)^N$ -fold matrix for the spin system and sum up for each energy interval $d\nu/n$ around ν/n . This is impossible. But it was recognized by Van Vleck in a now classical paper¹ that we can get some information about the lineshape through the moments defined as

$$\langle \nu^n \rangle = \int_0^{\infty} \nu^n f(\nu) d\nu \quad . \quad (1-1)$$

The moments can be expressed as diagonal sums of matrices including all spins, but since traces are invariant under similarity trans-

formations, we can calculate the trace in the most convenient representation, namely when all spins are individually diagonalized.

From $\langle \nu^n \rangle$, the moments $\langle \Delta \nu^n \rangle = \langle (\nu - \nu^*)^n \rangle$ around the unperturbed resonance frequency ν^* can be found. In the Van Vleck treatment, which is a high temperature approximation, the odd moments vanish, $\langle \Delta \nu^n \rangle = 0$ for $n = \text{odd}$. The second and sometimes the fourth moments have been calculated and compared to experimental values in a number of cases.

The moment calculations can be extended to low temperatures where $h\nu \geq kT$ by weighting each term in the traces by the proper Boltzmann factor $\exp(-h\nu/kT)$. This has been done by Bloembergen,² Pryce and Stevens,³ Kambe and Usui,⁴ and more explicitly by McMillan and Opechowski.⁵ It turns out that the odd moments are often finite, and the first moment, in particular, may show interesting temperature shifts. Except for the early demonstration by Bloembergen² that the proton resonance in $\text{CuSO}_4 \cdot 5\text{H}_2\text{O}$ splits up into a number of components at helium temperatures because of the alignment with the field of the Cu^{++} spins, there seems to have been no measurements of low temperature changes in resonance line moments.

The method of calculating line moments is exact, and in principle it should give all information needed about the lineshape. But in practice, it is hard to calculate the higher moments, and since the measured moments depend strongly upon the absorption far out in the weak wings of the line, it is often hard to compare theory with experiment.

Another, more direct approach to the problem of resonance line-shapes has been attempted by Anderson and Weiss^{6,7} and by Kubo and Tomita.^{8,9,10} They are able to derive the actual lineshape from the Fourier transform of the relaxation function of the magnetic moment. By proper use of Boltzmann factors it can also be shown by this method that the lines narrow at low temperature, as has been done for a special case by Moriya and Obata.¹¹ But again the calculations are complicated and so many approximations necessary, that for quantitative comparison with experiments this approach is no better than the moment method in most cases. Therefore, only the qualitative conclusions from this theory will be discussed briefly in Section 1.6.

1.2. Outline of moment calculation when $h\nu \geq kT$.

In this section we review the moment theory as given by Kambe and Usui,⁴ but we will use the notation of McMillan and Opechowski.⁵ The theory can be applied to nuclear resonance as well as to electron resonance, but only in the latter case can we experimentally realize the condition $h\nu \approx kT$.

The Hamiltonian for a system of N interacting spins is

$$\mathcal{H} = \sum_{i=1}^N \mathcal{H}_i^{(0)} + \frac{1}{2} \sum_{i,j}' \mathcal{H}_{ij}^{(1)} \quad (1-2)$$

where $\sum_{i,j}'$ is to be taken over all values i and j so that $i \neq j$, and $\mathcal{H}_i^{(0)}$ is the energy operator for an individual spin in a constant external magnetic field \vec{H}_0 . It will now be assumed that all spins are

identical in the sense that their spectra are identical and overlapping. In Section 1.4 the formulas will be extended to the case when there are two or more different species of interacting spins.

The perturbation $\mathcal{K}_{ij}^{(1)}$ is the sum of the dipolar and possible exchange interactions between spins i and j .

The classical interaction potential $\mathcal{K}_{ij \text{ dip}}$ for two dipoles $\vec{\mu}_i$ and $\vec{\mu}_j$ joined by a vector \vec{r}_{ij} is¹²

$$\mathcal{K}_{ij \text{ dip}} = \left(\frac{\vec{\mu}_i \cdot \vec{\mu}_j}{r_{ij}^3} \right) - \frac{3(\vec{\mu}_i \cdot \vec{r}_{ij})(\vec{\mu}_j \cdot \vec{r}_{ij})}{r_{ij}^5} \quad (1-3)$$

In general, the g -value of a spin is a tensor, so $\vec{\mu}_i = \beta \vec{g} \vec{S}_i$ where β is the Bohr magneton and \vec{S} is the spin operator. The matrix elements of $\mathcal{K}_{ij \text{ dip}}$ are found by expanding it in terms of S_{zi} , $S_{\pm i} = S_{xi} \pm i S_{yi}$.

As an example, when spins i and j have g_{\parallel} along the direction of \vec{H}_0 (z-axis) and g_{\perp} in the x-y plane, we have

$$V_{ij \text{ dip}} = \frac{\beta^2}{r_{ij}^3} (a + b + c + d + e + f) \quad (1-4)$$

where

$$a = g_{\parallel}^2 S_{zi} S_{zj} (1 - 3 \cos^2 \theta_{ij})$$

$$b = -\frac{1}{4} g_{\perp}^2 [S_{-i} S_{+j} + S_{+i} S_{-j}] (1 - 3 \cos^2 \theta_{ij})$$

$$c = -\frac{3}{2} g_{\parallel} g_{\perp} [S_{+i} S_{zj} + S_{+j} S_{zi}] \sin \theta_{ij} \cos \theta_{ij} \exp(-i \phi_{ij})$$

$$d = -\frac{3}{2} g_{\parallel} g_{\perp} [S_{-i} S_{zi} + S_{-j} S_{zi}] \sin \theta_{ij} \cos \theta_{ij} \exp(i \phi_{ij})$$

$$e = -\frac{3}{4} g_{\perp}^2 [S_{+i} S_{+j}] \sin^2 \theta_{ij} \exp(-2i \phi_{ij})$$

$$f = -\frac{3}{4} g_{\perp}^2 [S_{-i} S_{-j}] \sin^2 \theta_{ij} \exp(2i \phi_{ij})$$

θ_{ij} is the polar angle that \vec{r}_{ij} makes with \vec{H}_0 , and ϕ_{ij} is the azimuthal angle of \vec{r}_{ij} .

The ordinary exchange interaction is caused by a slight overlap of the wavefunctions from different spins together with the exclusion principle that prevents two electrons from being in the same state at the same time. Superexchange is interaction via other ions, usually oxygen, lying between the spins. This is probably the source of the weak coupling in most of the hydrated salts we have investigated. Since the wave functions in the crystals are at best only crudely known, it is not possible to calculate the strength of the exchange from first principles. It has to be found from experiments, and we usually take it to be isotropic ,

$$\mathcal{K}_{ij\text{ex}} = \tilde{A}_{ij} \vec{S}_i \cdot \vec{S}_j = \tilde{A}_{ij} (S_{zi} S_{zj} + \frac{1}{2} (S_{+i} S_{-j} + S_{-i} S_{+j})). \quad (1-5)$$

Since the wavefunctions fall off exponentially with distance, it is usually assumed that this coupling is important only between nearest neighbor spins. A positive \tilde{A}_{ij} in (1 - 5) corresponds to anti-ferromagnetic coupling, a negative \tilde{A}_{ij} to ferromagnetic coupling.

The approximation in the moment calculation is to treat $\mathcal{K}_{ij}^{(1)} = \mathcal{K}_{ij\text{dip}} + \mathcal{K}_{ij\text{ex}}$ as small compared to the Zeeman energy $\mathcal{K}_i^{(0)}$ and keep only first-order perturbation terms, that is, the terms in $\mathcal{K}_{ij}^{(1)}$

that commute with $\mathcal{K}_i^{(0)}$ and that can be diagonalized in a representation where $\mathcal{K}_i^{(0)}$ is diagonal. These terms will slightly shift the energy levels a_r of a single spin. If we look upon the N spins, each with $(2S + 1) = R$ levels, as a coupled system, the states are $\dots n, \dots n', \dots$ with energies $\dots E_n \dots E_{n'}$. In the absence of the perturbation, a large number N_a of states has the same energy $E_a = N_1 a_1 + N_2 a_2 + \dots N_R a_R$ where $N = \sum_{r=1}^R N_r$. The first-order interaction terms couple states within this manifold of degenerate states, the degeneracy is lifted, and the energy states are spread out slightly around E_a .

The second-order terms in $\mathcal{K}_{ij}^{(1)}$ would weakly couple together different levels $a_r \dots a_{r'}$ of a single spin and permit transitions in the microwave field of $\Delta m = \pm 1$. For a system of spins without crystal-line field splitting, the terms $c - f$ in (1 - 4) would thus cause weak satellite lines at $h\nu = 0, 2g\beta H_0, 3g\beta H_0$ in addition to the main line at $h\nu = g\beta H_0$. Since their separation from the main line is large, these weak lines would give considerable contribution to the higher moments. The calculation would, therefore, not be improved, but made incorrect by including the second-order terms in the approximation, and the noncommuting part of the interaction operator has to be thrown away.

The properly truncated $\mathcal{K}^{(1)}$ we will designate $\bar{\mathcal{K}}^{(1)}$ and we will also use $\bar{\mathcal{K}} = \mathcal{K}^{(0)} + \bar{\mathcal{K}}^{(1)}$. It should be remembered that if a crystal-line field of low symmetry mixes the states of the unperturbed spin, then $\bar{\mathcal{K}}^{(1)}$ may also contain contributions from the terms $c - f$ in (1 - 4).

When a crystalline field is present and the spectrum consists of more than one line, the microwave field operator M also has to be truncated to \hat{M} to include only the matrix elements for the resonance transition in which we are interested.

The power $P(\nu)d\nu$ absorbed by the spin system from the microwave field of frequency ν is proportional to

$$h\nu \sum_{nn'}^{\Delta} (b_n^{E_n} - b_{n'}^{E_{n'}}) |(n|\hat{M}|n')|^2 \quad (1-6)$$

where $\sum_{nn'}^{\Delta}$ means summation over all states $|n\rangle$ and $|n'\rangle$ such that

$$h\nu \leq E_{n'} - E_n \leq h(\nu + d\nu)$$

and the Boltzmann factors are written

$$b_n^{E_n} = e^{-E_n/kT} \quad (1-7)$$

The lineshape function is then

$$f(\nu) = \frac{P(\nu)}{\int_0^{\infty} P(\nu)d\nu} = \frac{\sum_{nn'}^{\Delta} (b_n^{E_n} - b_{n'}^{E_{n'}}) |(n|\hat{M}|n')|^2}{\sum_{nn'}^{+} (b_n^{E_n} - b_{n'}^{E_{n'}}) |(n|\hat{M}|n')|^2} \quad (1-8)$$

where $\sum_{nn'}^{+}$ means summation over all states $|n\rangle$ and $|n'\rangle$ such that $E_{n'} \geq E_n$.

From the definition (1-1) we can write the ℓ^{th} moment as

$$h^t \langle v^t \rangle = \frac{\sum_{nn'}^+ (E_{n'} - E_n)^t (b^{E_n} - b^{E_{n'}}) |(n|\hat{M}|n')|^2}{\sum_{nn'}^+ (b^{E_n} - b^{E_{n'}}) |(n|\hat{M}|n')|^2} \quad (1-9)$$

To avoid the summation $\sum_{nn'}^+$, Kambe and Usui introduce the operators

$$\begin{aligned} (n|\hat{M}_+|n') &= \begin{cases} (n|\hat{M}|n') & \text{for } E_{n'} < E_n \\ 0 & \text{otherwise} \end{cases} \\ (n|\hat{M}_-|n') &= \begin{cases} (n|\hat{M}|n') & \text{for } E_{n'} > E_n \\ 0 & \text{otherwise} \end{cases} \end{aligned} \quad (1-10)$$

Then the moments can be written in invariant trace form

$$h \langle v \rangle = \frac{1}{2} \frac{\text{Trace} (b^{\bar{\mathcal{K}}} [\hat{M}_-, [\bar{\mathcal{K}}, \hat{M}_+]])}{\text{Trace} (b^{\bar{\mathcal{K}}} [\hat{M}_-, \hat{M}_+])} \quad (1-11)$$

$$h^2 \langle v^2 \rangle = \frac{\text{Trace} (b^{\bar{\mathcal{K}}} [[\hat{M}_-, \bar{\mathcal{K}}], [\bar{\mathcal{K}}, \hat{M}_+]])}{\text{Trace} (b^{\bar{\mathcal{K}}} [\hat{M}_-, \hat{M}_+])} \quad (1-12)$$

In these expressions \hat{M}_\pm and $\bar{\mathcal{K}}$ are supposed to act on the system eigenfunctions $|n,k\rangle$ of $\sum_i \mathcal{K}_i^{(0)}$ where k stands for the degeneracy of the state with energy E_n . But the states $|n,k\rangle$ are made up by all linear combinations of the eigenfunctions of a single spin, and

we can, therefore, evaluate the traces with respect to the functions

$$|a\rangle_1 |b\rangle_2 |c\rangle_3 \dots |d\rangle_N = |a, b, \dots d\rangle \text{ using}$$

$$\hat{M}_{\pm} = \sum_i \hat{m}_{\pm i} \quad \bar{K} = \sum_i K_i^{(0)} + \frac{1}{2} \sum_{ij} \bar{K}_{ij}^{(1)}. \quad (1-13)$$

Here $|g\rangle_l$ is the g^{th} eigenfunction of the l^{th} spin, so that

$$K^{(0)} |a, b, \dots d\rangle = E_n |a, b, \dots d\rangle$$

$$\text{if } a_a + a_b + a_c + \dots + a_d = E_n.$$

The density matrix can be approximated by

$$b^{\bar{K}} \sim \prod_i b^{a_i} \quad (1-14)$$

In this first approximation the interaction terms are neglected in the density matrix expansion. This is only valid far above the Curie temperature.

With the substitutions of (1-13) and (1-14), the traces in (1-11) and (1-12) become

$$\begin{aligned} & \text{Trace } (b^{\bar{K}} [\hat{M}_-, \hat{M}_+]) \\ &= \sum_{r=1}^R b^{a_{r1} + a_{r2} + \dots + a_{ri} + \dots} \sum_i [\hat{m}_{-i}, \hat{m}_{+i}] \\ &= (\text{Trace } (b^a))^{N-1} \sum_i \text{Trace } (b^{a_i} [\hat{m}_{-i}, \hat{m}_{+i}]) \end{aligned} \quad (1-15)$$

$$\begin{aligned}
& \text{Trace } (b^{\bar{\mathcal{K}}} [\hat{\mathcal{M}}, [\bar{\mathcal{K}}, \hat{\mathcal{M}}]]) \\
&= \sum_i \sum_r b^{a_{r_1} + \dots + a_{r_i} + \dots + a_{r_j} + \dots} \sum_j' [(\hat{m}_i + \hat{m}_j), \\
&\quad [(\mathcal{K}_i^{(0)} + \frac{1}{2} \bar{\mathcal{K}}_{ij}^{(1)}), (\hat{m}_i + \hat{m}_j)]] \\
&= (\text{Trace } (b^a))^{N-1} \sum_i \text{Trace } (b^{a_i} [\hat{m}_i, [\mathcal{K}_i^{(0)}, \hat{m}_i]]) \\
&+ (\text{Trace } (b^a))^{N-2} \sum_{ij}' \text{Trace } (b^{a_i + a_j} [\hat{m}_i [\bar{\mathcal{K}}_{ij}^{(1)}, \hat{m}_i + \hat{m}_j]]) \quad (1-16)
\end{aligned}$$

$$\begin{aligned}
& \text{Trace } b^{\bar{\mathcal{K}}} [[\hat{\mathcal{M}}_-, \bar{\mathcal{K}}], [\bar{\mathcal{K}}, \hat{\mathcal{M}}_+]] \\
&= \sum_r b^{a_{r_1} + \dots + a_{r_i} + \dots + a_{r_j} + \dots} [[\sum_{ij}' (\mathcal{K}_i^{(0)} + \frac{1}{2} \bar{\mathcal{K}}_{ij}^{(1)}), (\hat{m}_{+i} + \hat{m}_{+j})],
\end{aligned}$$

$$[[\sum_{k\ell}' (\mathcal{K}_k^{(0)} + \frac{1}{2} \bar{\mathcal{K}}_{k\ell}^{(1)}), (\hat{m}_{-k} + \hat{m}_{-\ell})]]$$

$$\begin{aligned}
&= (\text{Trace } (b^a))^{N-1} \sum_i \text{Trace } (b^{a_i} [[\mathcal{K}_i^{(0)}, \hat{m}_{+i}], [\mathcal{K}_i^{(0)}, \hat{m}_{-i}]] \\
&+ (\text{Trace } (b^a))^{N-2} \sum_{ij}' \text{Trace } (b^{a_i + a_j} \{ [[\bar{\mathcal{K}}_{ij}^{(1)}, (\hat{m}_{+i} + \hat{m}_{+j})],
\end{aligned}$$

$$[\mathcal{K}_i^{(0)}, \hat{m}_{-i}]] + [[\mathcal{K}_i^{(0)}, \hat{m}_{+i}], [\bar{\mathcal{K}}_{ij}^{(1)}, (\hat{m}_{-i} + \hat{m}_{-j})]]$$

$$\begin{aligned}
& + \frac{1}{2} \left[\left[\mathcal{K}_{ij}^{(1)}, (\hat{m}_{+i} + \hat{m}_{+j}) \right], \left[\mathcal{K}_{ij}^{(1)}, (\hat{m}_{-i} + \hat{m}_{-j}) \right] \right] \Big\} \\
& + (\text{Trace } (b^a))^{N-3} \sum_{ijk}' \text{Trace } (b^{a_i + a_j + a_k} \\
& \left[\left[\mathcal{K}_{ij}^{(1)}, (\hat{m}_{+i} + \hat{m}_{+j}) \right], \left[\mathcal{K}_{ik}^{(1)}, (\hat{m}_{-i} + \hat{m}_{-k}) \right] \right] \Big) . \quad (1-17)
\end{aligned}$$

These formulas were derived by Kambe and Usui.⁴ They can be applied to special cases by substituting the proper values of $\mathcal{K}_i^{(0)}$, $\overline{\mathcal{K}}_{ij}^{(1)}$ and $\hat{m}_{\pm i}$.

1.3. Applications of the moment formulas to interaction between like neighbors.

A simple example to which Kambe and Usui⁴ applied the formulas (1-11) to (1-17) is the case of no crystalline field splitting of the lowest state. Their results will be repeated here since it will be of use later. The unperturbed Hamiltonian for isotropic g is

$$\mathcal{K}_i^{(0)} = g\beta H_0 S_z \quad (1-18)$$

where the field H_0 is taken to be along the z -direction. The truncated interaction $\overline{\mathcal{K}}^{(1)}$ will contain the exchange (1-5) plus the terms a and b of the dipolar energy (1-4). This we write as

$$\overline{\mathcal{K}}_{ij}^{(1)} = A_{ij} \vec{S}_i \cdot \vec{S}_j + B_{ij} S_{zi} \cdot S_{zj} \quad (1-19)$$

where

$$A_{ij} = \tilde{A}_{ij} + \frac{g^2 \beta^2}{2r_{ij}^3} (3 \cos^2 \theta_{ij} - 1) \quad (1-20)$$

$$B_{ij} = - \frac{3g^2 \beta^2}{2r_{ij}^3} (3 \cos^2 \theta_{ij} - 1) \quad (1-21)$$

The oscillating microwave field is along the x-axis; hence,

$$\hat{m}_i = g\beta S_{xi} \quad \hat{m}_{\pm i} = \frac{g\beta}{2} S_{\pm i} \quad (1-22)$$

When (1-18), (1-19) and (1-22) are inserted in (1-15), (1-16), and (1-17), the commutators can be simplified by using the relations

$$[S_{zi}, S_{\pm j}] = \pm \delta_{ij} S_{\pm i} \quad [S_{\pm i}, S_{-j}] = 2 \delta_{ij} S_{zi} \quad (1-23)$$

In this way, Kambe and Usui find the mean deviation from the unperturbed transition frequency $\nu^* = g\beta H_0/h$

$$h \langle \Delta \nu \rangle = - S B_s(y) \sum_i B_{ij} \quad (1-24)$$

and the mean square deviation about $\nu = \nu^* + \langle \Delta \nu \rangle$

$$\langle \Delta \nu^2 \rangle = \frac{1}{h^2} S^2 \frac{d}{dy} B_s(y) \sum_i B_{ij}^2 \quad (1-25)$$

$B_s(y)$ is the Brillouin function

$$B_s(y) = \frac{2S+1}{2S} \coth \left(\frac{2S+1}{2S} y \right) - \frac{1}{2S} \coth \left(\frac{y}{2S} \right) \quad (1-26)$$

where $y = g\beta H_0 S/kT$. At low temperatures $B_g \rightarrow 1$ for $T \rightarrow 0$; so, depending upon the lattice sum, we may have a finite first moment shift. The sum $\sum_j B_{ij}$ gives the effect of sample magnetization which will be discussed in more detail in Section 1.5. Here we only note that for a cubic lattice and spherically-shaped sample it vanishes. On the other hand, $dB_g(y)/dy \rightarrow 0$ for $T \rightarrow 0$ and the second moment vanishes at low temperatures as it should. Isotropic exchange between like spins does not influence the first or the second moment.

For spin $S = \frac{1}{2}$, the g-tensor in many cases has axial symmetry. If the magnetic field then is along the symmetry axis, the moments are already given by (1-24) and (1-25) if we use

$$A_{ij} = \tilde{A}_{ij} + \frac{g_{\perp}^2 \beta^2}{2r_{ij}^3} (3 \cos^2 \theta_{ij} - 1) \quad (1-20a)$$

$$B_{ij} = - \frac{(2g_{\parallel}^2 + g_{\perp}^2) \beta^2}{2r_{ij}^3} (3 \cos^2 \theta - 1) \quad (1-21a)$$

Another case that can be calculated directly and which applies to the case of $\text{Ni SiF}_6 \cdot 6\text{H}_2\text{O}$ discussed later is when

$$S = 1 \quad \mathcal{K}_i^{(0)} = g\beta \vec{S}_i \vec{H}_0 + D(S_{zi}^2 - 2/3) \quad (1-27)$$

For H_0 along the z-axis, we will then have two resonances, and $\mathcal{K}_i^{(1)}$ and $m_{\pm i}$ have to be truncated more than in the previous case. Then we must be very careful in using the commutator relations (1-23)

so that only the right terms are included. But if everything is written out in matrices, the multiplications are straightforward. We have

$$\kappa_i^{(0)} = \begin{pmatrix} e + \frac{1}{3}D & 0 & 0 \\ 0 & -\frac{2}{3}D & 0 \\ 0 & 0 & -e + \frac{1}{3}D \end{pmatrix} = \begin{pmatrix} a_3 & 0 & 0 \\ 0 & a_2 & 0 \\ 0 & 0 & a_1 \end{pmatrix} \quad (1-28)$$

where $g\beta H_0 = e$

$$m_{+i} = \begin{pmatrix} 0 & x & 0 \\ 0 & 0 & x \\ 0 & 0 & 0 \end{pmatrix}$$

where $x = g\beta \sqrt{2} H_{rf}$

If we observe the transition $(a_2 - a_1) = (e - D)$, we have to truncate m_{+i} to

$$\hat{m}_{+i} = \begin{pmatrix} 0 & 0 & 0 \\ 0 & 0 & x \\ 0 & 0 & 0 \end{pmatrix} \quad (1-29)$$

Similarly,

$$\hat{m}_{-i} = \begin{pmatrix} 0 & 0 & 0 \\ 0 & 0 & 0 \\ 0 & x & 0 \end{pmatrix} \quad (1-30)$$

By matrix multiplication, we find

$$[\hat{m}_{-i}, m_{+i}] = \begin{pmatrix} 0 & 0 & 0 \\ 0 & -x^2 & 0 \\ 0 & 0 & x^2 \end{pmatrix} \quad (1-31)$$

and

$$[\hat{m}_i, [\mathcal{K}_i^{(0)}, \hat{m}_i]] = \begin{pmatrix} 0 & 0 & 0 \\ 0 & 2(-e+D)x^2 & 0 \\ 0 & 0 & -2(-e+D)x^2 \end{pmatrix} \quad (1-32)$$

For two spins i and j the energy matrix is

$m_i \backslash m_j$		1			0			-1		
		1	0	-1	1	0	-1	1	0	-1
$\mathcal{K}_i^{(0)} + \mathcal{K}_j^{(0)} = 0$	1	1	$2(e + \frac{1}{3}D)$							
	0	$(e - \frac{1}{3}D)$								
	-1		$\frac{2}{3}D$					0		
	1		$(e - \frac{1}{3}D)$							
	0			$-\frac{4}{3}D$						
	-1				$(-e - \frac{1}{3}D)$					
	1						$\frac{2}{3}D$			
	0							$(-e - \frac{1}{3}D)$		
	-1								$2(-e + \frac{1}{3}D)$	(1-33)

The truncated interaction is in the same representation:

Combining (1-31), (1-32) and (1-35) with (1-11), (1-15) and (1-16), we find the first moment for the transition $(a_2 \leftrightarrow a_1)$

$$h < \Delta \nu > = \sum_j \frac{[(A_{ij} + B_{ij}) b^{a_3} - A_{ij} b^{a_2} - B_{ij} b^{a_1}]}{(b^{a_1} + b^{a_2} + b^{a_3})} \quad (1-36)$$

The trigonal lattice of $\text{NiSiF}_6 \cdot 6\text{H}_2\text{O}$ is sufficiently close to cubic so that for a spherical sample the dipolar part of the interaction in (1-36) cancels. The exchange part of A_{ij} , however, will give a characteristic temperature dependent shift in the first moment, and from the observed shift we can find the magnitude and sign of \tilde{A}_{ij} .

The first moment for the transition $(a_3 \leftrightarrow a_2)$ can be calculated the same way. But to find the second moment, we would have to work with $(2S + 1)^3 = 27$ - fold matrices, and while this should not be impossible, it is an unnecessarily hard way of doing the calculation. McMillan and Opechowski⁵ have calculated the commutators in (1-11) and (1-12) in a general way using the technique of projection operators. Their formulas for the first and second moment are given in Appendix 1. These formulas only involve summations over the truncated matrix elements connecting the unperturbed energy states.

1.4. Line moments from interaction between unlike spins.

The previous moment calculation can be extended to include the effect of unlike spins. The importance of differentiating between "like" and "unlike" neighbors comes from the fact that for

interaction between unlike spins a further truncation of $\mathcal{K}^{(1)}$ is necessary, because then terms like $S_{+i} S_{-i}$ do not connect states of the same energy.

The criterion for "unlikeness" is that the spins have unperturbed transitions sufficiently different in energy so that the resonance lines have little or no overlap. It is obvious that different chemical species of ions may have different magnetic properties. But also chemically identical ions may be unlike in this sense, for instance, if the crystalline field is different in strength or direction on different crystalline sites, or if identical spins interact so strongly with a particular neighbor or the nuclear spin that separate lines are created. Whether the interaction is like or unlike depends to some extent on the strength of spin interaction; strong interaction will tend to make separate lines overlap.

The Hamiltonian for two kinds of interacting spins, primed and unprimed, is

$$\begin{aligned} \overline{\mathcal{K}} = & \sum_i \mathcal{K}_i^{(0)} + \sum_{k'} \mathcal{K}_{k'}^{(0)} + \frac{1}{2} \sum_{i,j}' \overline{\mathcal{K}}_{ij}^{(1)} \\ & + \sum_{i,k}' \overline{\mathcal{K}}_{ik}^{(1)} + \frac{1}{2} \sum_{k',e}' \overline{\mathcal{K}}_{k'e}^{(1)} \quad (1-37) \end{aligned}$$

The density matrix now has to be approximated by

$$b^{\bar{\mathcal{K}}} \approx \prod_{i,k}^{N_i, N_{k'}} \frac{a_i}{b} \frac{a_{k'}}{b} \quad (1-38)$$

We may suppose that we are looking at a resonance of the unprimed system.

When now the traces in (1-11) and (1-12) are expanded the same way as before, we find that the additional terms in the moments due to interaction with unlike neighbors are :

$$h < \Delta \nu >_{\text{unlike}} = \frac{1}{2} \frac{\sum_k \text{Trace} (b^{a_i + a_{k'}} [\hat{m}_i, [\bar{\mathcal{K}}_{ik}^{(1)}, \hat{m}_i]])}{\text{Trace } b^{a_{k'}} \text{Trace} (b^{a_i} [\hat{m}_{-i}, \hat{m}_{+i}])} \quad (1-39)$$

$$h^2 < \Delta \nu^2 >_{\text{unlike}}$$

$$= \sum_{k'} \text{Trace} (b^{a_i + a_{k'}} \left\{ [[\bar{\mathcal{K}}_{ik}^{(1)}, \hat{m}_{+i}], [\mathcal{K}_i^{(0)}, \hat{m}_{-i}]] \right.$$

$$+ [[\mathcal{K}_i^{(0)}, \hat{m}_{+i}], [\bar{\mathcal{K}}_{ik}^{(1)}, \hat{m}_{-i}]]$$

$$\left. + [[\bar{\mathcal{K}}_{ik}^{(1)}, \hat{m}_{+i}], [\bar{\mathcal{K}}_{ik}^{(1)}, \hat{m}_{-i}]] \right\})$$

$$\left\{ \text{Trace } b^{a_{k'}} \text{Trace} (b^{a_i} [\hat{m}_{-i}, \hat{m}_{+i}]) \right\}^{-1}$$

$$\begin{aligned}
& + \sum_{k' e'} \text{Trace} (b^{a_i + a_{k'} + a_{e'}} [[\bar{\mathcal{K}}_{ik}^{(1)}, \hat{m}_{+i}] , \\
& [\bar{\mathcal{K}}_{ie}^{(1)}, \hat{m}_{-i}]]) \left\{ \text{Trace} (b^{a_{k'} + a_{e'}} \right. \\
& \left. \text{Trace} (b^{a_i} [\hat{m}_{-i}, \hat{m}_{+i}]) \right\}^{-1} \\
& + \sum_{k j} \text{Trace} (b^{a_i + a_j + a_{k'}} \left\{ [[\bar{\mathcal{K}}_{ik}^{(1)}, \hat{m}_{+i}] , \right. \\
& \left. [\bar{\mathcal{K}}_{ij}^{(1)}, (\hat{m}_{-i} + \hat{m}_{-j})]] \right. \\
& \left. + [[\bar{\mathcal{K}}_{ij}^{(1)}, (\hat{m}_{+i} + \hat{m}_{+j})] , [\bar{\mathcal{K}}_{ik}^{(1)}, \hat{m}_{-i}]] \right\}) \\
& \left\{ \text{Trace} b^{a_{k'} + a_j} \text{Trace} b^{a_i} [\hat{m}_{-i}, \hat{m}_{+i}] \right\}^{-1} . \quad (1-40)
\end{aligned}$$

We see that for more than one kind of different neighbors the contribution to $h < \Delta v >$ can simply be added for each specie. The last terms in $h^2 < \Delta v^2 >_{\text{unlike}}$ are cross terms between like and unlike neighbors. But such cross terms can be expected to cancel out when we calculate the more useful central second moment of a line.

Equations (1-39) and (1-40) will now be applied to a special case : Two magnetic species, both of which have spin $S = \frac{1}{2}$ and g-tensors with symmetry axis along the direction of the magnetic

field. The results will be used later to explain the measurements on neodymium ethylsulfate.

Using

$$\mathcal{H}^{(0)} = \sum_i g_{\parallel} \beta S_{zi} H_0 + \sum_{k'} g_{\parallel}' \beta S_{zk'} H_0 \quad (1-41)$$

$$\overline{\mathcal{H}}_{ij}^{(1)} = A_{ij} \frac{1}{2} (S_{-i} S_{+j} + S_{+i} S_{-j}) + (A_{ij} + B_{ij}) S_{zi} S_{zj} \quad (1-42)$$

$$\overline{\mathcal{H}}_{ik}^{(1)} = (A_{ik} + B_{ik}) S_{zi} S_{zk}'$$

where

$$A_{i\zeta} = \tilde{A}_{i\zeta} + \frac{1}{2} \frac{g_{\perp i} g_{\perp \zeta} \beta^2}{r_{i\zeta}^3} (3 \cos^2 \theta_{i\zeta} - 1)$$

$$B_{i\zeta} = - \frac{1}{2} \frac{(2g_{\parallel i} g_{\parallel \zeta} + g_{\perp i} g_{\perp \zeta}) \beta^2}{r_{i\zeta}^3} (3 \cos^2 \theta_{i\zeta} - 1)$$

and ζ stands for j or k' , the first moment shift becomes

$$h \langle \Delta \nu \rangle = h \langle \Delta \nu \rangle_{\text{like}} + h \langle \Delta \nu \rangle_{\text{unlike}}$$

$$= \langle S_{zi} \rangle \sum_j' B_{ij} + \langle S_{zk'} \rangle \sum_{k'}' (A_{ik} + B_{ik}) \quad (1-43)$$

Here

$$\langle S_{z\zeta} \rangle = -\frac{1}{2} \frac{(1 - b \parallel \zeta^{\beta H_0})}{(1 + b \parallel \zeta^{\beta H_0})} \quad (1-44)$$

The second central moment becomes, in this case,

$$\begin{aligned} h^2 \langle \Delta \nu^2 \rangle_{\text{central}} &= h^2 \langle \nu^2 \rangle - (h \langle \Delta \nu \rangle)^2 \\ &= (\langle S_{zi}^2 \rangle - \langle S_{zi} \rangle^2) \sum_j B_{ij}^2 \\ &+ (\langle S_{zk}^2 \rangle - \langle S_{zk} \rangle^2) \sum_k (A_{ik} + B_{ik})^2 \end{aligned} \quad (1-45)$$

where

$$\langle S_{z\zeta}^2 \rangle = \frac{1}{3} S_{\zeta} (S_{\zeta} + 1) = \frac{1}{4} \quad (1-46)$$

Here we should note that $B_{i\zeta}$ and the dipolar part of $A_{i\zeta}$ are defined with opposite signs so that they partially cancel when they appear together in a sum. Then we see, as is well known,¹ the unlike neighbors are less efficient in dipolar broadening of a resonance line. But exchange between unlike neighbors will contribute to the second moment. We should also note that at low temperature where $\langle S_{zk} \rangle$ is finite, we will have an exchange induced shift of the first moment.

1. 5. Discussion of demagnetizing effects.

We have seen that in the calculation of line moments we have to evaluate sums over the lattice of the form

$$\sum_j \frac{(3 \cos^2 \theta_{ij} - 1)}{r_{ij}^3} \quad (1-47)$$

Such a sum is only slowly converging. But following the classical theory of demagnetization,¹³ the summation can be performed by dividing it into two parts. Close to the spin i expression (1-47) has to be summed over the lattice points. But outside a radius ζ from i we can treat the magnetization as being continuous rather than associated with discrete lattice points, and this part of the sum can be converted to an integral. This integral will depend on the shape of the crystal; and it will, in general, be different for different lattice points. Only for an ellipsoid will the integral be the same for all points i , and only for a sphere will it vanish. For a cubic lattice the sum inside ζ also vanishes.

When the field is along one of the ellipsoid axes, the shape dependent part of the sum (1-47) can be described by a demagnetizing factor N_z

$$\sum_{\substack{j \\ r_{ij} > \zeta}} \frac{3(\cos^2 \theta_{ij} - 1)}{r_{ij}^3} = N_1 \left(N_z - \frac{4\pi}{3} \right) \quad (1-48)$$

where N_1 is the density of spins.

The factor N_z equals $4\pi/3$ for a sphere. For ellipsoids of revolution around the z-axis, N_z is given by¹⁴

a) Prolate spheroid :

$$N_z = \frac{4\pi}{(m^2 - 1)} \left[\frac{m}{2(m^2 - 1)^{1/2}} \ln \left(\frac{m + (m^2 - 1)^{1/2}}{m - (m^2 - 1)^{1/2}} \right) - 1 \right] \quad (1-49)$$

where the axis ratio $m = r_z / r_x$.

b) Oblate spheroid :

$$N_z = \frac{4\pi m^2}{(m^2 - 1)} \left[1 - \frac{1}{(m^2 - 1)^{1/2}} \arcsin \left(\frac{m^2 - 1}{m^2} \right)^{1/2} \right] \quad (1-50)$$

where $m = r_x / r_z$.

From (1-24) we now get the change in first moment for free spins in a cubic lattice :

$$\langle \Delta v \rangle = - \frac{3}{2} \cdot \frac{g\beta}{h} \left(\frac{4\pi}{3} - N_z \right) \langle M_z \rangle \quad (1-51)$$

where the magnetization is given by

$$\langle M_z \rangle = N_1 g\beta \langle S_z \rangle = - N_1 g\beta S B_s \left(\frac{g\beta HS}{kT} \right) = - M . \quad (1-52)$$

Here N_1 is the number of spins per unit volume and B_s is the Brillouin function (1-26) .

It is interesting to compare the first moment shift (1-51) to the Kittel formula for ferromagnetic resonance¹⁵

$$\nu h = g\beta \left\{ [H_0 + (N_x - N_z) M] [H_0 + (N_y - N_z) M] \right\}^{1/2}. \quad (1-53)$$

Here N_x and N_y are the demagnetization factors in the x - and y -directions. They are related to N_z by

$$N_x + N_y + N_z = 4\pi. \quad (1-54)$$

For axial symmetry, so that $N_x = N_y = \frac{1}{2}(4\pi - N_z)$, the resonance condition (1-53) becomes

$$\begin{aligned} \nu h &= g\beta (H_0 + (N_x - N_z) M) \\ &= g\beta (H_0 + \frac{3}{2}(\frac{4\pi}{3} - N_z) M) \end{aligned} \quad (1-55)$$

Comparing (1-55) to (1-51), we see that the shape dependent lineshifts depend in the same way on the magnetization in these two cases as we expected. For a general ellipsoid with $N_x \neq N_y \neq N_z$, we see that the first moment shift (1-51) differs in order M^2/H_0 from the resonance condition (1-53). This is because the component of the magnetization in the direction of the applied field is not a constant of the motion in the case of a general ellipsoid, as has been pointed out by Van Vleck.¹⁶ The moment method is not strictly valid unless the sample has cylindrical symmetry around H_0 . Only in this case can we truncate the interaction Hamiltonian in the representation where M_z is constant.

The appearance of the factor N_x that signifies a dynamic demagnetizing effect in the formula for the first moment change, may be thought of as being caused by the spin-flip terms $S_{+i} S_{-j}$ in the

interaction. Suppose these terms were truncated out (in the case of no exchange) and we would get only the static demagnetization

$$h < \Delta \nu > = -g\beta \left(\frac{4\pi}{3} - N_z \right) < M_z > . \quad (1-56)$$

It is, therefore, not surprising that in the interaction between nonequal neighbors or when crystalline field splitting is present and further truncation is necessary, the Kittel resonance condition is not immediately valid in the sense that in (1-55) M cannot simply be replaced by the static magnetization $- < M_z >$. In the case of $\text{NiSiF}_6 \cdot 6\text{H}_2\text{O}$, for example, the magnetization relevant to the shape dependent first moment shift of the lower line is found from (1-36) to be

$$< M'_{a_1} >_{\leftrightarrow a_2} = - \frac{N_1 g \beta}{3} \frac{(3b^{a_1} - b^{a_2} - 2b^{a_3})}{(b^{a_1} + b^{a_2} + b^{a_3})} . \quad (1-57)$$

Similarly, for the upper line we get

$$< M'_{a_2} >_{\leftrightarrow a_3} = - \frac{N_1 g \beta}{3} \frac{(2b^{a_1} + b^{a_2} - 3b^{a_3})}{(b^{a_1} + b^{a_2} + b^{a_3})} . \quad (1-58)$$

The formulas (1-57) and (1-58) should replace $< M_z >$ in (1-51). This correction for elliptically-shaped samples is later applied to our measurements on $\text{NiSiF}_6 \cdot 6\text{H}_2\text{O}$.

If the crystal lattice is not cubic, we also have to consider the part of the sum (1-47) taken over $r_{ij} < \zeta$ which may give an additional line shift.

The second central moment formula involves only the rapidly-converging sum

$$\sum_j \left(\frac{g^2 \beta^2}{r_{ij}^3} (3 \cos^2 \theta_{ij} - 1) \right)^2 ,$$

and the second central moment will not depend on the sample shape as long as it is spheroidal.

When a sample deviates from exact ellipsoidal shape, the demagnetizing field will vary from spin to spin. We may expect this to have a relatively larger effect on the second moment than on the first moment, and in particular, we may not see the narrowing of the resonance lines at low temperature.

1.6. Comment on the fourth moment and the effect of exchange.

The method of calculating moments can, in principle, be extended to the n^{th} moment, and more information about the lineshape may be gained. Van Vleck¹ has calculated the fourth moment at high temperature for the case of no crystalline field splitting. He found:

a) Isotropic exchange with like spins will not change the second moment, but it will increase the fourth moment. This can only happen if the resonance line is being so-called exchange-narrowed -- made more narrow and sharp in the center and with longer wings on the sides.

b) If two unlike systems of spins are interacting, isotropic exchange between the spins in one system will exchange-narrow the resonance line of the other system.

The fourth moment at low temperature can be written as⁴

$$h^4 \langle \nu^4 \rangle = \frac{\text{Trace} (b^{\overline{\mathcal{K}}} [[\overline{\mathcal{K}}, [\overline{\mathcal{K}}, \hat{M}_-]], [\overline{\mathcal{K}}, [\overline{\mathcal{K}}, \hat{M}_+]]])}{\text{Trace} (b^{\overline{\mathcal{K}}} [\hat{M}_-, \hat{M}_+])} \quad (1-59)$$

The traces can again be calculated as in Section 1.2 by inserting

$$\overline{\mathcal{K}} = \sum_i \mathcal{K}_i^{(0)} + \frac{1}{2} \sum_{ij} \mathcal{K}_{ij}^{(1)} \quad \text{and} \quad \hat{M}_{\pm} = \sum_i \hat{m}_{\pm i}$$

and taking

$$b^{\overline{\mathcal{K}}} = \prod_i b^{ai}$$

as the approximation for the density matrix. This will lead to even more complicated formulas than those given by Van Vleck. At low temperature where $\text{Trace} (b^{ai} S_{zi})$ and $\text{Trace} (b^{ai} S_{zi}^3)$ are no longer zero, many terms involving these factors will appear.

These terms require that we perform awkward summations over the lattice like $\sum_{ijk} A_{ij} A_{jk} B_{ij} B_{ik}$ even before we can tell whether they are positive or negative or in other words whether they add to or subtract from the fourth moment at low temperatures. Because of the labor necessary and the limited information to be gained, we will not here try to calculate the fourth moment.

A more direct approach to the problem of resonance lineshapes and exchange-narrowing has been attempted by Anderson and Weiss.^{6,7}

They consider the exchange interaction to give a random frequency modulation to the dipolar-broadened resonance, similar to the motional modulation of nuclear spin-spin interaction in liquids treated by Bloembergen, Purcell and Pound.¹² The lineshape can then be found from the Fourier transform of an autocorrelation function

$$\phi(\tau) = \langle \mu_{ij}^*(t + \tau) \mu_{ij}(t) \rangle_{\text{average over } t} \quad (1-60)$$

$\phi(\tau)$ is a measure of the "memory" of the state μ_{ij} at the time $t + \tau$ for what it was at a time τ earlier. Strong exchange will cause rapid spin flips that reduce the correlation time and average out the dipolar field fluctuations, and the line will appear exchange-narrowed.

Assuming Gaussian random modulation, they find that the central part of an exchange-narrowed line must have Lorentzian shape. But the intensity of the line wings will decrease more rapidly, as expected, since a strictly Lorentzian line would have an infinite second moment. Qualitatively, in the case of strong exchange, the line-width is

$$\Delta H \approx H_d^2 / H_e \quad (1-61)$$

where H_d is the effective dipolar field and H_e is the effective field from exchange interactions. For more quantitative results, the line parameters would have to be fitted so that they give the same second and fourth moment as given by Van Vleck's theory.

In this model, Anderson⁷ also treats the case of two lines close together that merge into one as the exchange is increased. This is beyond the power of the moment method. From Fig. 2 in his article, it is clearly seen that increasing exchange between the unlike spins first broadens the two lines so that they overlap more and more, and at the same time the peaks move together. This behavior is observed in the case of $\text{CuSO}_4 \cdot 5\text{H}_2\text{O}$ to be described later.

For many lines close together, Anderson's qualitative result is that the exchange will broaden them and wash out their identity, but while still separated, the shift of each peak is negligible. If there are p lines separated by $h \Delta\nu$, we expect qualitatively that an exchange $\mathcal{K}_e' \approx h \Delta\nu$ will make exchange spin flips possible between neighboring lines and, therefore, broaden the separate lines into one. But a considerably stronger exchange $\mathcal{K}_e'' \approx (p-1) h \Delta\nu$ is required to exchange-narrow appreciably the composite line. This seems to be the observed behavior of the hyperfine lines of Mn when the exchange is changed by varying the concentration.¹⁷ For an exchange \mathcal{K}_e in the approximate range $h \Delta\nu < \mathcal{K}_e < (p-1) h \Delta\nu$, we have to treat the interaction as partly between like and partly between unlike neighbors. Exchange between unlike neighbors, however, will lead to a shift of the resonance frequency at low temperatures, and we have found it necessary to use this model to explain the line shift in $\text{K}_2\text{Cu}(\text{SO}_4)_2 \cdot 6\text{H}_2\text{O}$ where the Cu resonance has $p = 4$ hyperfine lines.

Kubo and Tomita^{8,9,10} have given the ideas of Anderson and Weiss a more rigorous foundation by starting from the theory of irreversible processes in quantum-mechanical systems. Their treatment includes the Boltzmann factors necessary if we go to temperatures where $h\nu \approx kT$. The theory is essentially equivalent to the moment method: each higher order in the expansion of the relaxation function corresponding to $\phi(\tau)$ in (1-60) gives only the same information as the corresponding line moment, and requires about the same amount of work. Only for partly-overlapping lines or when the interaction fields are comparable in strength to the external field, does this approach seem to be superior.

It might be pointed out that in the latter case when the exchange is strong, all terms in the dipolar interaction (1-4) contribute to the linewidth and should not be truncated out.⁶ Physically, we can see that dipolar rearrangements that do not conserve energy become possible when the fluctuations in exchange energy are very great. Thus, the complete second moment for a highly exchange-narrowed line will be 10/3 times its value calculated from the truncated dipolar interaction.

1.7. Comment on McMillan and Opechowski's second approximation.

The approximation for the density matrix (1-14) can be made more accurate by using the fact that the interactions are weak, and the part of the Boltzmann factor containing these interactions can then

be expanded in powers of $(kT)^{-1}$. Such higher approximations in the derivation of the line moments have been considered by McMillan and Opechowski.^{5,18} Using the projection operator formalism explained in Appendix I, they write

$$\text{bol}(P_a K P_a) = \text{bol}(E_a P_a) \left[1 - \frac{P_a K^{(1)} P_a}{kT} + \dots \right] \quad (1-62)$$

In the first approximation, only the first term in the bracket is kept, and this is the approximation we have worked with so far. We write the resulting moments as $h^n < \Delta v^n >_1$. If the term $P_a K^{(1)} P_a / kT$ is also kept in (1-62), this leads to the second approximation moments $h^n < \Delta v^n >_2$. The labor involved in calculating higher approximations increases rapidly, and McMillan has given a formula only for $h < \Delta v >_2$. His general equation is copied in Appendix II.

Because of the extra term in (1-62), we expect the first moment in the second approximation to contain terms in $(K^{(1)})^2$. Even for a cubic lattice, this will give a finite shift, which is related to the magnitude of the second moment in the first approximation.

McMillan and Opechowski show quite generally that

$$\begin{aligned} < \Delta v >_2 \xrightarrow{T \rightarrow \infty} \frac{v^* < \Delta v >_1 + < \Delta v^2 >_1}{v^* + < \Delta v >_1} \\ &= \frac{< \Delta v^2 >_1}{v^*} \quad \text{for } < \Delta v >_1 \xrightarrow{T \rightarrow \infty} 0 \quad (1-63) \end{aligned}$$

Here ν^* is the unperturbed frequency of the resonance. The odd moments of the line generally vanish at high temperature in the first approximation.

Equation (1-63) can easily be derived. The spin-spin interaction causes a variation in local field, and the possible transition frequencies will have a distribution $S(\nu)$. The intensity of the absorption at each frequency ν is proportional to the population difference $(b^E - b^{E+h\nu})$ between the initial and final energy level. When the Boltzmann factors are expanded, the first moment in the second approximation is by definition

$$\langle \Delta \nu \rangle_2 = \frac{\int_{-\infty}^{\infty} x S(\nu^* + x) \left(1 - b^{h\nu^*} + \frac{b^{h\nu^*} x}{kT} \right) dx}{\int_{-\infty}^{\infty} S(\nu^* + x) \left(1 - b^{h\nu^*} + \frac{b^{h\nu^*} x}{kT} \right) dx} \quad (1-64)$$

We assume that the distribution $S(\nu)$ can be calculated from the spin-spin interaction, and $[S(\nu)]_n$ calculated will, in general, be different for each approximation n in $\mathcal{K}_{ij}^{(1)}/kT$. For $T \rightarrow \infty$, however, the population difference between energy levels goes to zero and in this limit $[S(\nu)]_n \xrightarrow{T \rightarrow \infty} S(\nu)$. From (1-64), we then get

$$\langle \Delta \nu \rangle_2 \xrightarrow{T \rightarrow \infty} \frac{\int_{-\infty}^{\infty} x [S(\nu^* + x)]_1 (\nu^* + x) dx}{\int_{-\infty}^{\infty} [S(\nu^* + x)]_1 (\nu^* + x) dx} \quad (1-65)$$

This directly gives (1-63) , since we also have, by definition

$$\langle \Delta \nu^m \rangle_1 = \frac{\int_{-\infty}^{\infty} x^m [S(\nu^* + x)]_1 dx}{\int_{-\infty}^{\infty} [S(\nu^* + x)]_1 dx} \quad (1-66)$$

The correction (1-63) is small and we have never seen it applied to measurements of g -values. It may be of importance when broad lines are measured at low frequency. If a resonance with second moment of $(500 \text{ gauss})^2$, say, is measured in a field of 2500 gauss, the relative error in g , if not corrected by (1-63) will be

$$\frac{\Delta g}{g} = \frac{1}{H_0} \frac{\langle \Delta H^2 \rangle_1}{H_0} = 4 \% \quad (1-67)$$

McMillan and Opechowski have applied their general equation for $\langle \Delta \nu \rangle_2$ to the transition in $\text{NiSiF}_6 \cdot 6\text{H}_2\text{O}$. The difference from the first approximation is small at all temperatures, and we will neglect higher approximation corrections in our discussion of experimental data.

1.8. Comment on the possibility of magnetostatic modes in para - magnetic crystals at low temperature.

It is well known that under certain circumstances ferromagnetic resonance experiments can be complicated by the appearance of magnetostatic modes in the sample, propagation effects in large samples

and spin wave instabilities at high microwave power levels. Paramagnetic salts become magnetized and similar to ferromagnets at low temperature when the spins are aligned by an external field. We may then ask whether we should see some of these effects in our lineshape experiments. In particular, magnetostatic modes have recently been observed in disks of $\text{K}_2\text{CuCl}_4 \cdot 2\text{H}_2\text{O}$,¹⁹ and we have also seen some extra lines in the spectra of $\text{CuSO}_4 \cdot 5\text{H}_2\text{O}$ and $\text{K}_2\text{Cu}(\text{SO}_4)_2 \cdot 6\text{H}_2\text{O}$ below 1°K that probably are caused by such modes. Here we will briefly review the theory for the various effects observed in ferromagnetic resonance. The experimental evidence for magnetostatic modes will be discussed in Section 5.5.

If the magnetizations in different parts of the sample precess with the same frequency but in different phases, the regions will interact via the dipolar fields, and the resonance condition may be changed relative to that of the uniform mode. Walker^{20,21} has given the resonance frequencies for a number of these magnetostatic modes by solving the equations

$$d\vec{M}/dt = \gamma (\vec{M} \times \vec{H}) \quad (1-68)$$

$$\text{curl } \vec{H}_1 = 0 \quad \text{div } (\vec{H}_1 + 4\pi \vec{M}_1) = 0 \quad (1-69)$$

in the limit of small deviations \vec{M}_1 from the equilibrium magnetization \vec{M}_0 and with the proper boundary conditions for a spheroid. The energy differences between the modes are proportional to M_0 and for a sphere, they fall over a frequency range of $\Delta\omega = \frac{1}{2} \gamma \cdot 4\pi M_0$.

Fletcher et al.²² and others have obtained good agreement between Walker's theory and measured mode positions.

Magnetostatic modes are a result of dipolar interaction only. The exchange forces are of short range compared to the mode wavelength and they are neglected in Walker's theory. His results should, therefore, be directly applicable to paramagnetic resonance at low temperature.

Whether a particular mode is excited or not depends on the symmetry of the microwave field at the sample. In a perfectly homogeneous driving field, only the fundamental mode would be excited. It is found²³ that unless special care is taken in mounting the sample away from field-disturbing dielectric materials, one is likely to excite a whole series of modes, and they may partly be so close together in frequency that they are not observed as separate lines.

Consider now the modes in a non-spherical sample. Dillon²³ found that small deviation from sphericity, such as results from tumble-grinding an anisotropic material, would slightly change the separation of the modes. Large deviations, however, will cause the demagnetizing field to vary through the sample, the magnetization in different regions will precess with different frequencies, and there will be no discrete modes for the crystal as a whole. It is hard to give a good criterion for how close to spheroidal shape the sample has to be before separate magnetostatic modes can be observed, but it may well be possible that a sample is good enough for measurements of first

moment lineshifts and still have sufficiently crude shape to prevent observation of discrete modes. Since we have observed these modes only in rather good spheres, it may even be advantageous to use crudely-shaped samples.

It should be noted that homogeneous broadening of the line by dipolar and hyperfine interactions will not prevent the possible excitation of magnetostatic modes. The macroscopic magnetization of one part of the sample will still precess on the average with the same frequency as that of another part. However, if the paramagnetic salt has two or more separate resonances, the microwave field will usually excite only one of them in a given external field. The energy difference between magnetostatic modes will then be given by the magnetization of that sub-lattice alone. The spectrum is likely to be complicated when the possible mode patterns of two separate resonances overlap.

We expect any single mode to have the same linewidth as the uniform mode. If higher modes are excited, line areas can no longer be used to measure resonance intensity, since each spin may resonate in a succession of modes as we sweep through the line.

If the sample is made so big that it becomes comparable to the driving-field wavelength, the finite propagation speed of the dipolar fields has to be accounted for by using the complete Maxwell's equations instead of the approximations (1-69).²⁴ This will change the resonance frequencies of the first few modes of long wavelength and,

in particular, the resonance condition for the uniform mode in a sphere becomes²⁵

$$\omega = \gamma H_0 \left\{ 1 - \frac{8\pi M_0}{9H_0} \left(1 + \frac{\epsilon}{5}\right) (kR_0)^2 + \dots \right\} \quad (1-70)$$

where

ϵ = dielectric constant

k = $2\pi/\lambda$ propagation constant

R_0 = sample radius .

The magnetization at $T = 0^\circ\text{K}$ for $\text{NiSiF}_6 \cdot 6\text{H}_2\text{O}$, for example, is from (1-52)

$$M_0 = N_1 g \beta S = 86 \text{ gauss}$$

for $N_1 = 4.16 \cdot 10^{21}$ ions/cm³, $g = 2.24$ and $S = 1$. If we take the dielectric constant for this salt to be $\epsilon \approx 2.5$, work at 30 kMc/s so that $k = 2\pi \text{ cm}^{-1}$ and use the sample size $R_0 \approx 0.075$ cm (wave-guide spectrometer), we find the size induced resonance shift for constant ω at $T = 0^\circ\text{K}$ to be

$$\Delta H = \frac{8\pi M_0}{9} \left(1 + \frac{\epsilon}{5}\right) (kR_0)^2 = 80 \text{ gauss.}$$

Our cavity spectrometer in which most of the experiments on $\text{NiSiF}_6 \cdot 6\text{H}_2\text{O}$ were done requires a sample size of about $R_0 \approx 0.015$ cm. Then the shift becomes $\Delta H \approx 4$ gauss, which is negligible.

In $\text{Nd}(\text{C}_2\text{H}_5\text{SO}_4)_3 \cdot 9\text{H}_2\text{O}$ and $\text{K}_2\text{Cu}(\text{SO}_4)_2 \cdot 6\text{H}_2\text{O}$ the saturation magnetization is smaller, and we have ignored the size effect even for measurements in the waveguide.

The higher order magnetostatic modes can be thought of as going gradually over into traveling spin waves obeying the dispersion relation²⁶

$$\omega(k) = \gamma \left[(H_0 - N_z M_0 + H_{\text{ex}} d^2 k^2) (H_0 - N_z M_0 + H_{\text{ex}} d^2 k^2 + 4\pi M_0 \sin^2 \theta) \right]^{\frac{1}{2}} \quad (1-71)$$

Here, N_z is the demagnetization factor in the direction \vec{H}_0 , d is the lattice spacing and θ is the angle between \vec{H}_0 and the spin-wave propagation vector \vec{k} . The term $H_{\text{ex}} d^2 k^2$ is important in ferromagnets where the exchange field is strong, but it is negligible in paramagnets magnetized in strong fields at low temperatures.

The various magnetostatic modes and spin waves are non-interacting in the first approximation, but they are weakly coupled by the dipolar fields, surface irregularities and lattice defects. The way the fundamental mode is coupled to high-order spin waves is very important for the spin-lattice relaxation process in ferromagnets,^{27,28} and the coupling may also cause instabilities of the resonance at high power levels.^{29,30} However, we will not here speculate on the possibility of such spin wave effects in paramagnets at $T \approx 0$ since we observed no instabilities and did not try to measure relaxation.

CHAPTER 2

DISCUSSION OF EXPERIMENTAL APPARATUS AND TECHNIQUE

2.1. Description of microwave and low-temperature systems.

In the line moment theory reviewed in the previous chapter, all shifts are functions of the Boltzmann factor $e^{-h\nu/kT}$. Resonance experiments have usually been done in magnetically diluted salts under conditions where $h\nu \ll kT$, and no observations of the temperature effect seem to have been reported before. The line moment changes can be clearly demonstrated only if the measurements are made down to a temperature where

$$T < h\nu/k \quad (2-1)$$

and on concentrated salts where the magnetic ions are close enough to interact moderately.

We satisfied the temperature-frequency condition (2-1) by working at 30 kMc/s and using a ^3He -cryostat for cooling the sample down to $0.3^\circ - 0.4^\circ\text{K}$. This temperature is three times lower than the approximately 1°K one can reach by pumping on ordinary liquid ^4He . Still lower temperatures can be obtained by adiabatic demagnetization, but that way of cooling is not very convenient for resonance experiments, and the problem of securing heat contact between the sample and the cold reservoir is likely to be serious. Spin resonance work at a frequency higher than 30 kMc/s may require a stronger magnetic field than the available magnets can give. A field of 10,700 gauss is needed for resonance in a salt with

$g \approx 2$ at 30 kMc/s . This is just below the approximately 11,500 gauss field limit of our 12" Varian magnet with 2" gap.

For $h\nu = 30 \text{ kMc/s}$, the Boltzmann factors are

T	$e^{-h\nu/kT}$
4.2° K	0.71
0.4° K	0.027

At $T = 0.4^\circ \text{ K}$, all but a few percent of the spins are in the lowest state, while at 4.2° K , the levels of a Kramers' doublet are nearly equally populated.

For a Kramers' doublet, the intensity of the resonance goes as $(1 - e^{-h\nu/kT})/(1 + e^{-h\nu/kT})$, and the line area, therefore, changes by a factor of 5.5 as we lower the temperature from 4.2° to 0.4° K . If the line narrows as expected, the peak intensity will increase even more. This makes the measurements difficult, since we may easily get too little resonance absorption for good signal-to-noise ratio at the high temperatures or too much absorption at low temperatures for linear response of the system. Spectrometer linearity will be discussed later in Section 2.5 .

In most microwave spectrometers, magnet modulation and lock-in detection are used to obtain a good signal-to-noise ratio. Working with our concentrated salt we expect linewidths of at least a few hundred gauss, and then we could not use a modulation scheme because :

a) The field modulation inside the shielding brass cavity and container would have to be a reasonable fraction of the linewidth for sensitivity, and we would have had trouble trying to modulate this big magnet with, say, 100 gauss at 30 c/s.

b) Even if we could modulate the magnet, the eddy currents set up in the ^3He system would represent a serious heat input and prevent us from reaching the lowest temperatures. In practice, at 0.4°K we began to see the heating effect if we increased the field modulation to more than the minimum of a few gauss necessary to see the proton resonance for field determination.

Since we could not use a lock-in system, we had to use larger samples and record the changes in reflected power as we swept the magnetic field slowly through resonance. This requires a stable microwave system which is hard to obtain at this high frequency, and we found it necessary to have the klystron frequency locked either to the sample cavity or to an external cavity. Even so, noise and klystron amplitude fluctuations usually were of the order of one percent of the power level, and a useful signal had to be well above that.

For work around 0.5°K , problems with sample saturation and poor heat contact require that the microwave power be kept very low as will be discussed in Sections 2.2 and 2.3. At the lowest temperatures we are forced to use the more sensitive, but more complicated superheterodyne detection scheme instead of simple crystal detection.

The microwave circuits used were modified occasionally; sometimes the sample was sitting in the maximum H-field of a resonant cavity, and sometimes it was sitting at the reflecting bottom of a waveguide. From the calculations in the next section, it appears that in the latter arrangement the danger of saturating the resonance is less, and while a larger sample is then required, it is usually no problem to get enough absorption at this frequency and temperature range.

The main features of the waveguide spectrometer are shown in Fig. 1. The measuring power comes from an EMI 9518 klystron which is frequency-locked to a fixed cavity for stability. The reflected power from the sample arm is detected in the balanced mixer, amplified and displayed with a recorder as the magnetic field is swept slowly through resonance. The local oscillator is a Varian X-12 klystron whose frequency is doubled in a crystal harmonic generator made by Mr. E. Royce. The X-12 frequency is locked to a wavemeter adjusted so that the beat frequency from the mixer is 30 Mc/s. The frequency stabilizing circuits were designed by Mr. S. Prévot. The klystrons are frequency-modulated slightly at 26 kc/s or 455 kc/s. If the mean frequency drifts slightly off the frequency of maximum absorption in the cavity, the microwaves will be amplitude-modulated at the modulation frequency. A phase-discriminating network then gives a negative feedback to the klystron repeller, returning the mean frequency to the maximum cavity absorption.

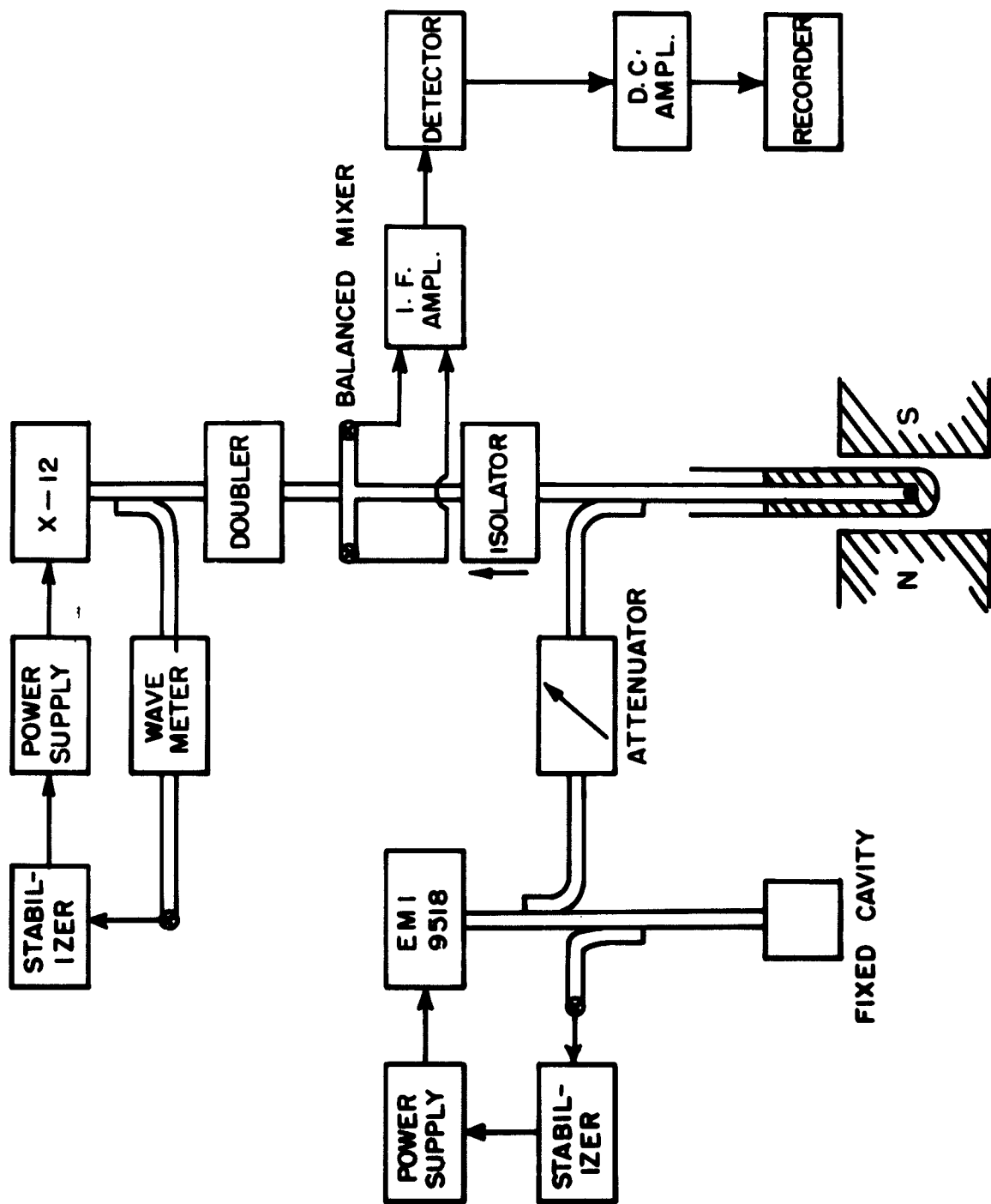


Fig. 1 Block Diagram of Waveguide Spectrometer.

A 30 db ferrite isolator is necessary to prevent local oscillator power from reaching the sample. The waveguide going into the cryostat is the somewhat oversized K dimension; a tapered transition connects this with the rest of the system in Ka-band.

The low temperature system is shown schematically in Fig. 2. The ^4He -bath can be pumped down to about 1.25°K with the big rotary pump, P_4 ; the oil diffusion pump, P_3 , could take it somewhat lower in temperature, but has seldom been used. The bath temperature can be found from its vapor pressure measured in the mercury and oil manometers M_3 . The Cartesian manostat CM can stabilize the ^4He pressure at any level above a few mm Hg, and this will keep the temperature constant to within 0.01°K .³¹

The vapor pressure of ^3He is considerably higher than that of ^4He at the same temperature. Also, ^3He is not a superfluid with film flow so heat leaks can be kept low. It is, therefore, relatively easy to pump a ^3He bath down to about $1\mu\text{mHg}$ pressure which corresponds to 0.3°K .

A ^3He cryostat similar to this one has been described by Seidel and Keesom.³² The expensive ^3He gas is normally kept in the storage containers V_1 , V_2 , and V_3 . When the gas is let into the thin-walled stainless steel tube T going through the ^4He bath at 1.25°K , it condenses and drips down into a little container which is inside an evacuated brass can that also encloses the sample S sitting in the

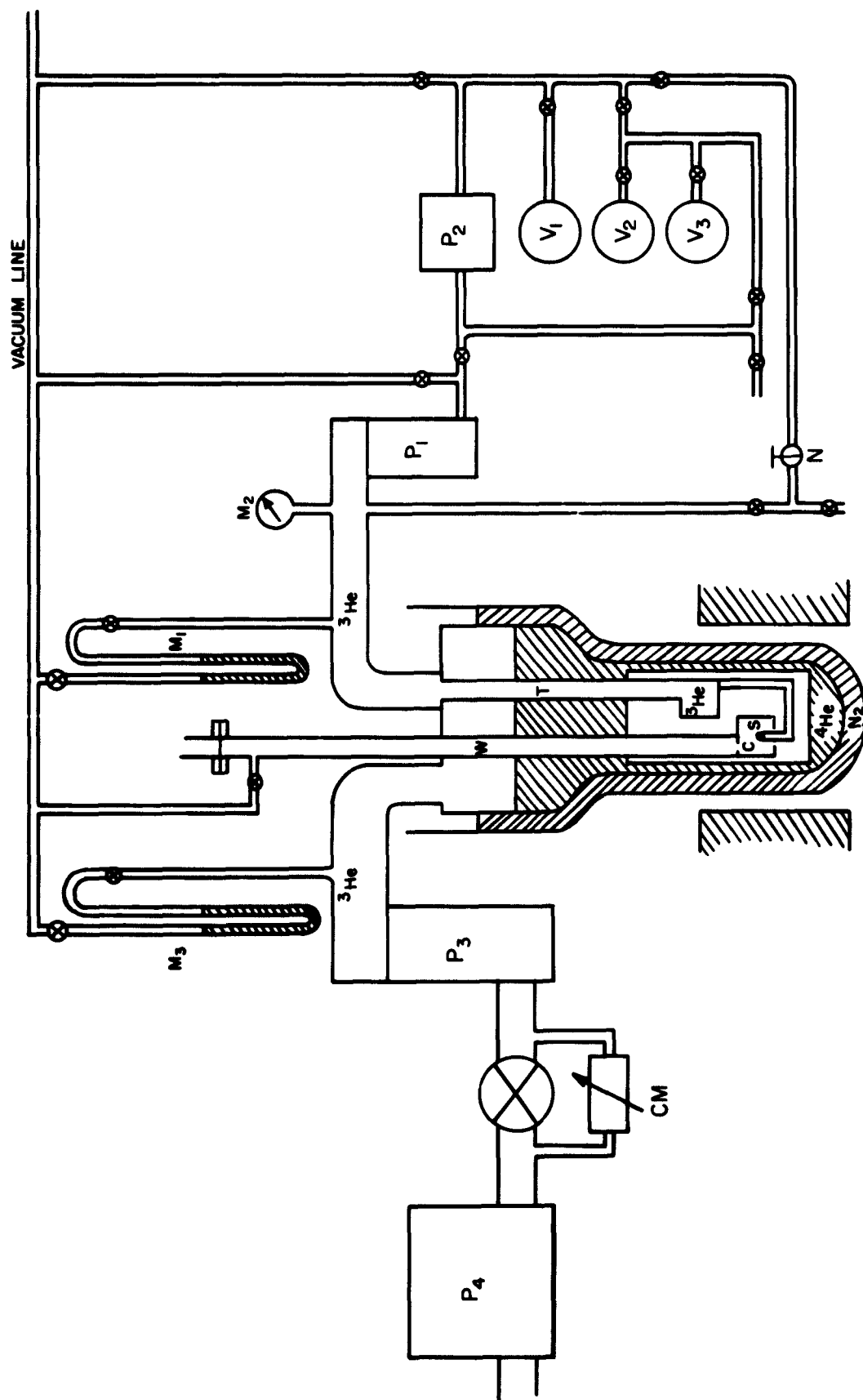


Fig. 2 Schematic Drawing of ^3He Cryostat.

microwave waveguide W or cavity C . From here the ^3He can be pumped back to storage with the oil diffusion pump P_1 and the vacuum-sealed rotary pump P_2 (Welch 1400 B), and in the process, the sample is cooled. The heat leak together with the pumping speed determines the equilibrium temperature of the ^3He -bath which can be measured from the gas pressure with the oil manometer and McLeod gauge M_1 . The effective pumping speed can be reduced by a controlled leak back through the needle valve N and the heat input can be increased by dissipation in an attached electric heater element. M_2 are thermocouple and ionization gauges that are used for checking the vacuum of the ^3He system between operations.

Seidel and Keesom measured a heat removal rate from their cryostat by ^3He evaporation of about 50 erg/s at $T = 0.3^\circ\text{K}$ and about 1000 erg/s at $T = 0.5^\circ\text{K}$. We are using about the same geometry and pump sizes, and this cooling capacity should be sufficient, since for sample saturation and heat contact reasons we will have to limit the microwave dissipation in the sample to less than 10 erg/sec. In practice, about 1 cm^3 of condensed ^3He will last for several hours before it is pumped away if the heat leak is kept small.

Figure 3 shows the means for heat contact between sample and ^3He bath. The sample S is glued onto a quartz post inside a quartz tube going through a hole in the cavity (or waveguide) bottom. The quartz tube is sealed to a platinum tube which again is soldered to a copper tube going to the wall of the ^3He container. This tube system

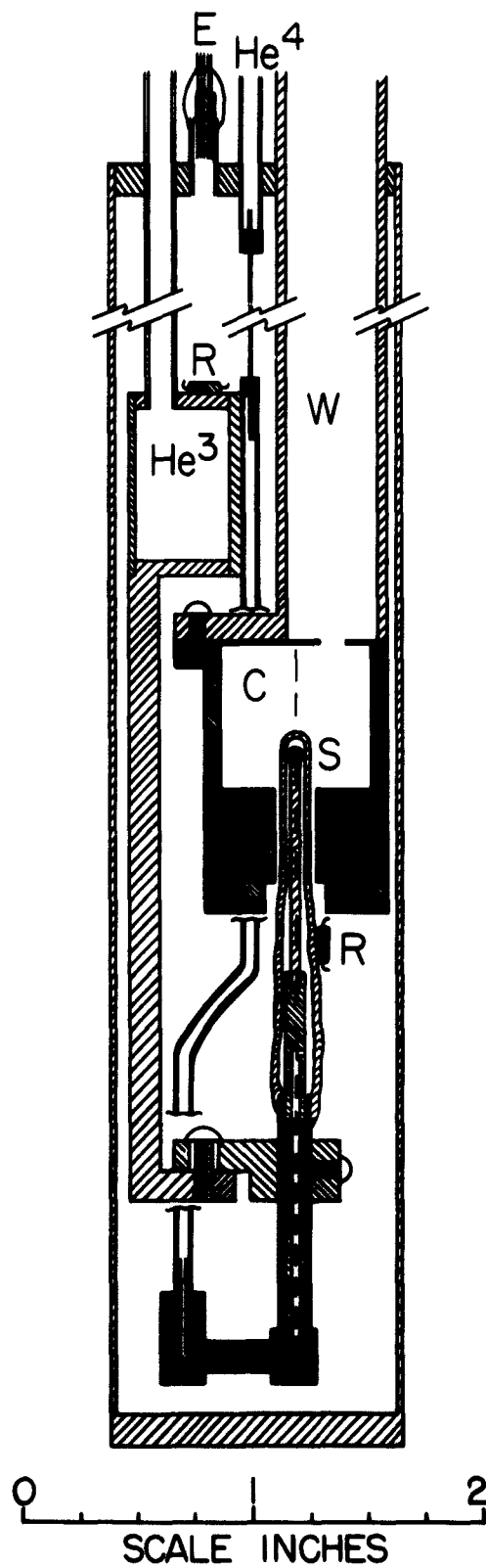


Fig. 3 Detail Showing Sample Mounted Inside Microwave Cavity and in Heat Contact with ^3He Reservoir.

can be filled with ^4He gas through a stainless steel capillary about 10 cm long, with 0.003" inside diameter. The ^4He will condense on the tube walls, form a superfluid film that flows to the sample and evaporates there to flow as gas carrying latent heat back to the wall of the ^3He bath where it will recondense. The efficiency of this heat contact will be estimated in Section 2.3 .

It should be noted that the waveguide and cavity are not cooled by ^3He , but remain at 1.25°K . This requires care in centering the quartz tube in the hole so that it does not touch the walls. The hole diameter d should be small enough to prevent any microwave power from coupling out. The size of the quartz tube and the necessary clearance forced us to use $d = 0.43\text{ cm}$. This hole, when empty, will not propagate waves of frequency 30 kMc/s , but it is not certain that the frequency is below cut-off when the tube is partly filled with quartz of dielectric constant 3.8 . For frequencies below cut-off, the microwave fields extend exponentially into the hole, and the hole should, therefore, be reasonably long to prevent coupling out.

The temperature was measured by the resistance of two standard $10\ \Omega$, $1/10\text{ W}$ resistors R calibrated against ^3He vapor pressure. One was glued onto the ^3He can and one was attached to the quartz tube as close as possible to the cavity hole. When the microwave power was kept sufficiently small, we saw no temperature difference between the two thermometers. From the discussion in Section 2.3 , it will appear that the most likely bottleneck for heat

transfer from the sample is the ^4He gas flow in the tube. If the two resistors read the same during measurements, it is then reasonable to believe that the sample is not significantly heated.

In Fig. 3 the seal E is for electrical leads to thermometers and heater. The waveguide also serves as a pumping tube for evacuation of the brass can, and it is vacuum-sealed on top with a seal of mica on O-ring. A piece of polyfoam in the waveguide prevents room temperature radiation from coming down and heating the quartz and sample.

The samples were grown from water solutions at room temperature. Some of the crystals could fairly easily be ground into spheres by blowing them around in a cylinder lined with emery paper. However, crystals like $\text{NiSiF}_6 \cdot 6\text{H}_2\text{O}$ that would easily split along the axial direction usually turned into ellipsoids, and in others like $\text{CuK}_2\text{Cl}_4 \cdot 2\text{H}_2\text{O}$, the crystal lattice seemed to distort under this treatment. Crystals of the latter type could be made into approximate spheres by carefully dissolving away corners with wet filter paper. The sample size needed in a waveguide was about 1 mm^2 , in a cavity 100 times less, and such small sizes of soft crystal were rather hard to handle. The samples were x-ray oriented and glued on the quartz rod with GE 1202 varnish or Shell Epon 828 epoxy. The crystal orientation in the horizontal plane could be checked by rotating the magnet and adjusting its angle for observation of extremal g-value or narrowest or broadest resonance line as required by the particular salt.

It is believed that crystal orientation usually was better than $\pm 2^\circ$.

2.2. Discussion of possible microwave saturation.

The spectrometer must operate at a low enough microwave level so that the spin system is kept essentially at the temperature of the ^3He bath. This will be most critical at the lowest temperatures where the spin-lattice relaxation time is long and the heat contact between crystal lattice and bath is poor. For the design of the spectrometer, it is helpful to estimate the order of magnitude of the heat transfer bottlenecks to see what the permissible microwave power levels are and whether a superheterodyne detection method is necessary.

To avoid spin saturation, we require¹²

$$\gamma^2 T_1 T_2 H_1^2 < 1, \quad (2-2)$$

where $\gamma = g\beta/\hbar$ = gyromagnetic ratio ,

T_1 = spin-lattice relaxation time,

T_2 = spin-spin relaxation time,

H_1 = amplitude of circularly polarized microwave magnetic field at the sample .

T_2 is related to the width of the line by

$$T_2 = \frac{1}{2} [f(\nu)_{\text{max}} / \int_0^\infty f(\nu) d\nu] \quad (2-3)$$

For a Lorentzian lineshape, $2T_2$ equals the width between half-power points.

The microwave field amplitude H_1 for a given input power will now be calculated and compared in the cases of cavity spectrometer and nonresonant waveguide spectrometer.

a) We used a cylindrical cavity having the dimensions: radius $a = 8.25$ mm, length $z_0 = 14.8$ mm. It was operated in the TE_{012} mode, and the sample was sitting on the vertical axis, one-quarter wavelength from the bottom. The field distribution in the cavity in terms of the microwave field H_s at the sample is ³³

$$H_z = H_s J_0(u' \frac{r}{a}) \cos \beta' z \quad (2-4)$$

$$H_r = H_s \frac{\beta' a}{u'} J_1(u' \frac{r}{a}) \sin \beta' z, \quad (2-5)$$

where $u' = 3.832$ = first zero-point argument of Bessel function

$$J_1(r)$$

$$\beta' = [(\frac{\omega}{c})^2 - (\frac{u'}{a})^2]^{\frac{1}{2}}$$

c = speed of light

ω = $2\pi \cdot 30$ kMc/s.

The energy content of the cavity is

$$U = \frac{1}{8\pi} \int H^2 dv$$

$$\begin{aligned}
&= H_s^2 z_0 \frac{a^2}{2} \left[1 + \left(\frac{\beta a}{u} \right)^2 \right] (J_0(u'))^2 \\
&= 18.6 \cdot 10^{-3} H_s^2 \text{ erg} \quad . \quad (2-6)
\end{aligned}$$

The Q of the cavity was never accurately measured, but in order of magnitude it was about 10,000 at helium temperatures.

The wall losses in terms of the microwave field at the sample would then be

$$W_e = \frac{\omega U}{Q} = 3.5 \cdot 10^5 H_s^2 \text{ erg/s} \quad . \quad (2-7)$$

For a critically coupled cavity, the wall losses would equal the input power W_i . In this case ,

$$H_s = \left(\frac{W_i}{3.5 \cdot 10^5} \right)^{\frac{1}{2}} \text{ gauss} \quad . \quad (2-8)$$

To avoid saturation, we demand that

$$\gamma^2 T_1 T_2 H_s^2 = \frac{g^2 \beta^2}{\hbar^2} T_1 T_2 \left(\frac{H_s}{2} \right)^2 \leq 0.1 \quad , \quad (2-9)$$

where the factor 2 under H_s comes in because the H_s is linearly polarized. Substituting for H_s from (2-8), we then find the maximum input power as

$$W_i \leq \frac{1.4 \cdot 10^5 \hbar^2}{g^2 \beta^2 T_1 T_2} \text{ erg/s} \quad . \quad (2-10)$$

For the reasonable values $T_1 \approx 10^{-1}$ sec , $T_2 \approx 10^{-8}$ sec ,
 $g \approx 2$, this becomes

$$W_i \leq 0.45 \text{ erg/s} \approx 0.05 \mu\text{W} . \quad (2-11)$$

b) The power flow in the dominant mode of a waveguide in terms of the maximum transverse magnetic field is³⁴

$$\begin{aligned} W_i &= \frac{c}{4\pi} \int \frac{\text{Re}}{2} [\vec{E} \times \vec{H}^*] \cdot d\vec{s} \\ &= \frac{c H_{si}^2 a_0 b_0}{16\pi [1 - (\frac{\lambda}{2a})^2]^{1/2}} . \end{aligned} \quad (2-12)$$

For a standard K-band waveguide, the dimensions are :

$a_0 = 1.07$ cm , $b_0 = 0.432$ cm . If the sample is sitting in the maximum field on a perfectly reflecting waveguide short, we have $H_s = 2H_{si}$. In this case the saturation condition (2-9) becomes

$$\begin{aligned} W_i &\leq \frac{1}{10} \cdot \frac{a_0 b_0 c \hbar^2}{16\pi [1 - (\lambda/2a)^2]^{1/2} T_1 T_2 g^2 \beta^2} \\ &\approx 100 \text{ erg/s} = 10 \mu\text{W} \end{aligned} \quad (2-13)$$

when we again use $T_1 \approx 10^{-1}$ sec , $T_2 \approx 10^{-8}$ sec , $g \approx 2$.

The sensitivity of a spectrometer is proportional to the square of the field amplitude H_1 at the sample. Here we have estimated the cavity spectrometer to be about 200 times more sensitive than the

waveguide spectrometer. This is in fair agreement with our experience that the sample for the waveguide would have to be about 100 times bigger than the sample for the cavity, and it does not necessarily contradict our assumption of a cavity $Q \approx 10,000$, since the field configurations in the two spectrometers are completely different.

It is doubtful from this order of magnitude calculation whether a cavity spectrometer can be safely used with only simple crystal detection. The signal-to-noise ratio from the detector will probably be too poor if the microwave power level has to be kept below $0.1 \mu W$. But straight detection should be possible without danger of saturation if a waveguide spectrometer is used with its smaller microwave field. This, however, means that we have to use a bigger sample, more power is dissipated in it, and lattice-bath thermal bottlenecks may become important. This will be discussed in the next section.

2.3. Discussion of heat contact between sample and ^3He system.

We would like to choose the sample size so that about 10 % of the incident microwave power is absorbed at resonance. According to our guess in the last section, this absorbed power may perhaps amount to $1 \mu W$ before we start saturating the transition in the waveguide spectrometer case. Now we want to calculate whether we can safely dissipate this power without heating the sample. We should then be forewarned that even rough order of magnitude calculations may be misleading since heat transfer below $1^\circ K$ is complicated by little-known material constants and surface effects. Also, the tube connecting

the sample and the ^3He reservoir has a complicated geometry, and to simplify the calculation we have to assume that this is equivalent to the same length of uniform tubing.

We may visualize the heat transfer as being divided in these separate processes :

- a) Heat conduction from the interior of the sample to the surface.
- b) Heat resistance on the surface of the sample due to phonon mismatch.
- c) Evaporation of the ^4He film on sample, which has to be replenished by film flow.
- d) Flow of the gas containing the heat of vaporization through a narrow tube that offers resistance back to the wall of the ^3He reservoir for recondensation. Where the tube has thick copper walls, heat conduction in the copper may reduce the necessary gas flow considerably.

It will turn out from the following estimates that effect d) is the bottleneck that prevents us from reaching really low temperatures during measurements.

- a) Since we expect the resonating spins to give up energy in quanta of $h\nu^*$, we might look for the energy carrying properties of a band of "hot phonons" around ν^* which would take the dissipated energy to the sample surface. However, there are conflicting opinions about the reality of such "hot phonons" in most cases of spin

relaxation.³⁵ It appears likely that the Zeeman energy is mostly transferred to phonons of higher frequency via impurities, spins at irregular lattice points and strongly exchange-coupled pairs. Presumably, the phonon spectrum comes rapidly into thermal equilibrium in most relaxation experiments at liquid ^4He temperatures, and the energy transfer through the lattice can then probably be treated as simple heat conduction. We will here assume that this is valid even for temperatures below 0.5°K where the phonon mean free path is of the same order as the sample dimensions.

Casimir³⁶ has derived a formula for the heat conductivity K in pure crystals when only surface scattering of phonons is important. Measured values of conductivities are few in this temperature range, but they are generally somewhat smaller than predicted by Casimir's theory. At $T = 0.3^\circ\text{K}$ Garrett³⁷ found $K = 10^4 \text{ erg sec}^{-1} \text{ cm}^{-1} \text{ deg}^{-1}$ for $\text{K Cr (SO}_4)_2 \cdot 12\text{H}_2\text{O}$, which corresponds to a temperature-independent phonon mean free path of 0.5 mm . We will assume that the heat conductivity is approximately the same for our samples of hydrated crystals. A uniform heat dissipation of $P \approx 10/(\frac{4}{3}\pi a^3) \text{ erg sec}^{-1} \text{ cm}^{-3}$ in a sphere of radius a will, in the stable state, give a temperature difference between the center and the surface of³⁸

$$\Delta T = Pa^2/6K \approx 0.0005^\circ \text{ for } a = 0.075 \text{ cm}^{-1}. \quad (2-14)$$

This is insignificant, and unless this estimate for the heat conductivity is too small by more than an order of magnitude, heat trapping inside the sample does not seem to be important.

b) Phonon mismatch at the boundary between crystal and ^4He film will appear as a thermal resistance.^{39,40} The mismatch will depend on the vibration spectra of the two media, but the resistance even between polished copper and bulk ^4He does not agree too well with the existing theories. In our case we have additional complications : First, the sample surface is rather rough from grinding, and part of it is covered with glue of unknown properties. Second, the film thickness is of the order of the wavelength of the excited phonons at this temperature. The phonon spectrum is, therefore, likely to be changed relative to that of bulk liquid.

Instead of relying on the theory, we may then as well use the heat transfer rate between copper and bulk liquid ^4He as measured by Fairbanks and Wilks⁴¹ in the range 0.3 to 1°K

$$\frac{\Delta T}{W} = \frac{45}{T^2} \text{ cm}^2 \text{ deg/watt} \quad (2-15)$$

For $W = 10^{-6}$ watt, $T \approx 0.4^\circ\text{K}$ and a sample surface of $\approx 4\pi a^2$ where $a = 0.075$ cm, we get

$$\Delta T \approx 0.004^\circ\text{K}$$

The boundary resistance seems to be unimportant.

c) The critical flow in a saturated ^4He film is proportional to the perimeter of the narrowest constriction of the flow. At $T \approx 0.5^\circ\text{K}$ the liquid flow rate is about $10^{-4} \text{ cm}^3/(\text{sec cm})$.⁴² The specific weight of ^4He is 0.1455 g/cm^3 and its molecular weight 4 ; so with a

smallest diameter taken to be ≈ 0.05 cm , the maximum flow rate should be

$$F \approx 3.14 \cdot 10^{-5} \text{ cm}^3/\text{sec} = 1.15 \cdot 10^{-6} \text{ mole/sec.}$$

The heat of vaporization of ^4He is about 70 joules/mole at $T \approx 0.5^\circ\text{K}$.⁴³ Therefore, to carry away an energy of $1 \mu\text{W}$ a flow of $0.14 \cdot 10^{-7}$ mole/sec is needed, and the film flow should easily take care of this.

d) The saturation pressure of ^4He is given by⁴⁴

$$\log_{10} P_{\text{mm Hg}} = 2.19260 - \frac{3.10710}{T_{\text{oK}}} + \frac{5}{2} \log_{10} T_{\text{oK}} \quad (2-16)$$

Other terms appearing in more accurate expressions for $p(T)$ are negligibly small below 1°K . In this empirically-fitted, theoretical equation, p and T have to be taken as dimensionless quantities in the units indicated.

The mode of flow of the evaporated gas back to the cold reservoir will depend upon whether the mean free path of the ^4He atoms in the vapor is smaller or larger than the diameter of the tube. However, it is here hardly appropriate to speak of a mean free path as an analog to the classical case of hard, elastic spheres colliding with each other. For helium molecule collisions at low temperature wave mechanical resonance effects appear and the cross-sections vary widely with the energies of the colliding particles. To see the order of magnitude of the mean free path, we may then as well use the following

equation given by Keesom,⁴⁵ although the empirical formula for the viscosity used in deriving it is not very good below 3°K .

$$\ell = 2.159 \cdot 10^{-5} \frac{T^{1.147}}{P_{\text{mm Hg}}} \text{ cm} . \quad (2-17)$$

For $T = 0.5^{\circ}$ we find from (2-16) , $p = 16 \cdot 10^{-6}$ mmHg, and the mean free path is approximately

$$\ell_{0.5^{\circ} \text{ K}} = 0.6 \text{ cm} .$$

The vapor pressure is varying very rapidly, and at $T = 0.4^{\circ}$ K and $T = 0.6^{\circ}$ K we find

$$\ell_{0.4^{\circ} \text{ K}} = 30 \text{ cm} \quad \ell_{0.6^{\circ} \text{ K}} = 0.04 \text{ cm} .$$

We see that below $T \approx 0.5^{\circ}$ K the gas flow has to be treated as free molecular diffusion or Knudsen flow. The formula for the flow through a tube of radius a and length L under a pressure of $\Delta p = (p_1 - p_2)$ is⁴⁶

$$F_{\text{free mol}} = \frac{2a^3}{3L} \left(\frac{8\pi}{RMT} \right)^{1/2} \Delta p \text{ mole/sec} \quad (2-18)$$

where

$R = 8.317 \cdot 10^7$ ergs/(deg mole) = gas constant

$M = 4$ g/mole for ^4He .

Equation (2-18) is derived under the condition that the molecules are re-emitted in completely random directions after each collision with the film-covered tube wall. If the molecules were reflected

from the film, keeping part of their forward momentum, the gas flow could be considerably larger. In view of the molecule-molecule collision anomalies in the ^4He at this very low temperature, it might perhaps be interesting to try to check experimentally by heat conduction in narrow tubes whether molecule-film collisions are specular reflections or essentially condensations and re-evaporations.

From (2-16)

$$\begin{aligned} p &= \frac{10^{2.19260} T^{5/2}}{10^{3.107/T}} \text{ mm Hg} \\ &= \frac{2.06 \cdot 10^5 T^{5/2}}{10^{3.107/T}} \text{ dyn/cm}^2 \end{aligned} \quad (2-19)$$

By differentiating

$$\Delta p = 2.06 \cdot 10^5 \frac{T^{1/2} \left(\frac{5}{2} T + 3.107 \ln 10 \right) \Delta T}{10^{3.107/T}} \text{ dyn/cm}^2 \quad (2-20)$$

Combining (2-20) with (2-18) and multiplying with the heat of vaporization $C_e = 70$ joule/mole, we get the flow of latent heat :

$$\dot{Q}_{\text{free mol}} = F C_e = \frac{0.265 \cdot 10^4 a^3 \left(\frac{5}{2} T + 7.17 \right) \Delta T}{L 10^{3.107/T}} \text{ watt} \quad (2-21)$$

The total length of the tube connecting the sample to the cold wall of the ^3He can is about 10 cm . Most of it is made of copper. The heat conductivity of the copper walls will vary greatly with metal purity, heat treatment, and machining, and soldered joints will reduce

it. However, by extrapolating from the data summarized by White,⁴⁷ we may take the copper heat conductivity to be of the order $0.1 \text{ W cm}^{-1} \text{ deg}^{-1}$ at 0.5°K . A tube $\approx 8 \text{ cm}$ long and with $\approx 10 \text{ mm}^2$ average wall cross section will then conduct about 10^{-5} watt for a temperature difference of 0.01° between ends. We can, therefore, assume that the gas has to flow only through the quartz tube to the beginning of the copper tube. In (2-21) we, therefore, take $L \approx 2.5 \text{ cm}$, $a \approx 0.1 \text{ cm}$, and if we specify that the temperature difference ΔT is to be kept below 0.01° , the permissible heat input is

$$\begin{array}{ccccccc} T & = & 0.30 & 0.40 & 0.50 & (0.60)^\circ\text{K} \\ \dot{Q}_{\text{free mol}} \leq & 0.35 \cdot 10^{-11} & 1.5 \cdot 10^{-9} & 5.5 \cdot 10^{-8} & (6.0 \cdot 10^{-7}) \text{ watt} . \end{array}$$

At the temperatures above 0.5°K it is more correct to treat the flow of gas as viscous or Poiseuille flow. The formula for this is⁴⁸

$$F_{\text{visc}} = \frac{\pi a^4 p \Delta p}{8 \eta R T L} + \frac{3\pi}{16} F_{\text{free mol}} \quad (2-22)$$

The last term in this formula is a theoretical correction term for "slip" along the tube walls. η is the viscosity coefficient which we take for ^4He gas around 0.6°K as $\eta \approx 3 \cdot 10^{-6}$ poise.⁴⁹ Plugging (2-19) and (2-20) into (2-22) and using the previous values of a , L , and C_e , we get for the flow of latent heat in this case :

$$\dot{Q}_{\text{visc}} = F_{\text{visc}} \cdot C_e$$

$$= \left[\frac{18.6 \cdot 10^4 T^2 \left(\frac{5}{2} T + 7.17 \right) \Delta T}{10^{6.214/T}} + \frac{0.63 \left(\frac{5}{2} T + 7.17 \right) \Delta T}{10^{3.107/T}} \right] \text{ watt. (2-23)}$$

If we again specify $\Delta T \leq 0.01^\circ$, we get the values

T	=	0.6	0.7	0.8	0.9	1.0°K
$\dot{Q}_{\text{visc}} \leq$		$6.3 \cdot 10^{-7}$	$1.3 \cdot 10^{-5}$	$1.8 \cdot 10^{-4}$	$1.7 \cdot 10^{-3}$	$1.1 \cdot 10^{-2}$ watt

It should again be stressed that the calculated numbers represent at best only the order of magnitude heat flow in the actual case, since we can only guess the magnitude of the material constants involved, and perhaps the formulas used are not even approximately valid. But in spite of these uncertainties, it seems clear that the gas flow presents the most serious bottleneck to the heat transfer from the sample, and that a dissipation of 10^{-6} W may appreciably heat up the sample below about 0.6°K . Only with a heat input of about 10^{-9} watt or less can we hope to take measurements at 0.4°K , and this certainly requires a superheterodyne system.

2.4. Heat leak through capillary.

The ^4He film used to cool the sample is supplied through a thin-walled, stainless steel capillary. Flow of gas, film and perhaps bulk liquid ^4He through this capillary will represent a heat leak from the ^4He bath at approximately 1.25°K to the ^3He system. We can reduce this heat leak by pumping the gas away from the warm end of

the capillary. When the warm end is not pumped, we estimate the heat leak to be about 10^{-4} watt from the observed rate of ^3He evaporation, and we get only down to about 0.5°K in temperature.

The capillary is about 10 cm long and has an internal diameter of 0.003 " ($a = 3.8 \cdot 10^{-3}$ cm). If we apply equations (2-18) and (2-22) to the problem of heat conduction in this capillary, we find that the temperature gradient is concentrated very close to the cold end which is kept at the ^3He temperature. The heat leak from film and gas flow calculated this way is of order 10^{-6} watt when the warm end is not pumped. This may seem surprisingly large compared to the rather poor heat contact we calculated for the sample. It is a result of the good heat conduction in the larger part of the capillary which has almost the temperature of the ^4He bath. However, it does not explain the observed heat leak which is larger by two orders of magnitude.

We must then assume that the capillary and the sample tube will get filled with liquid ^4He if we do not pump the gas away after condensation. The flow of heat in ^4He -filled capillaries can be considerable, but it is a nonlinear function of the temperature gradient,⁵⁰ and no estimate of such a heat leak will be attempted. We should note, however, that if the sample tube is filled with liquid helium, there should be no problem with heat conduction away from the sample.

If we pump on the warm end of the capillary, we may be able to bring the gas pressure down to the saturation pressure of ^4He at

$T \approx 0.8^\circ \text{K}$. In this case, the heat leak will be given by the gas flow formula (2-18) which we now write

$$\dot{Q} = \frac{0.265 \cdot 10^4 a^3 \left(\frac{5}{2} T + 7.17\right) dT}{10^{3.107/T} dL} \approx \frac{12.4 \cdot 10^{-4} dT}{10^{3.107/T} dL} \quad (2-24)$$

where we have used $\left(\frac{5}{2} T + 7.17\right) \approx 8.5$.

We take the cold end of the capillary to be at $\approx 0.4^\circ \text{K}$ and integrate along the tube

$$\int_0^L \dot{Q} dL = 12.4 \cdot 10^{-4} \int_{0.4}^{0.8} \frac{dT}{10^{3.107/T}} \quad (2-25)$$

The integral on the right side cannot easily be solved. But since the overwhelming temperature dependence is in the exponent, we multiply under the integral by $0.6^2/T^2 \approx 1$. Then we get approximately

$$\begin{aligned} \dot{Q}L &\approx 12.4 \cdot 10^{-4} \cdot 0.36 \int_{0.4}^{0.8} \frac{10^{-3.107/T}}{3.107 \ln 10} \\ &= 0.8 \cdot 10^{-8} \end{aligned} \quad (2-26)$$

For $L = 10 \text{ cm}$ we, therefore, calculate the approximate heat leak when the gas is pumped away

$$\dot{Q} \approx 10^{-9} \text{ watt.}$$

Now, helium is removed from the sample tube at the critical rate of film flow in the capillary. The critical flow rate is $\sigma \approx 10^{-4} \text{ cm}^3/(\text{cm sec})$,⁴² and for the capillary, this corresponds to

$$F = \sigma \cdot 2\pi a = 8.6 \cdot 10^{-3} \text{ cm}^3/\text{hour} .$$

Filling the sample tube goes somewhat faster, since it is done by gravity flow of bulk helium. Once the tube is filled, we should be able to work for a few hours before re-filling, and this is also our practical experience.

2.5. Discussion of spectrometer linearity and large-signal corrections.

As shown in Section 2.1, we require that the spectrometer have a fairly large dynamic range where the output preferably is a linear function of the imaginary part of the susceptibility χ'' , or is at least a known function of χ'' . The large-signal behavior of a cavity and waveguide spectrometer will now be discussed.

First, we note that it does not matter for the linearity (but certainly for the sensitivity) whether we use direct detection or super-heterodyne amplification followed by a low-level square-law detector. In both cases the final recording will be proportional to the microwave power of the detector. The linearity of the detecting system can be simply checked by inserting and varying a precision attenuator, which has been done.

Secondly, any attempt to correct for large-signal nonlinearity resulting from too large a sample will be very unreliable because we

then violate the requirement that the presence of the sample be only a small perturbation on the microwave field. A big field perturbation will have the following effects :

- a) The absorption in the sample is proportional to $\chi'' H_1^2$ where H_1 is the microwave field at the sample. For a large perturbation, the average H_1 may change.
- b) With a different field distribution the wall losses may change.
- c) If the sample in a cavity perturbs the field at the coupling iris, the cavity coupling may change.

It is very hard to estimate the importance of the effects a) - c) in a given experiment. If for part of the measurements large signals cannot be avoided, the following formulas for the response of the spectrometer should only be taken as an indication of how the output is likely to change.

A. Cavity spectrometer.

The magnetic resonance is accompanied by dispersion which will change the frequency of the loaded cavity. But when the klystron frequency is coupled to the cavity, this will have no first-order effect.

The power absorbed in the sample is ⁵¹

$$P_s = \frac{1}{2} \omega \chi'' \int_{V_s} H_1^2 dV \quad (2-27)$$

where $\omega/2\pi$ is the frequency and V_s is the volume of the sample.

The Q factor of the cavity is defined as

$$Q_1 = \omega \frac{\text{Energy stored}}{\text{Energy lost/sec}}$$

$$= \frac{\frac{1}{8} \pi \int_{V_c} H_1^2 dV}{P_w + P_s} = \frac{1}{1/Q_0 + 4\pi \chi'' \eta} \quad (2-28)$$

where the filling factor η is

$$\eta = \int_{V_s} H_1^2 dV / \int_{V_c} H_1^2 dV \quad (2-29)$$

V_c is the volume of the cavity, P_w is the power lost in the cavity walls, and Q_0 is the corresponding quality factor for the empty cavity.

The coupled losses of the cavity can likewise be described by an external Q factor, and the coupling coefficient is defined by

$$\beta^{-1} = Q_{ex}/Q_1 = Q_{ex} \left(\frac{1}{Q_0} + 4\pi \chi'' \eta \right) \quad (2-30)$$

The power reflected from the cavity for the undercoupled case

$\beta < 1$ is

$$P_r = \frac{P_o (1 - \beta)^2}{(1 + \beta)^2} = P_o \frac{\left(\frac{Q_{ex}}{Q_0} - 1 + 4\pi \chi'' \eta Q_{ex} \right)^2}{\left(\frac{Q_{ex}}{Q_0} + 1 + 4\pi \chi'' \eta Q_{ex} \right)^2}$$

$$\begin{aligned}
= P_o \left\{ \frac{\left(\frac{Q_{ex}}{Q_o} - 1\right)^2}{\left(\frac{Q_{ex}}{Q_o} + 1\right)^2} + 4 \frac{\left(\frac{Q_{ex}}{Q_o} - 1\right)}{\left(\frac{Q_{ex}}{Q_o} + 1\right)^3} 4\pi \eta Q_{ex} \chi'' \right. \\
\left. + \frac{4\left(2 - \frac{Q_{ex}}{Q_o}\right)}{\left(\frac{Q_{ex}}{Q_o} + 1\right)^4} (4\pi \eta Q_{ex} \chi'')^2 + \dots \right\} \quad (2-31)
\end{aligned}$$

where P_o is the incident power.

We see that for linear response we want

$$\frac{\left(\frac{Q_{ex}}{Q_o} - 1\right)}{\left(\frac{Q_{ex}}{Q_o} + 1\right)} \gg 4\pi \chi'' \eta Q_{ex} \frac{\left(2 - \frac{Q_{ex}}{Q_o}\right)}{\left(\frac{Q_{ex}}{Q_o} + 1\right)}, \quad (2-32)$$

and in particular, we must avoid critical coupling $\beta_o = Q_{ex}/Q_o = 1$ for the unloaded cavity. The second-order term is seen to vanish for $\beta_o = Q_o/Q_{ex} = \frac{1}{2}$ which corresponds to an unloaded cavity reflection of $P_r = P_o (1 - \beta_o)^2 / (1 + \beta_o)^2 = \frac{1}{9} P_o$, and we should try to use an iris corresponding to this coupling.

The ratio P_r/P_o can be easily measured on an oscilloscope when the klystron frequency is swept through its mode. Doing this for no magnetic resonance and maximum magnetic resonance, say, we can then calibrate the chart records and find the relative values of χ'' from (2-31). The reflected power according to formula (2-31) is

plotted in Fig. 4 for varying coupling and magnetic absorption.

B. Waveguide spectrometer.

For a crystal mounted close to the bottom of a perfectly-reflecting waveguide short, dispersion is not expected to have any first-order effect on the reflected power.

A wave traveling through an absorbing medium will be attenuated exponentially, and we have

$$P_r = P_o e^{-a\chi''} \quad (2-33)$$

Since the crystal is small compared to the wavelength and is sitting in a node of the magnetic field, it may be more appropriate to use the following formulas :

The field amplitude at the crystal is

$$H_1 \sim \sqrt{P_o} + \sqrt{P_r} \quad (2-34)$$

The absorbed power P_a is

$$P_a = b\chi'' (\sqrt{P_o} + \sqrt{P_r})^2 \quad (2-35)$$

We also have

$$P_r = P_o - P_a \quad (2-36)$$

Solving these equations we get

$$P_r = P_o \left[\frac{2 - b^2 \chi''^2 - b\chi'' \sqrt{4 - 3b^2 \chi''^2}}{2(1 + b\chi'')^2} \right]$$

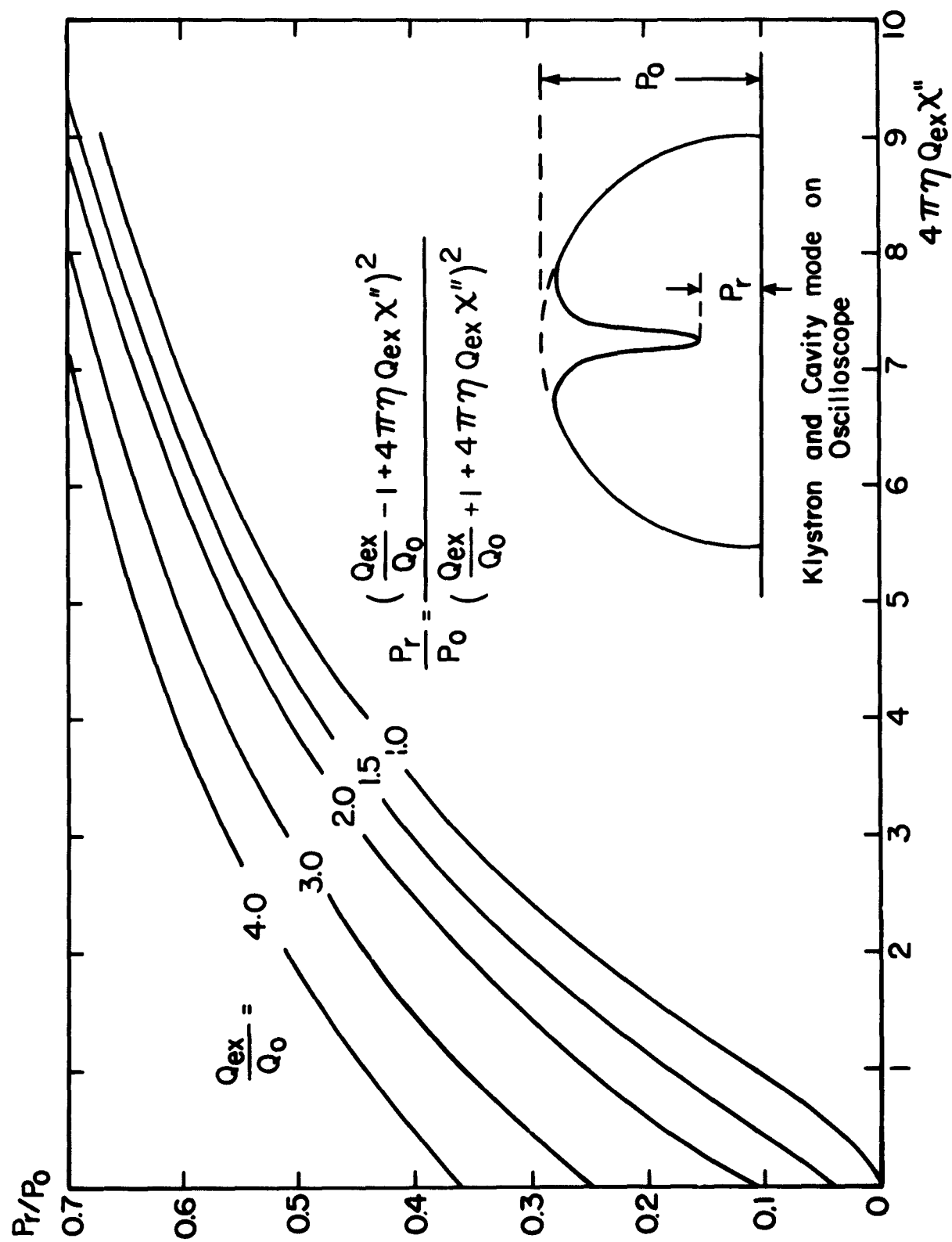


Fig. 4 Reflected Power from Cavity as Function of Absorption in Sample .

$$\approx P_0 \left[1 - 3b\chi'' + \frac{9}{2}b^2\chi''^2 + \frac{45}{8}b^3\chi''^3 + \dots \right]. \quad (2-37)$$

Including terms to second order, this expansion is identical to the expansion of (2-33) with $a = 3b$, and it does not matter much then whether we use correction formula (2-33) or (2-37).

C. Waveguide spectrometer with microwave bucking.

In order to reduce the dc bias on the signal in a waveguide spectrometer and reduce the klystron noise, one sometimes balances or "bucks out" part of the microwave power in a bridge. This may take the form of a T where the sample sits in one of the equivalent arms and the other arm contains an adjustable attenuator and a sliding short. Then we can add a signal of arbitrary phase and amplitude.

Such a system will be very similar to an overcoupled cavity. As for a cavity, the magnetic dispersion in the sample will change the tuning and the klystron frequency should be locked for right balance.

From the same reasoning as in Part B, the output of a balanced system is

$$P_r = P_0 \left(\sqrt{e^{-a\chi''}} + e^{-i\phi} \sqrt{b} \right)^2. \quad (2-38)$$

The balancing signal of relative power b should be added in opposite phase, so that $e^{-i\phi} = -1$. Expanding the exponential in this case, we get

$$P_r = P_0 \left[(1 + b - 2\sqrt{b}) - (1 - \sqrt{b}) a\chi'' + \frac{1}{4}(1 - \sqrt{b}) a^2\chi''^2 + \dots \right]. \quad (2-39)$$

For complete balance when $\chi'' = 0$, we need to have $b = \frac{1}{2}$ and as for a cavity we have then no linear term in χ'' in the response. The second-order term will only vanish when $b = 4$, and this requires some attenuation in the sample arm.

In practice, it is hard to determine the amount of bucking; proper large-signal correction is, therefore, very difficult and should not be attempted.

CHAPTER 3

MEASUREMENTS ON NEODYMIUM ETHYL SULFATE

3.1. Description of neodymium ethyl sulfate.

The rare earths form a series of isomorphic, hexagonal ethyl sulfates, $M(C_2H_5SO_4)_3 \cdot 9H_2O$, and these salts have been widely used in paramagnetic experiments. Ketelaar⁵² determined the structure from x-ray studies, and gave the space group as C_{6h}^2 . The unit cell is shown in Fig 5a, and the two rare earth ions are at the positions $\pm(\frac{1}{3} \frac{2}{3} \frac{1}{4})$. The dimensions of the unit cell vary slightly with the size of the rare earth ion; for $Nd(C_2H_5SO_4)_3 \cdot 9H_2O$ it is $a_0 = 13.992 \text{ \AA}$ and $c_0 = 7.07 \text{ \AA}$. Each Nd^{+++} ion will, therefore, have two nearest Nd neighbors 7.07 \AA away along the hexagonal axis as indicated in the drawing. The other ion in the same cell is 8.85 \AA away in a direction making an angle $\theta = 66.4^\circ$ with the hexagonal axis.

Each Nd^{+++} ion is surrounded by 9 water molecules, and the arrangement is probably as shown in Fig. 5b. The water dipoles, together with some contribution from the more distant surroundings, give an electric field of axial symmetry C_{3h} at the position of the rare earth ion.⁵³ The free ion Nd^{+++} has the ground state $4f^3 4I_{9/2}$; the field will split this into five Kramers' doublets, and the field symmetry is reflected in the axial symmetry of the g-tensors. The first excited doublet is about 130 cm^{-1} above the lowest doublet, and only the latter will be populated at

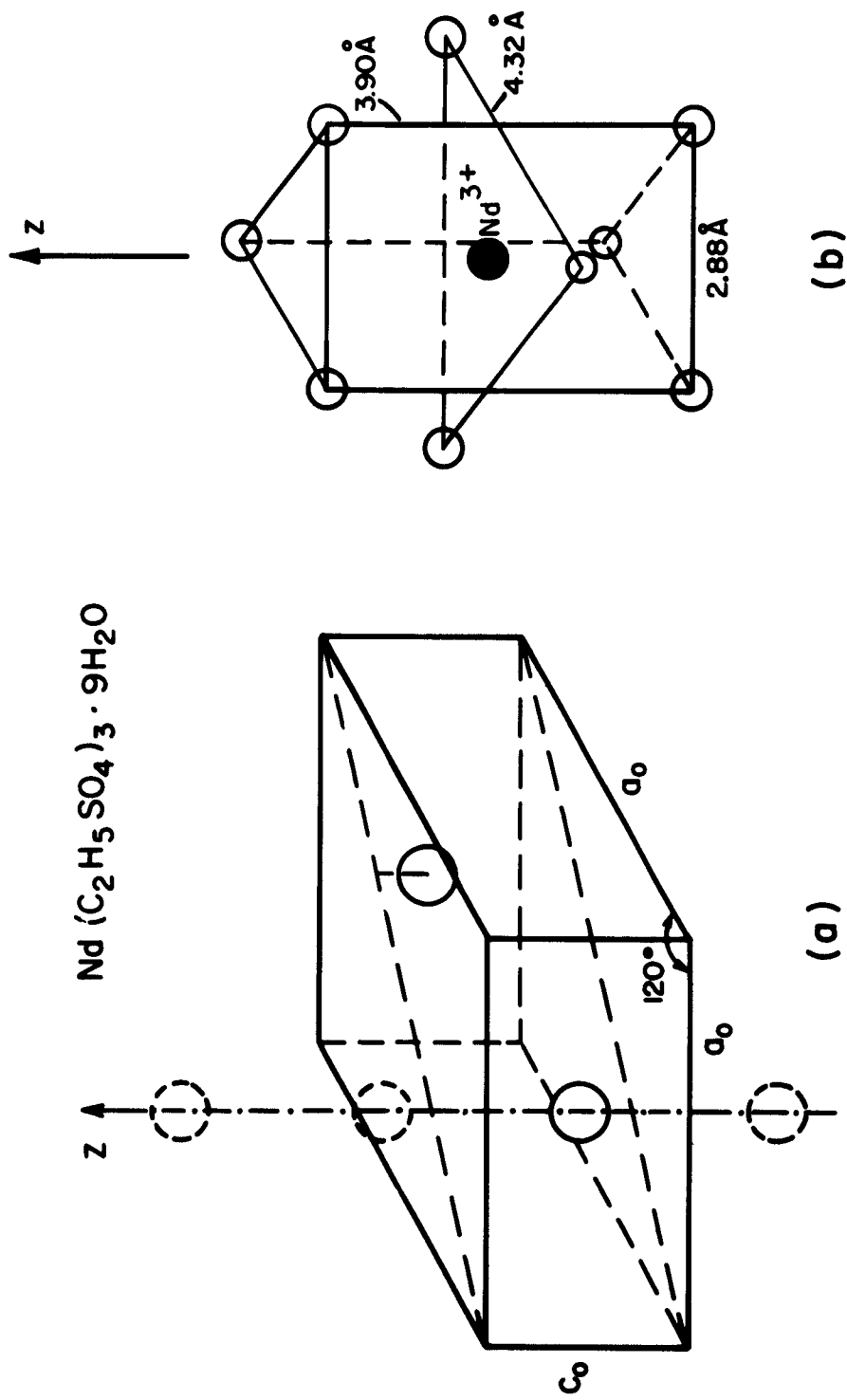


Fig. 5a Unit Cell of $\text{Nd}(\text{C}_2\text{H}_5\text{SO}_4)_3 \cdot 9\text{H}_2\text{O}$ Showing String of Nearest

Neighbors.

Fig. 5b Probable Arrangement of Water Molecules Around the Neodymium

Ion.

liquid helium temperatures. The magnetic behavior is the same for both ions in the unit cell, and it is given by the approximate spin-Hamiltonian for spin $S = \frac{1}{2}$.

$$\begin{aligned} \mathcal{H} = & \beta g_{\parallel} H_z S_z + \beta g_{\perp} (H_x S_x + H_y S_y) + A I_z S_z \\ & + B (S_x I_x + S_y I_y) + P (I_z^2 - 3I(I+1)) . \end{aligned} \quad (3-1)$$

The g -values for neodymium ethyl sulfate measured in salts where the Nd^{+++} have been diluted 1:200 with unmagnetic La^{+++} are⁵⁴

$$g_{\parallel} = 3.535 \pm 0.001 \quad g_{\perp} = 2.072 \pm 0.001$$

The even isotopes of Nd of mass 142, 144, 146, 148, and 150, which have a total natural abundance of 79.5 %, have no nuclear spin and, for these, the three last terms in (3-1) vanish. The isotopes 143 (abundance 12.2 %) and 145 (abundance 8.3 %) both have spin $I = 7/2$ which will give a number of weak hyperfine lines. Their positions, when the field is parallel to the crystal axis, can be given more accurately by⁵⁴

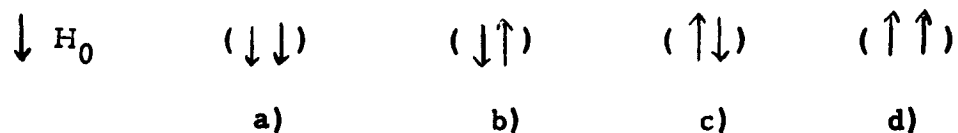
$$\begin{aligned} g_{\parallel} \beta H = & h\nu - A m \left[1 + \frac{B^2}{4(h\nu)^2} \right] - \frac{B^2}{2h\nu} [I(I+1) - m^2] \\ & + \frac{B^2 P}{2(h\nu)^2} [2m^3 - m(2I^2 + 2I - 1)] , \end{aligned} \quad (3-2)$$

where m is the nuclear magnetic quantum number, and the interaction constants are :

Isotope	$10^4 A(\text{cm}^{-1})$	$10^4 B(\text{cm}^{-1})$	$10^4 P(\text{cm}^{-1})$
143	380.3 ± 0.1	198.9 ± 0.5	< 2
145	236.4 ± 0.1	123.7 ± 0.5	< 2

In concentrated salts we expect the spin-Hamiltonian constants to have about the same values as in the diluted salts. We find g_{\parallel} a little larger, however; $g_{\parallel} = 3.60$, and this value will be used in the following calculations. But a new effect also appears here. The main resonance line splits up into three almost separated peaks when measured with the external field along the hexagonal axis. This was first seen and explained on the basis of spin-spin interaction by Bleaney et al.⁵⁵

The dominant interaction in this case is the dipolar field from the two nearest neighbors. Since each spin can be either parallel or anti-parallel to the external field, four arrangements of the nearest neighbors are possible, and this will be indicated by arrows :



At high temperatures, each of these arrangements is equally probable. The static dipolar field in case a) and case d) will shift the line by $\pm 2g_{\parallel}\beta/r^3 = \pm 188$ gauss. Case b) and c) have no effect on line position, and the central peak, therefore, should have twice the intensity of the side peaks ≈ 188 gauss away.

At low temperatures and in high fields that will line up the spins in the lowest state, we expect case a) to become more and case d) to become less probable. Professor Bloembergen suggested that we look at this lineshape as an example of spin alignment.

3.2. Measurements of line areas.

We measured two approximately spherical samples of Nd $(C_2H_5SO_4)_3 \cdot 9H_2O$ in the waveguide spectrometer at 30.00 kMc/s using superheterodyne detection. The crystals were generously given to us by Mr. Rieckhoff, Vancouver.* The magnetic field was along the hexagonal axis, and a typical change in lineshape and intensity is shown in Fig. 6. The strong line appears on the low field side of the unperturbed resonance, since in this geometry the dipolar field will aid the external field. At $T = 0.5^\circ K$ the absorption was rather too strong; about 50 % of the incident power, and the nonlinear response had to be corrected as indicated in Section 2.5.

The probability that any spin is parallel to the field is

$$p_{\downarrow} = 1/(1 + b^{\Delta E}) \quad (3-3)$$

*

We tried, without success, to grow crystals of Nd $(C_2H_5SO_4)_3 \cdot 9H_2O$ at room temperature. The ethyl sulfates are rather unstable, and we got only the monoclinic $Nd_2(SO_4)_3 \cdot 8H_2O$. The spin-Hamiltonian of this salt does not seem to have been published, although the resonance has been investigated at low frequency.⁵⁶ We observed up to 4 separated lines with g-factors varying from 2.9 to 1.2, but we did not seriously attempt to determine the principal axis of the g-tensors. X-ray studies of this crystal indicate $8Nd^{++}$ ions per unit cell.⁵⁷

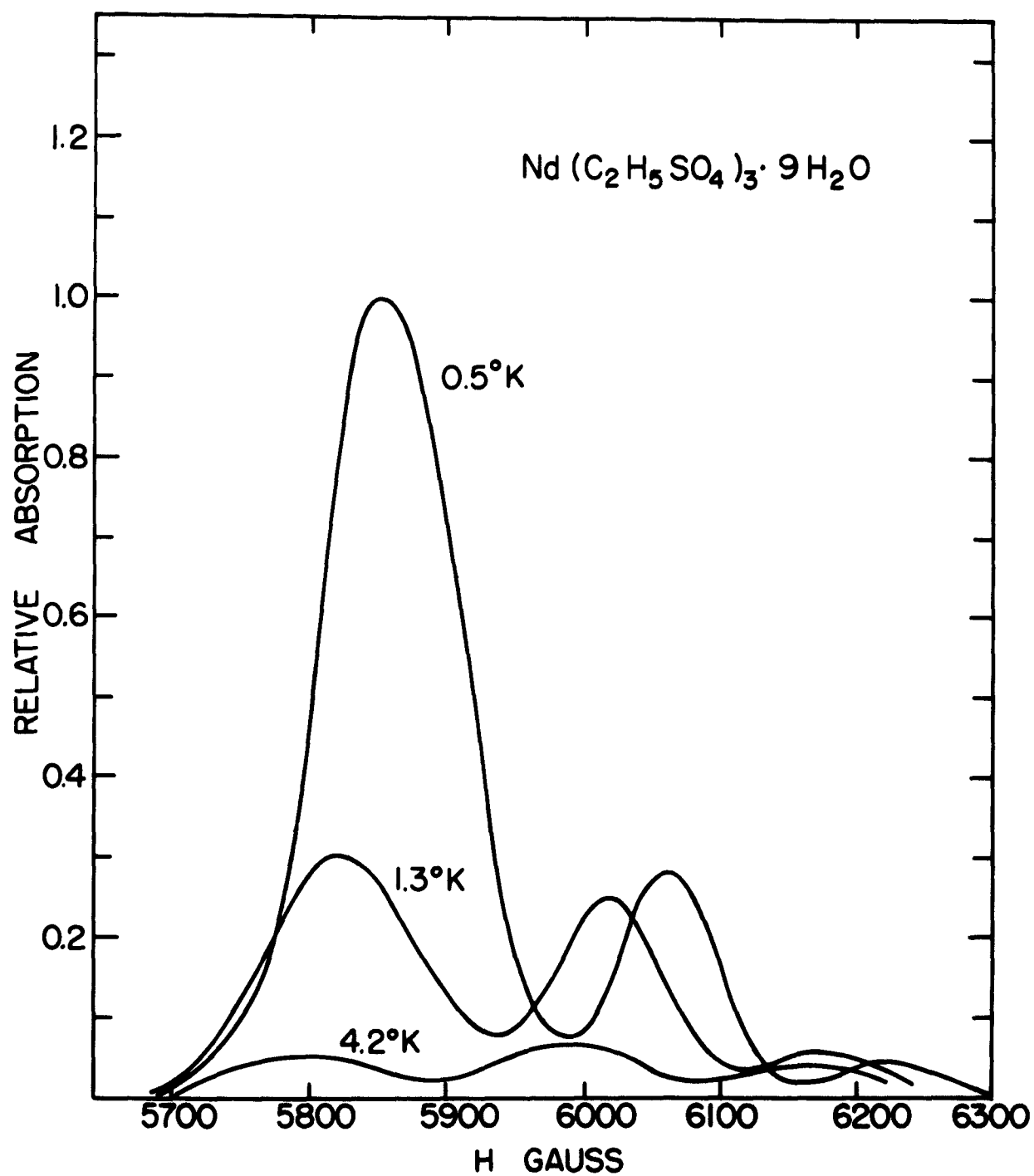


Fig. 6 Resonance Lineshape in $\text{Nd}(\text{C}_2\text{H}_5\text{SO}_4)_3 \cdot 9\text{H}_2\text{O}$ as Function of Temperature.

where the Boltzmann factor is written

$$b = e^{-g \beta H_0 / kT}$$

Here and in the following treatment, we neglect any influence of the interaction on the Boltzmann factors. This corresponds to the first approximation of McMillan and Opechowski, which Lee⁵⁸ has found to agree very well with the exact solution for an Ising chain.

The probability that any spin is anti-parallel is

$$p_{\uparrow} = b^{\Delta E} / (1 + b^{\Delta E}) \quad (3-4)$$

The probability that the two neighbors of a resonating spin are both parallel is

$$p_{\downarrow\downarrow} = (p_{\downarrow})^2 = 1 / (1 + b^{\Delta E})^2 \quad (3-5)$$

Similarly, the probabilities for the other arrangements of two neighbors are :

$$p_{\uparrow\uparrow} = (p_{\uparrow})^2 = b^{2\Delta E} / (1 + b^{\Delta E})^2 \quad (3-6)$$

$$p_{\downarrow\uparrow} = 2p_{\downarrow}p_{\uparrow} = 2b^{\Delta E} / (1 + b^{\Delta E})^2 \quad (3-7)$$

If the probabilities (3-5), (3-6), and (3-7) for the neighbor arrangements are multiplied by the probability

$$p = (1 - b^{\Delta E}) / (1 + b^{\Delta E}) \quad (3-8)$$

of resonance absorption, we get expressions for the relative intensities

of the three lines as a function of temperature. This is plotted in Fig. 7 for $\Delta E = h \cdot 30 \text{ kMc/s} = 1 \text{ cm}^{-1}$, together with the areas of experimental lines like those in Fig. 6 measured with planimeter in arbitrary units and fitted to the probability curves.

Lines from two different samples were measured and then separately fitted as indicated by different symbols. The indicated uncertainties are partly given by the spread in areas of different lines and partly by an estimated minimum of $\pm 20\%$ uncertainty in measured areas because of line overlap and nonlinearity from the large intensity range of 2:100 the spectrometer had to cover.

In spite of the cited difficulties, the measured line areas agree closely with the calculated intensities, except that the weakest line appears to be about 10 times too strong at $T = 0.5^\circ \text{ K}$.

But the main part of this particular line can be explained as coming from hyperfine components of the strong line. Formula (3-2) with the given values of the constants, predicts hyperfine lines of both isotope 143 ($m = -\frac{3}{2}$) at $H = 325$ gauss and of isotope 145 ($m = -\frac{5}{2}$) at $H = 350$ gauss on the high field side of each resonance line. These lines will overlap, and since each isotope has 8 hyperfine lines, the intensity of the combined line should be $20 \cdot 5/8 = 2.5\%$ of the strong line. This is just the intensity of the line we observe ≈ 350 gauss away from the strong line.

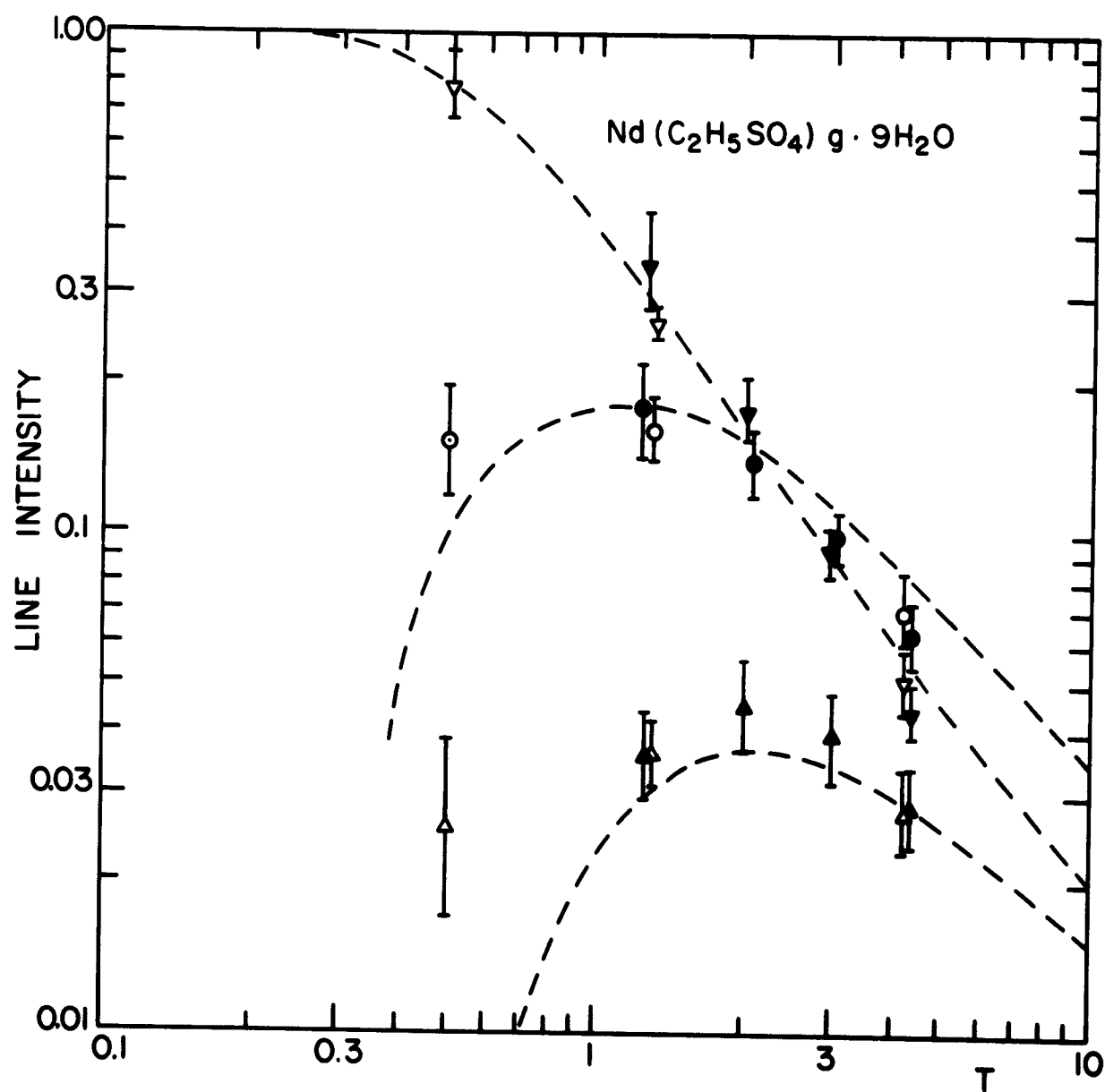


Fig. 7 Measured Areas of the Three Resonance Lines in $\text{Nd}(\text{C}_2\text{H}_5\text{SO}_4)_3 \cdot 9\text{H}_2\text{O}$ Compared to the Theoretical Absorption Ratios.

3.3. First moment changes.

In Fig. 6 a small shift in the position of each line is seen as we lower the temperature. The peaks are also not quite evenly spaced. Since each line looks reasonably symmetric and moments of each component are difficult to measure because of the overlap, we will, in this section, use the peak position of the lines and explain their shift on the basis of the first moment theory outlined in Chapter 1 .

The measured peak positions, as a function of temperature, are shown in Fig. 8 . The field was measured with proton resonance markers, and each line was swept through a number of times, going alternately up and down in field to average out possible hysteresis or recorder lag.

In the moment theory we stressed the importance of differentiating between like and unlike neighbors, since they required different truncation of the interaction Hamiltonian. Here, since we see three lines, although all spins are magnetically identical, we have to treat neighbors as like or unlike depending upon whether their respective instantaneous neighbor arrangements are the same or not. The probability of "like" or "unlike" neighbor interaction will, therefore, depend upon the temperature, since the probability for a given neighbor arrangement is a function of T .

The interaction between spin i and spin j can be divided into four parts :

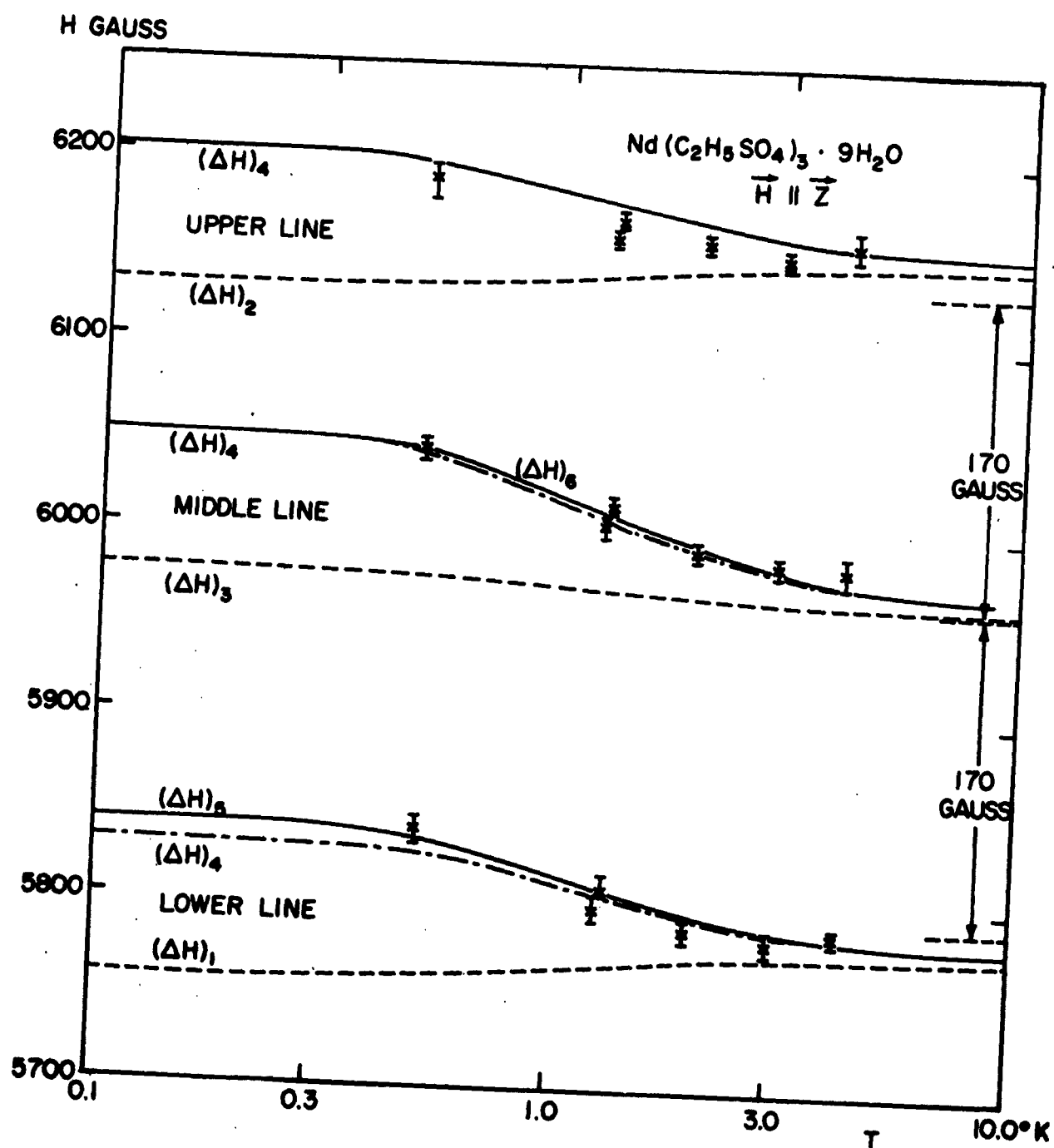


Fig. 8 Peak Position of Lines in $\text{Nd}(\text{C}_2\text{H}_5\text{SO}_4)_3 \cdot 9\text{H}_2\text{O}$ Compared to Calculated First Moment Shifts.

a) Static interaction from $S_{zi} S_{zj}$ terms with the two nearest neighbors. This gives the line splitting and is, thus, already taken care of.

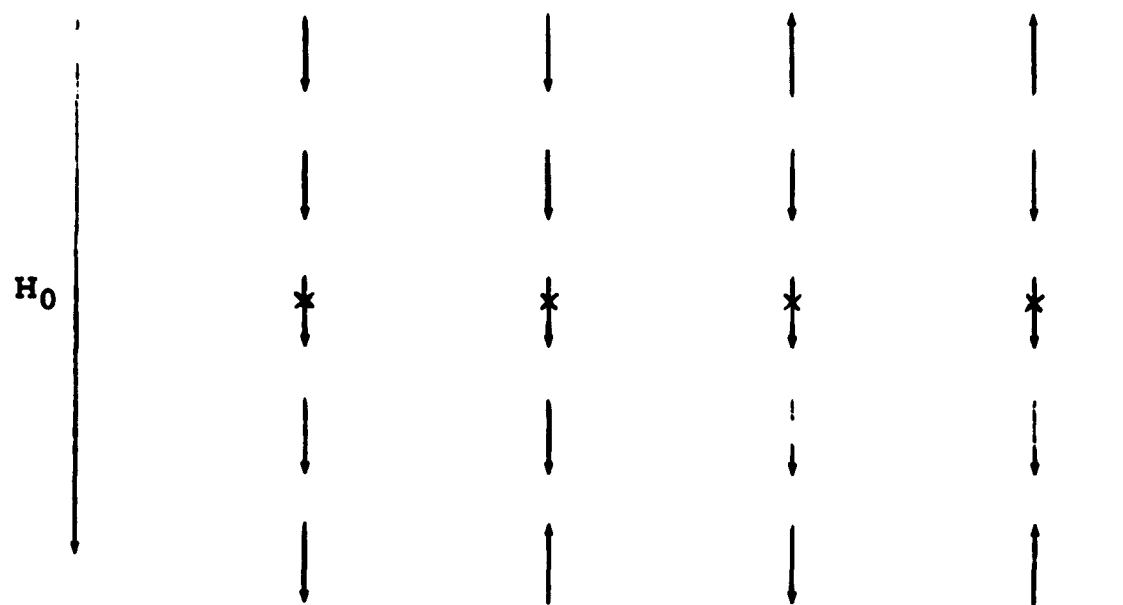
b) Spin-flip interaction from terms $S_{+i} S_{-j}$ with the two nearest neighbors. This is only possible when the flipping spins conserve dipolar energy.

c) Interaction $S_{zi} S_{zj}$ with all the more distant neighbors.

d) Interaction $S_{+i} S_{-j}$ with all the more distant neighbors that are "like."

We first treat the nearest neighbor interactions a) and b). Whether or not the spin-flip interaction b) needs to be considered depends on whether an ion and its neighbor are like or not; i. e., the nearest neighbors of the two interacting spins must be in the same state for b) to be included. In other words, the change in resonance frequency of an ion as a result of nearest neighbor interaction is a function of nearest neighbor-next nearest neighbor interactions.

Consider the case of an ion contributing to the low field line. Speaking semiclassically, its nearest neighbors are by necessity parallel to the external field. Its next nearest neighbors can then have the several different possibilities illustrated in Fig. 9. In case i), both nearest neighbors are like the spin denoted by the cross and the resonance frequency of this spin is shifted according to (1-43) with $\cos \theta_{ij} = 1$ by the amount $\langle h \Delta \nu \rangle = g_{\parallel}^2 + g_{\perp}^2 \beta^2 r_{ij}^{-3}$. In cases ii) and iii) one neighboring spin is like and the other unlike, so that the frequency shift is $(2g_{\parallel}^2 + \frac{1}{2} g_{\perp}^2) \beta^2 r_{ij}^{-3}$, whereas for case iv) it is $2g_{\parallel}^2 \beta^2 r_{ij}^{-3}$.



Probabilities i)

ii)

iii)

iv)

$$\left(\frac{1}{1 + b^{\Delta E}} \right)^2 \quad \frac{b^{\Delta E}}{(1 + b^{\Delta E})^2} \quad \frac{b^{\Delta E}}{(1 + b^{\Delta E})^2} \quad \left(\frac{b^{\Delta E}}{1 + b^{\Delta E}} \right)^2$$

**Fig. 9 Schematic Representation of Various Neighbor Arrangements
for Low Field Line in $\text{Nd}(\text{C}_2\text{H}_5\text{SO}_4)_3 \cdot 9\text{H}_2\text{O}$.**

Weighting these four cases by their probabilities of occurrence, the change of the first moment of this low field line becomes

$$\begin{aligned} \langle h \Delta \nu \rangle = & \beta^2 r_{ij}^{-3} \left[(2g_{\parallel}^2 + g_{\perp}^2) \frac{1}{(1 + b \frac{\Delta E}{\Delta E})^2} + (2g_{\parallel}^2 + \frac{1}{2}g_{\perp}^2) \frac{2b \frac{\Delta E}{\Delta E}}{(1 + b \frac{\Delta E}{\Delta E})^2} \right. \\ & \left. + 2g_{\parallel}^2 \left(\frac{b \frac{\Delta E}{\Delta E}}{1 + b \frac{\Delta E}{\Delta E}} \right)^2 \right] - \beta^2 r_{ij}^{-3} \left[2g_{\parallel}^2 + g_{\perp}^2 \frac{1}{(1 + b \frac{\Delta E}{\Delta E})} \right] \end{aligned} \quad (3-9)$$

Hence, the mean field shift of this low field line resulting from nearest neighbor spin-flip interactions b) is

$$(\Delta H)_1 = - \frac{g_{\perp}^2 \beta}{g_{\parallel} r_{ij}^3} \frac{1}{(1 + b \frac{\Delta E}{\Delta E})} \quad (3-10)$$

Similar reasoning gives, for the line shift of the upper line due to interactions b)

$$(\Delta H)_2 = \frac{g_{\perp}^2 \beta}{g_{\parallel} r_{ij}^3} \frac{b \frac{\Delta E}{\Delta E}}{1 + b \frac{\Delta E}{\Delta E}}, \quad (3-11)$$

and for the middle line

$$(\Delta H)_3 = \frac{g_{\perp}^2 \beta}{g_{\parallel} r_{ij}^3} \frac{1 - b \frac{\Delta E}{\Delta E}}{2(1 + b \frac{\Delta E}{\Delta E})} \quad (3-12)$$

These contributions to the shifts of the lines are calculated below for several temperatures.

T	=	0	0.5	1.0	2.0	∞ °K
$(\Delta H)_1$	=	-32	-31	-26	-21	-16 gauss
$(\Delta H)_2$	=	0	1	6	11	16 gauss
$(\Delta H)_3$	=	16	15	10	5	0 gauss

In case c), the static field from all neighbors except the two nearest gives all three lines the same shift given from (1-43)

$$(\Delta H)_4 = - \frac{2g_{\parallel}^2 \beta}{4g_{\parallel}} \left(\frac{1 - b \Delta E}{1 + b \Delta E} \right) \sum_j^* \frac{3 \cos^2 \theta_{ij} - 1}{r_{ij}^3} \quad (3-13)$$

where the star on the summation means all neighbors except the two nearest ones.

Daniels⁵⁹ has given the total lattice sum over all ions closer than $a_0 \sqrt{10}$ as $18.7 \times a_0^{-3}$. From this result it is easy to find the lattice sum needed here.

$$\sum_j^* \frac{3 \cos^2 \theta_{ij} - 1}{r_{ij}^3} = \frac{18.7}{13.992^3 \cdot 10^{-24}} - \frac{2 \times 2}{7.07^3 \cdot 10^{-24}} = -43.3 \cdot 10^{20} \text{ cm}^{-3} \quad (3-14)$$

The shift becomes

T	=	0	0.5	1.0	2.0	∞ °K
$(\Delta H)_4$	=	73	66	45	25	0 gauss

In case d), the shift from spin-flip interaction with all next nearest neighbors is proportional to the probability of finding the neighbor in the same state. So we get for the lower lineshift

$$(\Delta H)_5 = - \frac{\beta g_{\perp}^2}{4 g_{\parallel}} \left(\frac{1 - b \Delta E}{1 + b \Delta E} \right) \frac{1}{(1 + b \Delta E)^2} \sum_j^* \frac{3 \cos^2 \theta_{ij} - 1}{r_{ij}^3}, \quad (3-15)$$

middle lineshift

$$(\Delta H)_6 = - \frac{\beta g_{\perp}^2}{4 g_{\parallel}} \left(\frac{1 - b \Delta E}{1 + b \Delta E} \right) \frac{2 b \Delta E}{(1 + b \Delta E)^2} \sum_j^* \frac{3 \cos^2 \theta_{ij} - 1}{r_{ij}^3}, \quad (3-16)$$

and upper lineshift

$$(\Delta H)_7 = - \frac{\beta g_{\perp}^2}{4 g_{\parallel}} \left(\frac{1 - b \Delta E}{1 + b \Delta E} \right) \frac{b^2 \Delta E}{(1 + b \Delta E)^2} \sum_j^* \frac{3 \cos^2 \theta_{ij} - 1}{r_{ij}^3}. \quad (3-17)$$

Numerical values for these shifts are

T	=	0	0.5	1.0	2.0	4.0	∞° K
$(\Delta H)_5$	=	11	9	4	2	1	0 gauss
$(\Delta H)_6$	=	0	1	2	2	1	0 gauss
$(\Delta H)_7$	=	0	0	0	0	0	0 gauss .

The various shifts $(\Delta H)_1$ to $(\Delta H)_7$ are added together and fitted to the measured peak positions in Fig. 8 . The temperature shifts and the unequal line spacing are seen to be explained reasonably well by this theory. Since the upper weak line is mostly hyperfine

components of the other lines at $T = 0.5^\circ \text{ K}$, we do not expect any good agreement for this one.

Two points about the line positions should be noted. First, the unperturbed position for the middle line seems to be 5960 gauss. For a frequency of 30.0 Mc/s, this corresponds to $g = 3.60$ which is somewhat higher than the reported $g = 3.535$ for the diluted salt. Second, the splitting caused by the static part of the dipolar interaction would have to be only about 170 gauss instead of the calculated $\Delta H = 2g_{\parallel} \beta / r_{ij}^3 = 188$ gauss. The possible explanation of this difference will be discussed in Section 3.5.

3.4. Second moment changes.

The second moment for interaction between two species of spins is given by (1-45). For all but the two nearest neighbors we have to multiply the lattice sums by the probability that the neighbors of any spin make it "like" or "unlike" with respect to the line considered. For the lowest line, for example, this contribution to the second central moment becomes

$$\begin{aligned}
 (h^2 \langle \Delta \nu^2 \rangle)_a = & \frac{1}{4} \left(1 - \frac{(1 - b \Delta E)^2}{(1 + b \Delta E)} \right) \left[p_{\downarrow\downarrow} \sum_j^* B_{ij}^2 \right. \\
 & \left. + (1 - p_{\downarrow\downarrow}) \sum_k^* (A_{ik} + B_{ik})^2 \right]
 \end{aligned}$$

$$= \frac{b^{\Delta E} \beta^4}{4(1+b^{\Delta E})^2} \left[\frac{(2g_{\parallel}^2 + g_{\perp}^2)^2}{(1+b^{\Delta E})^2} + \left(1 - \frac{1}{(1+b^{\Delta E})^2}\right) 4g_{\parallel}^4 \right] \sum_j^* \frac{(3 \cos^2 \theta - 1)^2}{r_{ij}^6} \quad (3-18)$$

The spin-flip with the two nearest neighbors will cause some broadening too. As found before, there is a probability $p_{\downarrow} = 1/(1+b^{\Delta E})$ that one of the next nearest neighbors will be arranged so as to give the lower line a shift of $s = g_{\perp}^2 \beta^2 / 2 r_1^3$. The resulting contribution to the second moment around the mean position from two neighbors will be

$$\begin{aligned} \langle h^2 < \Delta v^2 > \rangle_b &= 2 [(1 - p_{\downarrow}) (p_{\downarrow} s)^2 + p_{\downarrow} (s - p_{\downarrow} s)^2] \\ &= 2(p_{\downarrow} - p_{\downarrow}^2) s^2 = \frac{g_{\perp}^4 \beta^4}{2 r_1^6} \left[\frac{1}{1+b^{\Delta E}} - \frac{1}{(1+b^{\Delta E})^2} \right]. \quad (3-19) \end{aligned}$$

The total second moment will be the sum of (3-18) and (3-19).

The lattice sum in (3-18) can be found by summing over all lattice points inside a sphere of radius R and integrating over an assumed uniform density of dipoles outside the sphere. If the summation is taken over the 64 next nearest neighbors within $R = 21.5 \text{ \AA}$, we find (please see following page)

$$\begin{aligned}
& \sum_j^* \frac{(3 \cos^2 \theta_{ij} - 1)^2}{r_{ij}^6} \\
&= \sum_{\substack{j \\ r < R}}^* \frac{(3 \cos^2 \theta_{ij} - 1)^2}{r_{ij}^6} + \int_{\phi=0}^{2\pi} \int_{\theta=0}^{\pi} \int_{r=R}^{\infty} \frac{(3 \cos^2 \theta - 1) \zeta r^2 dr}{r^6} d\phi d\theta
\end{aligned}$$

$$\approx (640 + 150) \cdot 10^{40} = 790 \cdot 10^{40} \text{ cm}^{-6} \quad (3-20)$$

Here we have used the dipole density

$$\zeta = \frac{2}{a_0^2 \sin 60^\circ \cdot c_0} = \frac{1}{600} \text{ \AA}^{-3}$$

The square root of the theoretical total second moment for the lower line is plotted as a function of temperature in Fig. 10 for $g_{\parallel} \beta H_0 = 1 \text{ cm}^{-1}$.

Since interaction between like neighbors broadens a line more than interaction between unlike spins, and since the probability for finding like neighbors increases for this line as we lower the temperature, we might expect the second moment to have a maximum at some low temperature. This would indeed happen if the ratio g_{\perp}/g_{\parallel} had been larger.

In the same way, the total second moment for the middle line becomes :

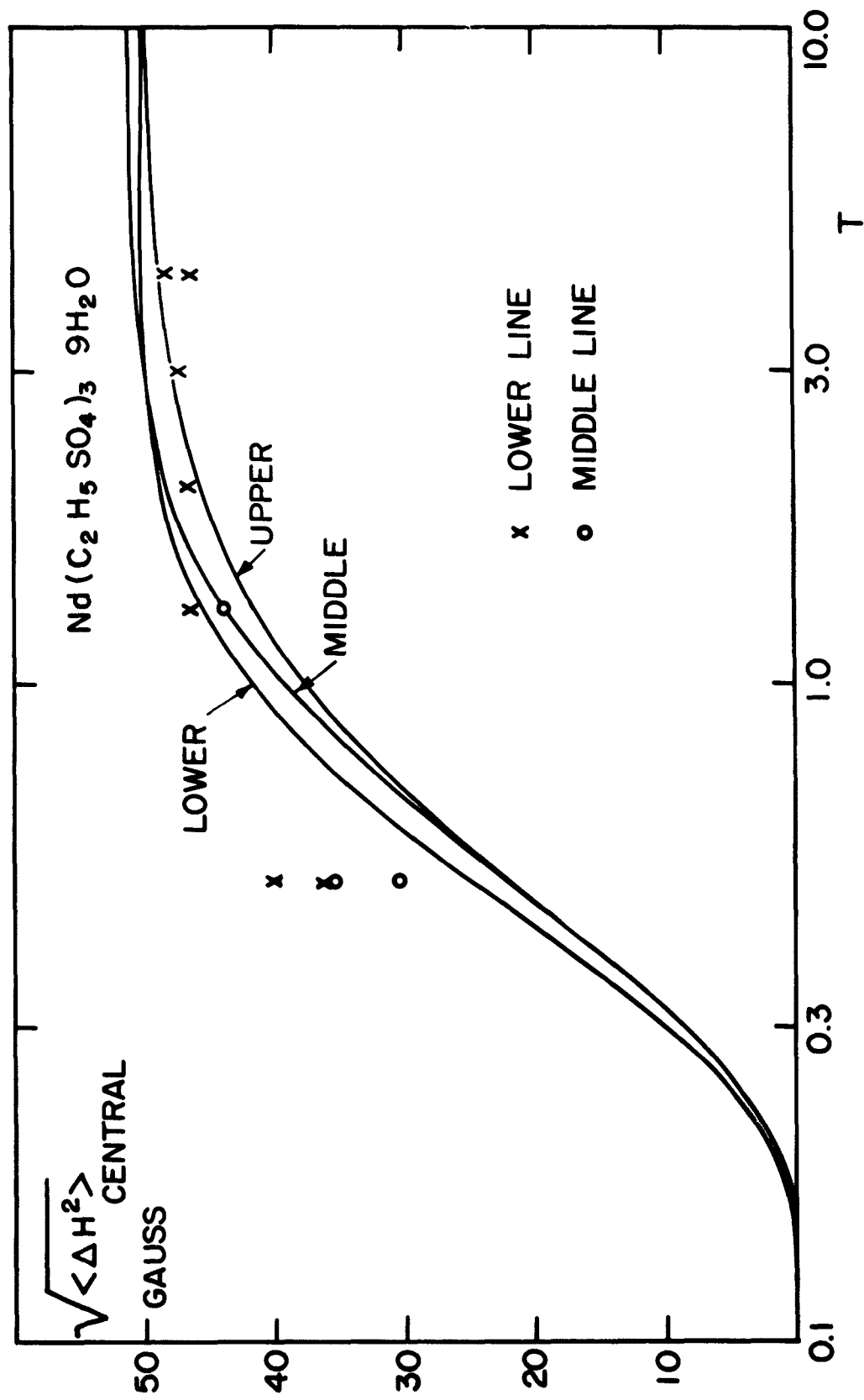


Fig. 10 Calculated Square Roots of Second Moments as Function of Temperature in $\text{Nd}(\text{C}_2\text{H}_5\text{SO}_4)_3 \cdot 9\text{H}_2\text{O}$ Compared to Some Measured Values.

$$\begin{aligned}
h^2 < \Delta v^2 >_{\text{middle}} &= \frac{b^{\Delta E} \beta^4}{4(1 + b^{\Delta E})} \left[\frac{2b^{\Delta E} (2g_{\parallel}^2 + g_{\perp}^2)^2}{(1 + b^{\Delta E})^2} \right. \\
&\quad \left. + \left(1 - \frac{2b^{\Delta E}}{(1 + b^{\Delta E})} \right) 4g_{\parallel}^4 \right] \sum_j^* \frac{(3 \cos^2 \theta_{ij} - 1)^2}{r_{ij}^6} \\
&\quad + \frac{g_{\perp}^4 \beta^4}{4r_1^6} \left[\left(\frac{1 - b^{\Delta E}}{1 + b^{\Delta E}} \right) - \left(\frac{1 - b^{\Delta E}}{1 + b^{\Delta E}} \right)^2 \right] \quad (3-21)
\end{aligned}$$

And for the upper line we find

$$\begin{aligned}
h^2 < \Delta v^2 >_{\text{upper}} &= \frac{b^{\Delta E} \beta^4}{4(1 + b^{\Delta E})} \left[\frac{b^{2\Delta E} (2g_{\parallel}^2 + g_{\perp}^2)^2}{(1 + b^{\Delta E})^2} \right. \\
&\quad \left. + \left(1 - \frac{b^{2\Delta E}}{1 + b^{\Delta E}} \right) 4g_{\parallel}^4 \right] \sum_j^* \frac{(3 \cos^2 \theta_{ij} - 1)^2}{r_{ij}^6} \\
&\quad + \frac{g_{\perp}^4 \beta^4}{2r_1^6} \left[\frac{b^{\Delta E}}{(1 + b^{\Delta E})} - \left(\frac{b^{\Delta E}}{1 + b^{\Delta E}} \right)^2 \right] \quad (3-22)
\end{aligned}$$

The square roots of these second moments are shown as functions of the temperature in Fig. 10. The small differences in second moment between the three lines reflects the different probability of spin-flip broadening.

It is difficult to compare the calculated moments to experimental data since the lines are partially overlapping. But one can measure

second central moments reasonably well on the side of a line where it does not overlap. This can always be done for the lower line, and some measured second moments for this line are given in Fig. 10. The upper line vanishes at sufficiently low temperature, and then measurements of the middle line can be done also.

The agreement is good above 2°K, but at lower temperatures the lines appear too broad. This is probably caused by variations in local field over the sample since the spheres used were rather crude.

In the previous section we saw that the distant neighbors would shift the lower line $g_{\perp}^2/2g_{\parallel}^2$ more than the other two lines at $T = 0^{\circ}\text{K}$ because of the possibility for spin-flip-caused shift. Likewise, variations in the local demagnetizing field will broaden the lower line more than the others by the same amount. Together with the extra broadening of the lower line shown in Fig. 10, this should account for the measured difference in second moment between the lower and middle line. Qualitatively one sees this difference just by looking at the lineshapes in Fig. 6.

3.5. Discussion of possible antiferromagnetic coupling in neodymium ethyl sulfate.

As we saw in the previous sections, the resonance line changes with temperature in neodymium ethyl sulfate are explained fairly well on the basis of dipolar interaction. But to fit the data, the line splitting from the static interaction with the two nearest neighbors had to be

taken as about 170 gauss instead of the calculated 188 gauss. Some of this difference can, perhaps, be accounted for as systematic error, since we used the peak positions instead of the first moments of slightly unsymmetric lines. It does not seem likely, however, that this error would amount to 18 gauss, and it is interesting to postulate some exchange interaction to explain this shift.

The exchange would have to be only to the two nearest neighbors of each spin since the upper and the lower lines have to be shifted in opposite directions. It would have to be antiferromagnetic in character since its effect is to reduce the dipolar splitting in this geometry. But it can hardly be isotropic since the resulting temperature-dependent shift from spin-flip of varying probability will tend to destroy the good agreement between calculated and measured temperature change of line positions.

We are then left with the possibility of the anisotropic exchange

$$K_{ij} = \tilde{A}_{ij} S_{zi} S_{zj} \quad \tilde{A}_{ij} = \begin{cases} \tilde{A} & \text{for near neighbors} \\ 0 & \text{otherwise} \end{cases} \quad (3-23)$$

which for $\tilde{A} = 6 \cdot 10^{-19}$ erg would give the required shift of

$$|\Delta H| = 2 \cdot \frac{1}{2} \tilde{A} / g \beta = 18 \text{ gauss} .$$

This is a very small exchange and alone corresponds roughly to a Curie temperature of ⁶⁰

$$\theta = - \frac{\tilde{A} S(S+1) Z}{3 k} = - 0.0018^\circ \text{ K} \quad (3-24)$$

when $Z = 2$ is the number of nearest neighbors.

Since the crystal is not cubic, the dipolar interaction also can give a spontaneous magnetization. From the crystal structure and the g -values for dilute salt, Daniels⁵⁹ calculated a powder Curie temperature of 0.007°K while Roberts, Sartain and Borie⁶¹ measured $\theta_{\text{powder}} = 0.013 \pm 0.005^\circ\text{K}$. The difference is probably not significant, but if it were, it predicts that the additional coupling should be ferromagnetic rather than antiferromagnetic.

The specific heat data allows a somewhat better comparison between theory and experiment for lattice interaction. Daniels calculates the specific heat from dipolar interactions as⁵⁹

$$\begin{aligned} \frac{CT^2}{2R} = & \frac{\beta^4}{64k^2} \left[(g_{\parallel}^4 + 5g_{\perp}^4) \sum_j' \frac{1}{r_{ij}^6} \right. \\ & - 6(g_{\parallel}^2 - g_{\perp}^2)(g_{\parallel}^2 - 2g_{\perp}^2) \sum_j' \frac{z_{ij}^2}{r_{ij}^8} \\ & \left. + 9(g_{\parallel}^2 - g_{\perp}^2)^2 \sum_j' \frac{z_{ij}^4}{r_{ij}^{10}} \right] = 8.95 \cdot 10^{-5} \quad (3-25) \end{aligned}$$

This is in excellent agreement with the experimental value of $8.85 \pm 0.25 \cdot 10^{-5}$,⁶¹ and does not seem to leave room for any exchange.

Equation (3-25) is derived without consideration as to whether spin neighbors are "like" or "unlike" as we had to do in the

calculation of moments. This is valid when no external field is present to quantize the spins in the z-direction. But (3-25) involves g_{\parallel} to the 4th power and r_{ij} to the 6th power, and small errors in these constants can easily upset the apparent agreement. The values of r_{ij} are from room temperature measurements; the coefficient of thermal expansion is unknown for neodymium ethyl sulfate, but it is quite possible that the dimensions could decrease by a factor of, say, $3 \cdot 10^{-3}$ from room temperature to helium temperatures as is the case for many materials. That would give a 2 % increase in $CT^2/2R$. And even more important, we have measured $g_{\parallel} = 3.60$ in the concentrated salt, and the use of this value in (3-25) instead of $g_{\parallel} = 3.535$ increases $CT^2/2R$ by about 6 %. The calculated specific heat is then too large, but when the small antiferromagnetic coupling (3-23) is included, it is reduced to agree again with the experimental data.

The easiest way to include the effect of the exchange in the specific heat is to change g_{\parallel} in (3-25) when interaction between nearest neighbors is considered. The coupling (3-23) added to the dipolar $S_{zi} S_{zj}$ -term in the interaction between nearest neighbors shifts the line by ≈ 18 gauss out of a total of 188 gauss, and the interaction energy is reduced to

$$K_{ij} = \left(\frac{170}{188}\right) \frac{2g_{\parallel}^2 \beta^2}{r_j^6} = \frac{2g_{\parallel}'^2 \beta^2}{r_j^6}$$

$$g_{\parallel}' = g_{\parallel} \sqrt{\frac{170}{188}} = 3.42 \quad (3-26)$$

This apparent $g_{//}^{'}$ should be used in (3-25) whenever the sums \sum_j involve one of the nearest neighbors. We use the total lattice sums as given by Daniels for neodymium ethyl sulfate and split them up in the contribution from the two nearest neighbors and all the rest as follows:

<u>Daniels</u>	<u>Two nearest</u>	<u>The rest</u>
----------------	--------------------	-----------------

$$\sum_j \frac{1}{r_{ij}^6} = \frac{245.53}{13.99^6 \cdot 10^{-48}} = (1.59 + 1.66) 10^{43}$$

$$\sum_j \frac{z_{ij}^2}{r_{ij}^8} = \frac{144.32}{13.99^6 \cdot 10^{-48}} = (1.59 + 0.32) 10^{43}$$

$$\sum_j \frac{z_{ij}^4}{r_{ij}^{10}} = \frac{128.07}{13.99^6 \cdot 10^{-48}} = (1.59 + 0.11) 10^{43}$$

We then find $CT^2/2R = 8.35 \cdot 10^{-5}$, and when this is increased by $\approx 2\%$ because of the decrease in the interionic distances, we get

$$\frac{S' T^2}{R} \approx 8.55 \cdot 10^{-5} \quad (3-27)$$

This is almost within the accuracy of the experimental result $CT^2/2R = 8.85 \pm 0.25 \cdot 10^{-5}$. But this agreement with specific heat data should not be taken as a proof for the existence of the coupling given by (3-23). In view of the uncertainties in g -value and ionic

spacings, probably all that can be said is that the specific heat data certainly does not rule out the possibility of such an interaction.

Some weak interaction, in addition to the dipolar forces, should not be too unexpected in neodymium ethyl sulfate. Demagnetization experiments⁶² on the isomorphic cerium ethyl sulfate give a specific heat for this salt that is six times larger than what we expect from the dipolar interaction alone. The Curie temperature in this salt is of the order -0.1°K which corresponds to an antiferromagnetic exchange ≈ 50 times stronger than the interaction (3-23).

Finkelstein and Mencher⁶³ have suggested that the anomalous behavior of cerium ethyl sulfate may be due to interactions between the atomic electric quadrupole moments of the magnetic ions. Such an interaction would depend upon the relative orientation of the spins and give terms in $S_{zi} S_{zj}$ and $S_{+i} S_{-j}$. But the relative strength of these terms is likely to depend on the anisotropy of the g-tensor, and we expect the spin-flip term to be smaller than the static term by a factor $g_{\perp}^2/g_{\parallel}^2 = 0.33$. Our experimental accuracy is not sufficient to decide whether a term like $\frac{1}{6} \tilde{A}_{ij} (S_{+i} S_{-j} + S_{-i} S_{+j})$ is needed in (3-23) or not. The quadrupole interaction would probably be important only for the nearest neighbors since it falls off as the 5th power of the interatomic distance.

Comparing cerium and neodymium, the quadrupole interaction would be proportional to the 8th power of the 4f electron orbit radius and proportional to the matrix elements connecting the ground

state with the lowest excited level of the ion. Cerium is the first member of the rare earth series, and we expect the mean radius for its 4f electron to be considerably larger than in neodymium. Also, the first excited state of Ce^{3+} in ethyl sulfate is only 4.8 cm^{-1} above the ground level,⁶² while in Nd^{3+} the splitting is about 130 cm^{-1} .⁵³ The electronic quadrupole interaction in neodymium ethyl sulfate should, therefore, be much smaller than in the corresponding cerium salt, and it could well be smaller by the two orders of magnitude that are required for the quadrupole interaction to agree with our postulated exchange. It is, therefore, not unreasonable to suggest that this may be the physical origin of the weak antiferromagnetic interaction that we have observed in neodymium ethyl sulfate.

Since this interaction is mainly static in character and between nearest neighbors only, it will not influence the second moments of the resonance lines.

CHAPTER 4

MEASUREMENTS ON NICKEL FLUOSILICATE

4.1. Description of nickel fluosilicate.

Nickel fluosilicate, $\text{NiSiF}_6 \cdot 6\text{H}_2\text{O}$ belongs to a large class of isomorphic crystals of formula $\text{M}^{2+} \text{N}^{4+} \text{A}_6^- \cdot 6\text{H}_2\text{O}$ where M^{2+} may be Ni, Cu, Fe, Co, Mn, Zn, Mg or Cd, N^{4+} may be Si, Ti, Sn, Zr, Pd or Pt, and A_6^- may be H, F or Cl. The structure of $\text{Ni SnCl}_6 \cdot 6\text{H}_2\text{O}$ has been determined from x-ray measurements by Pauling.⁶⁴ It is trigonal and the unit cell containing one molecule is shown in Fig. 11. The structure may be thought of as made up of $(\text{Ni} \cdot 6\text{H}_2\text{O})^{2+}$ and $(\text{SnCl}_6)^{2-}$ complexes arranged on a body-centered cubic lattice that has been trigonally distorted along the body diagonal denoted by z in Fig. 11. This body diagonal is the same as the hexagonal growth axis. Each complex is assumed to have the form of an almost regular octahedron surrounding the metallic ion.

The other members of the crystal series are assumed to have the same structure with only small changes in the dimensions of the unit cell. For the case of $\text{NiSiF}_6 \cdot 6\text{H}_2\text{O}$, the Ni - Ni distance OA in Fig. 11 is given⁶⁵ as 6.21 \AA and the angles α between the rhombohedral axes are $96^\circ 5'$. This is close enough to cubic symmetry ($\alpha = 90^\circ$) so that the lattice sum $\sum_j (3 \cos^2 \theta_{ij} - 1)/r_{ij}^3$ is found to be essentially the same as in the cubic case.⁶⁶

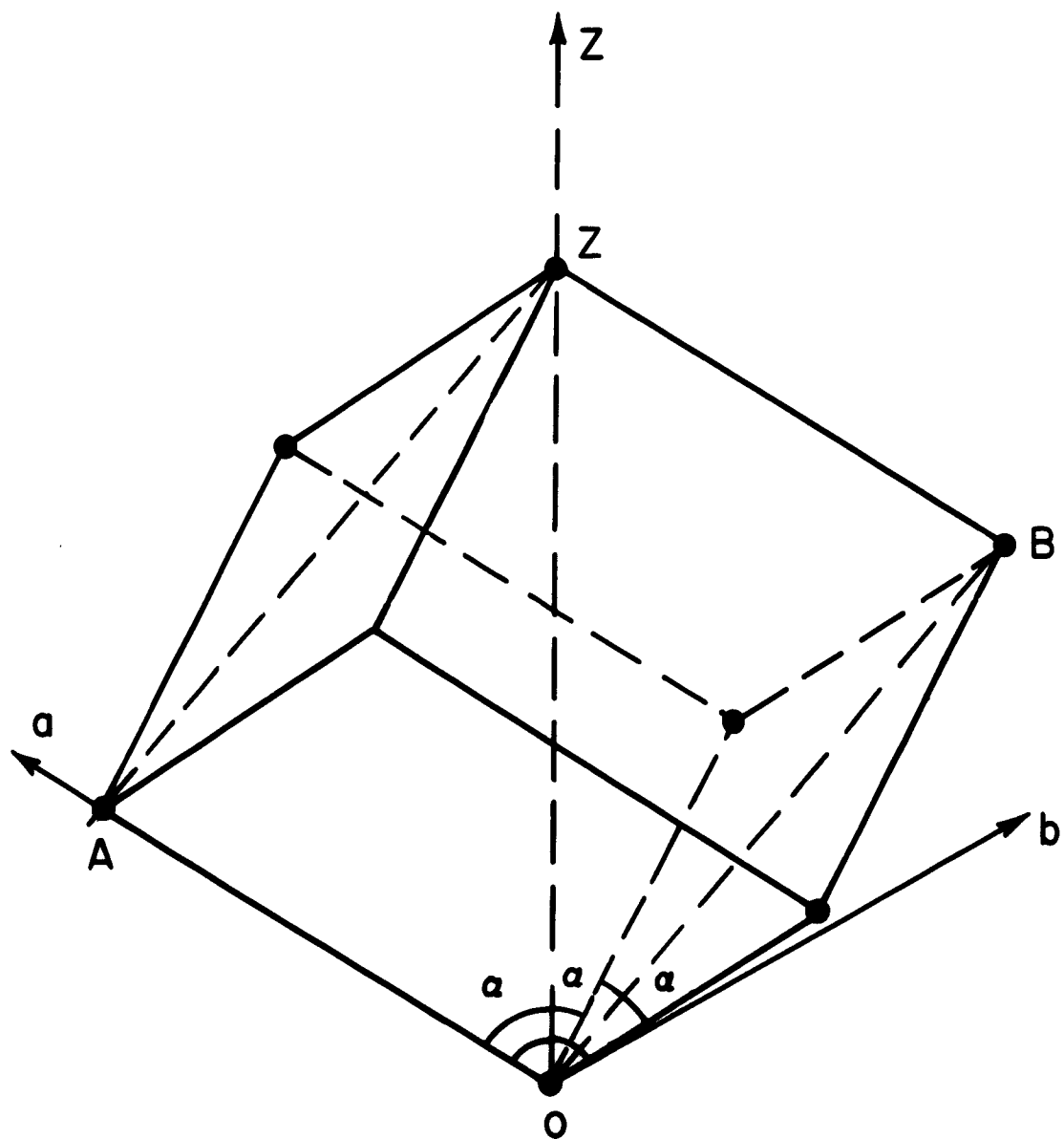


Fig. 11 Rhombohedral Unit Cell of $\text{NiSiF}_6 \cdot 6\text{H}_2\text{O}$.

This is the structure at room temperature. Walsh⁶⁷ has measured the thermal expansion of this crystal with strain gauges. He found the expansion coefficients to be highly anisotropic, and from his results we expect the deviation from cubic symmetry to be slightly larger at low temperatures. But the lattice sum can probably still be assumed to vanish for spherical samples.

From the structure we expect the Ni^{++} - ion to see a slightly trigonally distorted cubic electric field from the surrounding water dipoles. The cubic field splits the 3F_4 ground state of the free ion and leaves an orbital singlet level some $10,000 \text{ cm}^{-1}$ below the other states.⁶⁸ The triple spin degeneracy of this level is lifted by the trigonal field which splits it into a doublet and a singlet.⁶⁹ The magnetic behavior can then be described by the following spin-Hamiltonian for $S = 1$ ⁷⁰

$$H_i^{(0)} = \beta \vec{H}_0 \cdot \vec{g} \vec{S} + D (S_z^2 - 2/3) \quad (4-1)$$

No hyperfine interaction term needs to be included here since the Ni-isotope with nuclear spin has low abundance and small nuclear moment.

If the external field \vec{H}_0 makes an angle γ with the z-axis, and if we assume $g_x = g_y = g_z = g$, we find the energy levels of (4-1) by first-order perturbation calculation (exact for $\gamma = 0^\circ$).

$$\left. \begin{aligned} a_1 &= -g\beta H_0 + \frac{1}{3} D \left(\frac{3}{2} \cos^2 \gamma - \frac{1}{2} \right) \\ a_2 &= \frac{1}{3} D (1 - 3 \cos^2 \gamma) \\ a_3 &= g\beta H_0 + \frac{1}{3} D \left(\frac{3}{2} \cos^2 \gamma - \frac{1}{2} \right) \end{aligned} \right\} \quad (4-2)$$

The resonance transitions are

$$\begin{aligned} h\nu_1 &= a_2 - a_1 = g\beta H_0 - \frac{1}{2} D (3 \cos^2 \gamma - 1) \\ h\nu_2 &= a_3 - a_2 = g\beta H_0 + \frac{1}{2} D (3 \cos^2 \gamma - 1) \end{aligned} \quad (4-3)$$

For $\gamma \neq 0$, the crystalline field mixes the states and the transition $a_3 - a_1$ also becomes allowed, but with small probability when $g\beta H_0 \gg D$.

We have measured at helium temperatures $g = 2.24 \pm 0.01$, isotropic within the accuracy of the measurements. This is in good agreement with the $g = 2.25$ deduced from optical rotation data at low temperature⁶⁹ and does not differ significantly from the $g \approx 2.25 - 2.36$ reported in resonance experiments at higher temperatures.^{70,71}

We have found the splitting $D = -0.113 \pm 0.005 \text{ cm}^{-1}$ at helium temperatures. Above 20° K it is a function of temperature and increases to $D \approx -0.50 \text{ cm}^{-1}$ at room temperature.^{70,71} Hydrostatic pressure will decrease $|D|$ again, and Walsh⁶⁷ has shown that at room temperature D actually goes through zero and changes sign for $p = 6200 \text{ kg/cm}^2$. Since the splitting is so sensitive to lattice distortions, it is not unreasonable to expect that crystalline

defects, impurities and cooling strains will give a slight variation in the value of D from ion site to ion site. This view is supported by the fact that the narrowest resonance lines measured in Zn-diluted salts are about 30 gauss wide,⁷² much more than one should expect from dipolar interactions with the surrounding protons.

Earlier measurements of specific heat, magnetization and resonance linewidths of $\text{NiSiF}_6 \cdot 6\text{H}_2\text{O}$ have indicated the presence of moderately strong exchange in this salt. But there has been some confusion as to the magnitude of the exchange and whether it would have to be partly anisotropic. As will be seen, our measurements indicate an isotropic ferromagnetic exchange $A = -3.9 \cdot 10^{-18}$ erg in good agreement with some of the previous measurements.

Our lineshape data was taken mainly with the external field along the trigonal axis ($\gamma = 0$). Then we see two exchange-shifted and broadened lines separated at high temperature by $2|D|/g\beta$. However, we see from (4-3) that the two lines overlap for the field direction $\gamma \approx 55^\circ$ where $(3 \cos^2 \gamma - 1) = 0$. Here the combined line is exchange-narrowed and unshifted. But all directions $\gamma \approx 55^\circ$ do not give the same linewidth. In particular, the lattice sum $\sum_j (3 \cos^2 \theta_{ij} - 1)^2 / r_{ij}^6$ determining the second moment is very different for \vec{H}_0 parallel to the direction \vec{a} in Fig. 11, which happens to be almost along one of the rhombohedral axes, and for $\vec{H}_0 \parallel \vec{b}$, which is obtained by rotating \vec{H}_0 an angle $2 \times 55^\circ$ in the plane AZB. This difference in linewidth is interesting to observe, but is no more surprising than the variation in the square root of the

second moment 1 : 1.5 : 2.4 found for the directions (111) , (110) and (100) , respectively, in a cubic crystal.⁷³

4.2. First moment changes.

We tried to grind spheres of $\text{NiSiF}_6 \cdot 6\text{H}_2\text{O}$, but we did not succeed, since the crystals are soft and cleave very easily along the hexagonal axis. Instead, they came out as reasonably good ellipsoids of revolution with axial ratios ranging from 1.25 to 1.50 . The field for resonance then had to be corrected for demagnetization effect as discussed in Section 1.5 . For an axial ratio of 1.50 and a spin density of $4.16 \cdot 10^{21}$ ions/cm³ , we find, from (1-49) and (1-57) , a shape correction of 164 gauss at $T = 0^\circ \text{K}$ which is far from negligible.

The ellipticity of the samples had one beneficial effect, however; they were much easier to x-ray orient since we could see roughly the direction of the crystalline axis.

We measured four different samples in the cavity version of the spectrometer and two samples in the waveguide version. The frequencies used were slightly different; $f = 29.80 \text{ kMc/s}$ for the cavity and $f = 30.06 \text{ kMc/s}$ for the waveguide spectrometer. For comparison of the results we reduced the measured field values for waveguide resonance by $(29.80/30.06)$. Typical resonance lineshapes for \vec{H}_0 along the hexagonal z-axis are shown in Fig. 12 where the maximum amplitudes are normalized to the same value. In this plot the field values are not corrected for the effect of a nonspherical shape, but

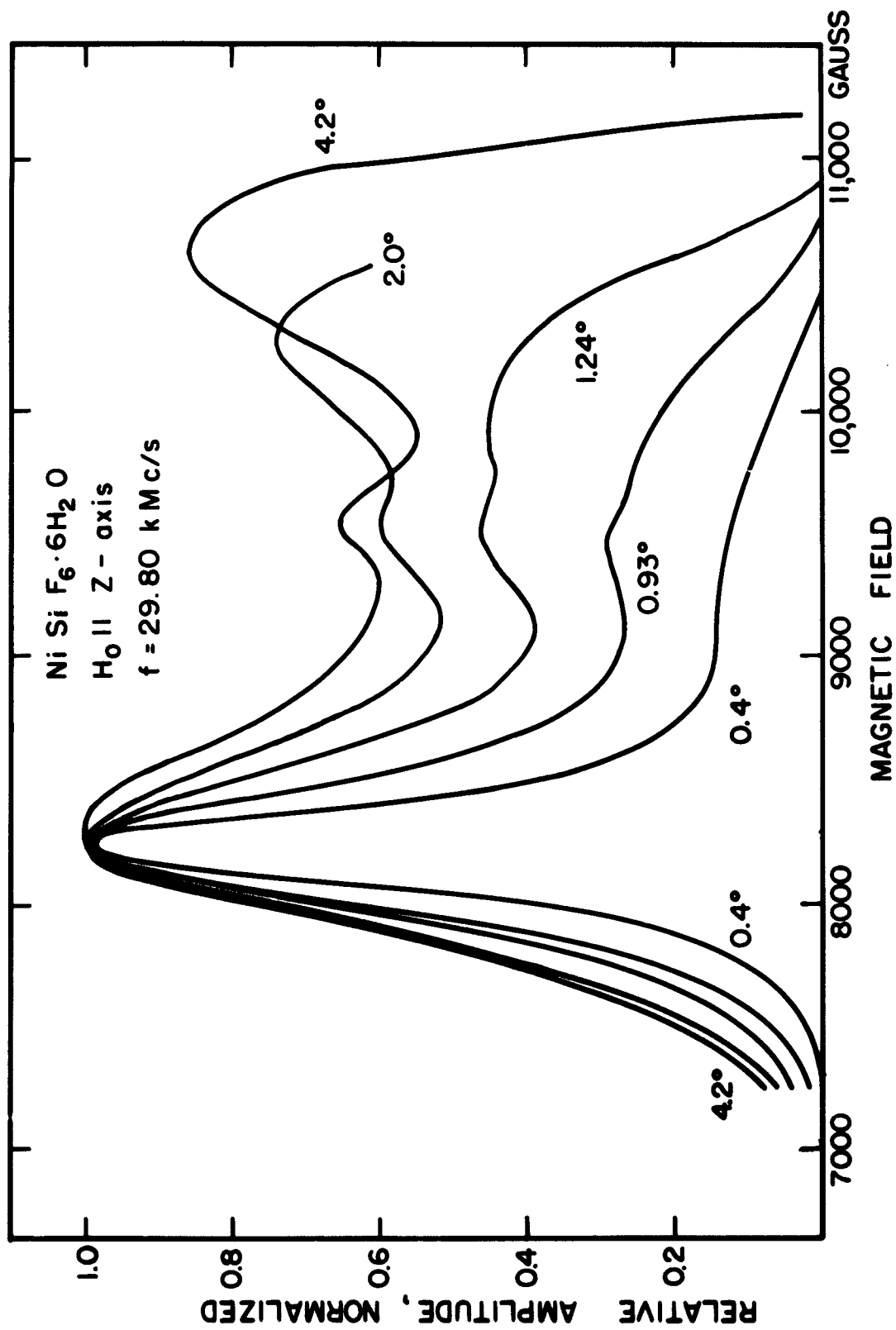


Fig. 12 Measured Resonance Lineshape in $\text{Ni Si F}_6 \cdot 6\text{H}_2\text{O}$ as Function of Temperature.

the lines at 0.4°K and 0.93°K are corrected for too much absorption by using formula (2-31). Completely off resonance we had $P_r/P_o \approx 0.05$; at resonance at $T = 0.4^{\circ}\text{K}$ we found $P_r/P_o \approx 0.70$.

From Fig. 12 we see that at 4.2°K we have two resonances of almost equal intensity as expected. Since $|D|$ is small, the line-splitting is not as large as we might have liked to have it, and the lines overlap somewhat. As we lower the temperature, the transition $a_3 - a_2$ at the higher field decreases in strength relative to the other transition, and it also changes position. Below 1°K it cannot be separated from the wing of the line $a_2 - a_1$ in the lower field. The lower line narrows considerably, and also moves somewhat. An additional weak line is seen right between the main peaks; the origin of this one is not known, but some possible explanations will be discussed in Section 4.4.

Because of the line overlap, it is difficult to measure first moments, and, therefore, we have again used the peak positions of the lines. The peak positions of the lower, strong line shown in Fig. 13a, are corrected for the demagnetizing shift according to (1-49) and (1-57). Since this salt is almost cubic, the dipolar parts of the lattice sum cancel and do not contribute to the first moment. However, as we saw in Section 1.3, isotropic exchange will shift the first moment of this line, and from (1-36) we find

$$h \langle \Delta v \rangle = -6\tilde{A} \frac{(b^{a_2} - b^{a_3})}{(b^{a_1} + b^{a_2} + b^{a_3})} . \quad (4-4)$$

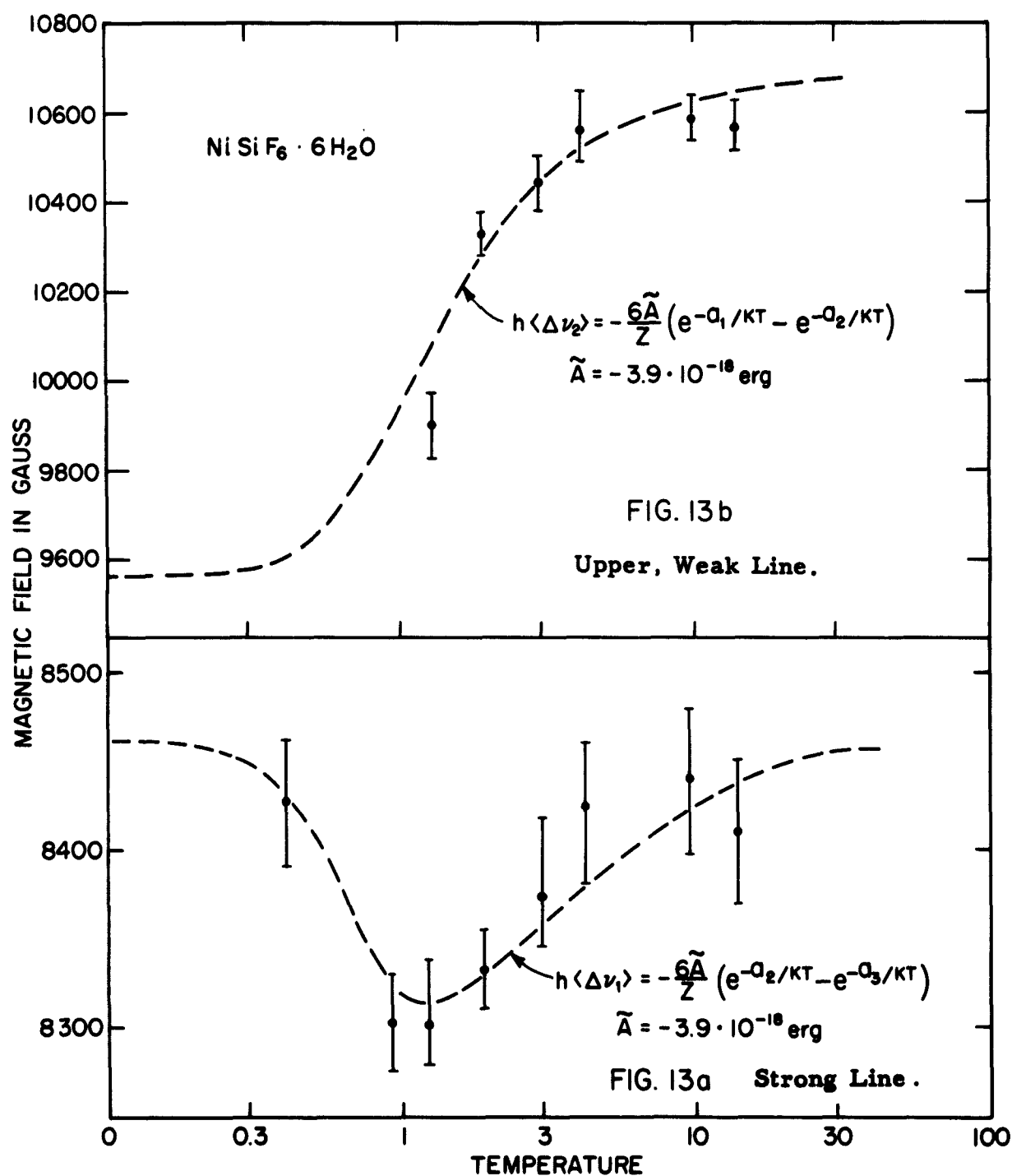


Fig. 13 Measured Peak Positions of Resonance Lines in $\text{NiSiF}_6 \cdot 6\text{H}_2\text{O}$
 Compared to Calculated First Moments.

Here we have assumed the exchange to have appreciable strength only to the six nearest neighbors of each spin. The best fit to the experimental values in Fig. 13a is seen to be for the choice of $\tilde{A} = -3.9 \cdot 10^{-18}$ erg. This is a ferromagnetic interaction. Antiferromagnetic exchange, $A > 0$, would have shifted the line the other way.

Similarly, the demagnetization-corrected peak position of the upper, weak line is plotted in Fig. 13b. Again, dipolar interaction does not change the first moment, and the exchange shifts it by

$$h \langle \Delta \nu \rangle = - \frac{6\tilde{A} (b^{a_1} - b^{a_2})}{(b^{a_1} + b^{a_2} + b^{a_3})} \quad (4-5)$$

The choice of $\tilde{A} = -3.9 \cdot 10^{-18}$ erg fits the measured values reasonably well.

The different shifts of the two lines can be explained as follows: In the lower line, the exchange term $S_{zi} S_{zj}$ will cause a shift proportional to $(b^{a_1} - b^{a_3})$. The spin-flip term $S_{+i} S_{-j}$ causes a shift in the opposite direction proportional to $(b^{a_1} - b^{a_2})$. Since the proportionality constants are the same, the net shift goes as $(b^{a_2} - b^{a_3})$, which is zero for $T \rightarrow \infty$ and $T \rightarrow 0$. For the upper line, however, spin-flips with near neighbors become less probable as the two upper levels are depopulated, and the shift proportional to $(b^{a_2} - b^{a_3})$ is insufficient to cancel the shift $(b^{a_1} - b^{a_3})$ caused by the $S_{zi} S_{zj}$ terms.

Qualitatively, we may think of a spin resonating in the lower transition as having a fictitious spin $\frac{1}{2}$. This spin will see only like

neighbors at temperatures so low that the uppermost level is effectively depopulated, and isotropic exchange cannot then shift the line. A spin resonating in the upper transition, however, can be thought of as seeing mainly unlike neighbors at low temperatures, and exchange will then change the first moment.

Anisotropic exchange would have given a very different first moment shift. If we were to assume anisotropic exchange of the form

$$H_{ij}^{(1)} = \tilde{A}_{ij\parallel} S_{zi} \cdot S_{zj} + A_{ij\perp} \cdot \frac{1}{2} (S_{+i} S_{-j} + S_{-i} S_{+j}) \quad (4-6)$$

where we write

$$\tan \Theta = \frac{A_{ij\perp}}{A_{ij\parallel}} \quad (4-7)$$

We see from the graphs of McMillan and Opechowski⁷⁴ that our measurements will only fit $\Theta = 45^\circ \pm 5^\circ$ which corresponds to

$$A_{ij\perp} = A_{ij\parallel} \quad \text{to within } \pm 20\%.$$

We also looked for possible temperature shift in line position when \vec{H}_0 made an angle of $\cos^2 \theta = 1/3$ with the hexagonal axis and the two lines overlapped. For this direction, the demagnetization correction should vanish in the first order. We saw no lineshift larger than the uncertainty in measurements, and this may be taken as additional indication of the absence of anisotropic exchange.

Anisotropic exchange having the same angular dependence as dipolar interaction could still, in principle, be present. This would

not affect first moments, since the crystal is almost cubic in form.

4.3. Second moment changes.

The second moments of the resonance lines in $\text{NiSiF}_6 \cdot 6\text{H}_2\text{O}$ have been calculated at infinite temperature by Ollom⁷⁵ and by Ishiguro, Usui and Kambe.⁶⁶ McMillan and Opechowski⁵ used this salt as an example for their formulas for the temperature dependence of the moments, and from (A-10), they find, for the transition $a_1 - a_2$ when H_0 is along the crystalline axis

$$\begin{aligned}
 h^2 \langle \Delta v^2 \rangle = & 6 \tilde{A} [Z^{-1} (b^{a_2} + 2b^{a_3}) + 5 Z^{-2} (b^{a_2} - b^{a_3})^2] \\
 & + 0.626 \frac{\beta^4 g^4}{d^6} \left\{ 1 + 4Z^{-1} (2b^{a_1} + b^{a_3}) \right. \\
 & - Z^{-2} (9b^{2a_1} - 6b^{a_1 a_2} + b^{2a_2} - 12b^{a_1 a_3} \\
 & \left. + 4b^{2a_3} + 4b^{a_2 a_3}) \right\} . \quad (4-8)
 \end{aligned}$$

Here we have used $g_{\parallel} = g_{\perp} = g$, $Z = (b^{a_1} + b^{a_2} + b^{a_3})$, and the result of the lattice summation

$$\frac{1}{4} \sum_j' (3 \cos^2 \theta_{ij} - 1)^2 / r_{ij}^6 = 0.626/d^6 , \quad (4-9)$$

where the lattice constant is $d = 6.21 \text{ \AA}$.

The second central moment can be found by combining (4-8) and (4-4)

$$\begin{aligned}
 h^2 \langle \Delta v^2 \rangle_{\text{central}} &= h^2 \langle \Delta v^2 \rangle - (h \langle \Delta v \rangle)^2 \\
 &= 6 \tilde{A}^2 [Z^{-1} (b^2 + 2b^3) - Z^{-2} (b^2 - b^3)^2] \\
 &+ 0.626 \frac{\beta^4 g^4}{d^6} \left\{ 1 + 4Z^{-1} (2b^1 + b^3) \right. \\
 &- Z^{-2} (9b^{2a_1} - 6b^{a_1 a_2} + b^{2a_2} - 12b^{a_1 a_3} \\
 &\left. + 4b^{2a_3} + 4b^{a_2 a_3}) \right\} \quad (4-10)
 \end{aligned}$$

The square root of (4-10) is plotted in Fig. 14 as a function of temperature for $v = 29.80$ kMc/s and $\tilde{A} = -3.9 \cdot 10^{-18}$ erg. This is compared to measured values of the square root of the second central moment taken on the non-overlapping low side of the lower line. The agreement is seen to be good. Since about 90 % of the second moment comes from the exchange term, this is a good check on the magnitude of \tilde{A} found from the first moment shifts, and the presence of any anisotropic exchange must be ruled out.

It is seen that even if the line clearly narrows at very low temperatures, the second moment remains somewhat larger than predicted by the theory. This is probably caused by imperfect elliptical shape of the samples, and possibly by nonlinearity from too much sample

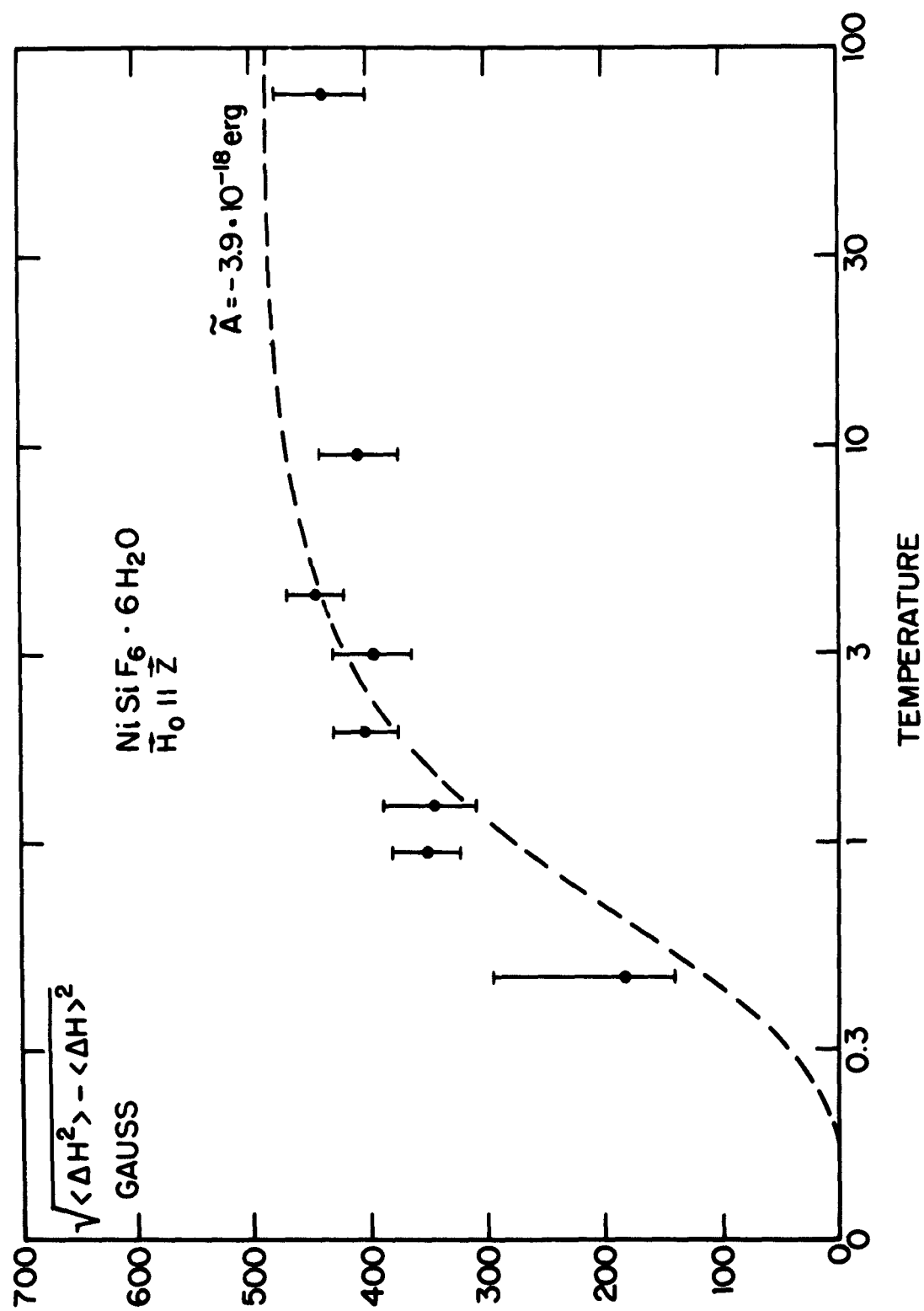


Fig. 14 Measured and Calculated Square Root of Second Moment of Lower

Line in $\text{NiSiF}_6 \cdot 6\text{H}_2\text{O}$ when $\vec{H}_0 \parallel \vec{z}$

saturation or sample heating at 0.4°K . A perfect spheroidal sample shape will not influence the second central moment measured in this orientation.

A similar formula could be given for the second moment of the other line, but this weak line disappears below 1°K , and the formula cannot very well be compared to experimental results.

At directions where the two lines overlap we find the second moment from (1-25) with $S = 1$

$$h^2 \langle \Delta v^2 \rangle = f(1 + 3f) \sum_j B_{ij}^2, \quad (4-11)$$

where

$$f = \frac{\frac{g\beta H_0/2}{b} - \frac{-g\beta H_0/2}{b}}{\frac{3g\beta H_0/2}{b} - \frac{-3g\beta H_0/2}{b}}$$

$$\rightarrow \frac{1}{3} \quad \text{for } T \rightarrow \infty. \quad (4-12)$$

In using formula (1-25) for this case, we have neglected small terms in the matrix elements between the levels of order $D^2/(g\beta H_0)^2$.

When the field is parallel to one of the rhombohedral axes (direction \vec{a} in Fig. 11) the lattice sum over 92 nearest neighbors is found to be

$$\sum_j (3 \cos^2 \theta_{ij} - 1)^2 / r_{ij}^6 = 224 \cdot 10^{42} \text{ cm}^{-6}. \quad (4-13)$$

The square root of the second moment for this direction of the field is

$$(\langle \Delta H^2 \rangle)^{\frac{1}{2}} = \left[\frac{f(1+3f)}{g^2 \beta^2} \frac{9}{4} g^4 \beta^4 \sum_j \frac{(3 \cos^2 \theta_{ij} - 1)^2}{r_{ij}^6} \right]^{\frac{1}{2}}$$

→ 380 gauss for $T \rightarrow \infty$. (4-14)

At the other resonance crossover point when H_0 is in direction \vec{b} of Fig. 11 the lattice sum is

$$\sum_j (3 \cos^2 \theta_{ij} - 1)^2 / r_{ij}^6 = 57.10^{42} \text{ cm}^{-6} , \quad (4-15)$$

and the square root of the second moment is

$$(\langle \Delta H^2 \rangle)^{\frac{1}{2}} = \left[f(1-3f) \cdot 5.60 \cdot 10^4 \right]^{\frac{1}{2}} \text{ gauss}$$

→ 193 gauss for $T \rightarrow \infty$. (4-16)

Formulas (4-14) and (4-16) as functions of temperature are shown in Fig. 15 together with some measured values of the square roots of the second moments. The agreement is fair. But most of our measured values are too small, and this shows how easy it is to underestimate the intensity in the wings of an exchange-narrowed line. For $\vec{H}_0 \parallel \vec{b}$, however, the measured width is much larger than predicted at 77°K. This is probably caused by beginning spin-lattice relaxation broadening. At room temperature we find all lines to be significantly broadened.

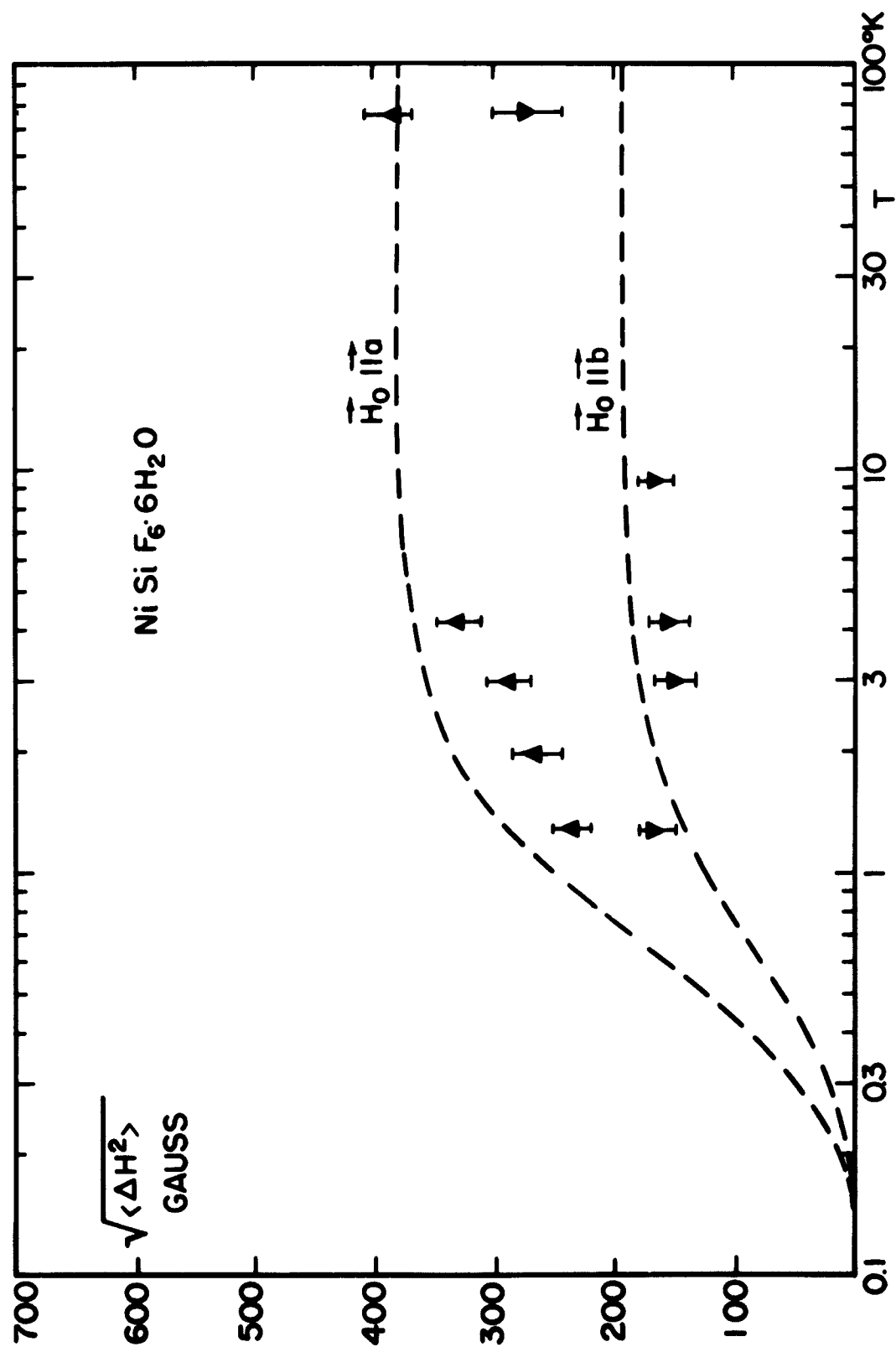


Fig. 15 Measured and Calculated Square Root of Second Moment in $\text{NiSiF}_6 \cdot 6\text{H}_2\text{O}$.

$6\text{H}_2\text{O}$ when the Magnetic Field is in a Direction where the Two Resonances Overlap.

Below 1°K the sample magnetization makes the moment calculation uncertain since the field is not along the spheroid axis. We are also likely to have experimental difficulties here because of too much signal, and therefore, no second moment measurements were made at the lowest temperature.

4.4. Discussion of the nickel fluosilicate results.

Our measurements of resonance line moments are in good agreement with the theory if we assume an isotropic, ferromagnetic interaction of strength $\tilde{A}_{ij} = -(3.9 \pm 0.4) \cdot 10^{-18}$ erg to the six nearest neighbors of each ion. We will now see how this compares with the results from other investigations.

The specific heat of $\text{NiSiF}_6 \cdot 6\text{H}_2\text{O}$ has been measured by Benzie and Cooke,⁷⁶ and the susceptibility has been found from the optical Faraday effect by Bequerel and Opechowski.⁶⁹ These results have been reanalyzed by Ollom and Van Vleck^{75,77} using the crystalline field splitting constant D given by paramagnetic resonance experiments. They found good agreement by assuming some exchange that would give a Curie temperature of $\theta = 0.1^\circ\text{K}$. From (3-24) this corresponds approximately to

$$\tilde{A} = -\frac{3k\theta}{2S(S+1)} = -3.5 \cdot 10^{-18} \text{ erg}$$

when we take the number of nearest neighbors to be $z = 6$. This is in close agreement with our result for \tilde{A} .

But earlier determinations of exchange strength from line moments served only to confuse the situation because of inadequate measurements. At room temperature we find the lines to be about 1800 gauss wide for \vec{H}_0 along the crystalline axis, but at 77°K they are only about 800 gauss wide. The resonance is obviously broadened by fast spin-lattice relaxation at room temperature, and one cannot use the lineshapes published by Holden, Kittel and Yager⁷¹ to determine the exchange as Ishiguro et al.⁶⁶ and Ollom⁷⁵ have done.

Trying to reconcile the linewidths with the magnetization and specific heat data, Ollom and Van Vleck^{77,75} introduced the possibility of anisotropic exchange. This would supposedly broaden the lines without giving much contribution to susceptibility and specific heat. In fairness, however, it should be said that they were not very happy with this explanation, and in the end they rather suspected the linewidth data.

Other support for the idea of anisotropic exchange seemed to come from the pressure experiments at room temperature by Walsh.⁶⁷ He expected to see the resonance line exchange-narrowed when the hydrostatic pressure caused the crystalline field splitting D to vanish. He attributed the failure to observe this to anisotropic exchange, but we have demonstrated that lifetime broadening at room temperature is the real cause and that the exchange is almost completely isotropic.

In Fig. 12, showing the shape of the resonances, there appears a weak line between the two main peaks. This line was also observed by Hempstead.⁷⁸ It could possibly be caused by two-photon transitions, but we found its relative intensity not to vary when we changed the microwave power level.

It is more likely that it is caused by some variation in the exchange and crystalline splitting parameters so that for a few percent of the spins $|D| < |\tilde{A}|$. Such variations can be caused by imperfections in the crystal lattice, by strain around cracks and impurities, etc. The resonance line for these ions will appear exchange-narrowed, and it will fall just between the two main lines.

From the relatively narrow lines observed in Zn-diluted $\text{NiSiF}_6 \cdot 6\text{H}_2\text{O}$ ⁷², it does not appear possible that the variation in D is sufficient to fulfill the condition $|D| < |\tilde{A}|$ for the required fraction of the spins. It is more likely that some pairs of spins are coupled by an exchange five times stronger than the average.

We investigated whether crushing of a crystal into a fine powder would strongly affect D or \tilde{A} by comparing the linewidth of the powder to the linewidth calculated from measurements on a single crystal in various field directions. The agreement was good, and no change of the constants by this treatment was detected.

CHAPTER 5

MEASUREMENTS ON COPPER POTASSIUM SULFATE AND COPPER SULFATE

5.1. Description of copper potassium sulfate.

Hydrated copper potassium sulfate, $K_2Cu(SO_4)_2 \cdot 6H_2O$, is a member of the long series of isomorphous double sulfates known as Tutton salts. The other salts in the series can be obtained by substituting for Cu^{++} : Mg, Zn, Cd, Ni, Co, Fe or Mn; for K^+ : Rb, Cs, (NH_4) or Tl, and the sulfate can be replaced by selenate. The salts are monoclinic with two ions per unit cell.

From goniometer and density measurements, Tutton⁷⁹ has given the topic axial ratios of $K_2Cu(SO_4)_2 \cdot 6H_2O$. We get the dimensions of the unit cell by multiplying these numbers by $(2/N)^{\frac{1}{3}} = 1.489 \cdot 10^{-8}$ cm where $N = 6.025 \cdot 10^{23}$ is Avogadro's number. We find

$$a_o = 9.040 \text{ \AA} \qquad b_o = 12.069 \text{ \AA} \qquad c_o = 6.141 \text{ \AA}.$$

The monoclinic angle is

$$\beta = 104^\circ 28'.$$

Hofmann⁸⁰ has x-ray analyzed a number of the salts, particularly the ammonia compounds. For $(NH_4)_2Mg(SO_4)_2 \cdot 6H_2O$, he found the space group to be C_{2h}^5 so that we can regard the position of the second molecule in the unit cell as being derived from the first

one by a translation from $(0, 0, 0)$ to $(\frac{1}{2}, \frac{1}{2}, 0)$ followed by a reflection in the ac -plane. The Mg^{++} ions are surrounded by distorted octahedrons of water molecules, four of which lie nearly in a square, each at a distance 1.9 \AA from the Mg^{++} and the other two at 2.15 \AA . The crystalline electric field should, therefore, have approximately tetragonal symmetry about the line joining the more distant waters. However, this structure has been criticized by Wyckoff,⁸¹ and anyway, we expect internal dimensions to be somewhat different in $K_2Cu(SO_4)_2 \cdot 6H_2O$.

The field of tetragonal symmetry will split the 2D -state of the free Cu^{++} ion and leave a Kramers' doublet some 20000 cm^{-1} below the other orbital levels.⁸² The tetragonal symmetry will be reflected via the spin-orbit coupling in an axial g -tensor for each of the two ions in the unit cell. However, if rhombic distortions are also present, there will be g -tensors with three principal axes, g_x , g_y and g_z .

The electron spin resonance behavior of the copper Tutton salts has been discussed by Bleaney and co-workers.^{83,84} Each magnetic complex can be described by the spin-Hamiltonian ($S = \frac{1}{2}$),

$$\mathcal{H}_0 = \beta \vec{H}_0 \cdot \vec{g} \cdot \vec{S} + \vec{S} \cdot \vec{B} \cdot \vec{I} + \vec{I} \cdot \vec{P} \cdot \vec{I} - \gamma \beta_n \vec{H}_0 \cdot \vec{I} \quad (5-1)$$

The copper isotopes ^{63}Cu (natural abundance 69 %) and ^{65}Cu (abundance 31 %) have both nuclear spin $I = \frac{3}{2}$. The tensor \vec{B} gives the electron-nucleus interaction. The tensor \vec{P} gives the electrostatic interaction with the nuclear electric quadrupole moment. The

last term in (5-1) is the direct interaction between the nuclear magnetic moment and the external field.

Susceptibility measurements on the Tutton salts are complicated by the presence of two ions per unit cell with different magnetic axes. If tetragonal symmetry for each ion is assumed, g -values can be deduced from the susceptibilities, but this assumption may not be warranted. In resonance measurements, however, one can find unambiguously the magnetic axis of each complex and the principal values of the g -tensors, but this is tedious work if the symmetry is rhombic.

In $K_2Cu(SO_4)_2 \cdot 6H_2O$ the directions for maximum $g = g_z$ is in the crystalline ab -plane making angles of about 45° with the a -axis.⁸⁴ In the concentrated salt, g_z is reported to be 2.36, but we have measured $g_z = 2.41$. In the plane perpendicular to this direction, g varies from 2.05 to 2.12 which signifies a considerable rhombic component of the crystalline field. In Zn-diluted salts, it is found that $g_z = 2.44$ and that the magnetic axis makes angles of $\alpha = (42 \pm 2)^\circ$ with the a -axis.⁸³

The spin-spin interaction broadens the resonance in concentrated salts, and only in magnetically diluted salts are the hyperfine lines seen separated. Normally, the allowed hyperfine transitions are those in which the nuclear orientation does not change ($\Delta m = 0$), but if the quadrupole interaction is comparable to the magnetic interaction, transitions corresponding to $\Delta m = \pm 2$ are also possible. In addition, $\Delta m = \pm 1$ transitions are allowed if the external magnetic field is not along a rhombic axis.

The hyperfine and quadrupole interaction constants are only 8% different for the two isotopes, and their weighted means are⁸³

$$B_z = (103 \pm 5) 10^{-4} \text{ cm}^{-1} ,$$

$$B_{\perp} = (34 \pm 5) 10^{-4} \text{ cm}^{-1} \text{ (measured in ab-plane)} ,$$

$$P = \frac{3}{2} P_z = (11 \pm 1) 10^{-4} \text{ cm}^{-1} ,$$

$$P_x = P_y \text{ is small} .$$

With the field along the magnetic z-axis of one type of ion, the hyperfine lines corresponding to $\Delta m = 0$ of this ion are shifted in energy by

$m = +3/2$	$h \Delta \nu = +3/2 B_z$	$\Delta H = -138 \text{ gauss}$
$m = +1/2$	$h \Delta \nu = +1/2 B_z$	$\Delta H = -46 \text{ gauss}$
$m = -1/2$	$h \Delta \nu = -1/2 B_z$	$\Delta H = 46 \text{ gauss}$
$m = -3/2$	$h \Delta \nu = -3/2 B_z$	$\Delta H = 138 \text{ gauss} . (5-2)$

Here we have used $g_z = 2.41$.

For other orientations, the splittings are smaller and more lines may appear.

Some weak exchange has been observed in $\text{K}_2\text{Cu}(\text{SO}_4)_2 \cdot 6\text{H}_2\text{O}$. This will be discussed in connection with the results of our first moment shifts in Section 5.3 .

5.2. First moment changes.

We have measured an approximately spherical sample of $\text{K}_2\text{Cu}(\text{SO}_4)_2 \cdot 6\text{H}_2\text{O}$ at 30.00 kMc/s, so mounted in the waveguide

spectrometer that the external field could be rotated in the crystalline ab-plane. The field direction could then be made parallel to the tetragonal axis of one of the magnetic complexes, and we observed two resonances with $g = g_z = 2.41$ (called line I below) and with $g = 2.11$ (line II). When the field was rotated 45° away from this position, the two lines did overlap as expected.

Line II is relatively narrow and appears symmetric at all temperatures. Line I is much broader because of the larger hyperfine splitting, and it becomes very unsymmetric at low temperatures as shown in Fig. 16. No separation of the hyperfine components is seen, and the line narrows at low temperature to a halfwidth of about 200 gauss as compared to the predicted hyperfine width of 280 gauss. In Fig. 17a we show the first moment shifts of the two lines when the field is in the direction of maximum line separation, and in Fig. 17b we show the change in line position when the field is along the crystalline b-axis and the two lines overlap.

When another sample of this salt, which had considerably better spherical shape, was measured, we found the resonance at the line overlap position to broaden below 1°K and split up into a number of separate peaks. The positions of the peaks did not correspond to the positions of the hyperfine lines calculated from (5-1). We, therefore, believe that these peaks must be the magnetostatic modes briefly explained in Section 1.8, and which will be discussed again in Section 5.5.

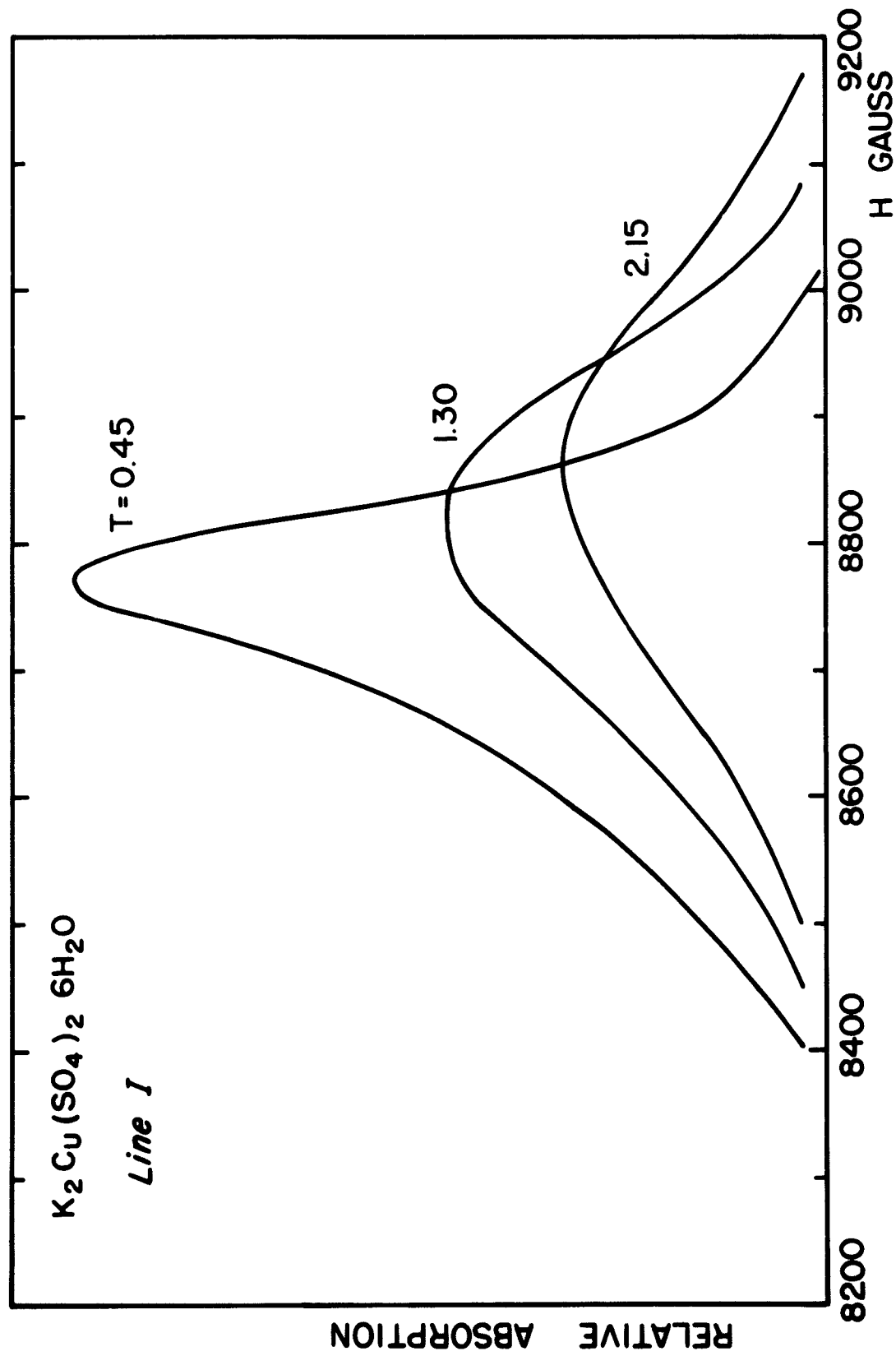


Fig. 16 Shape of Resonance Line I in $\text{K}_2\text{Cu}(\text{SO}_4)_2 \cdot 6\text{H}_2\text{O}$ as Function of Temperature.

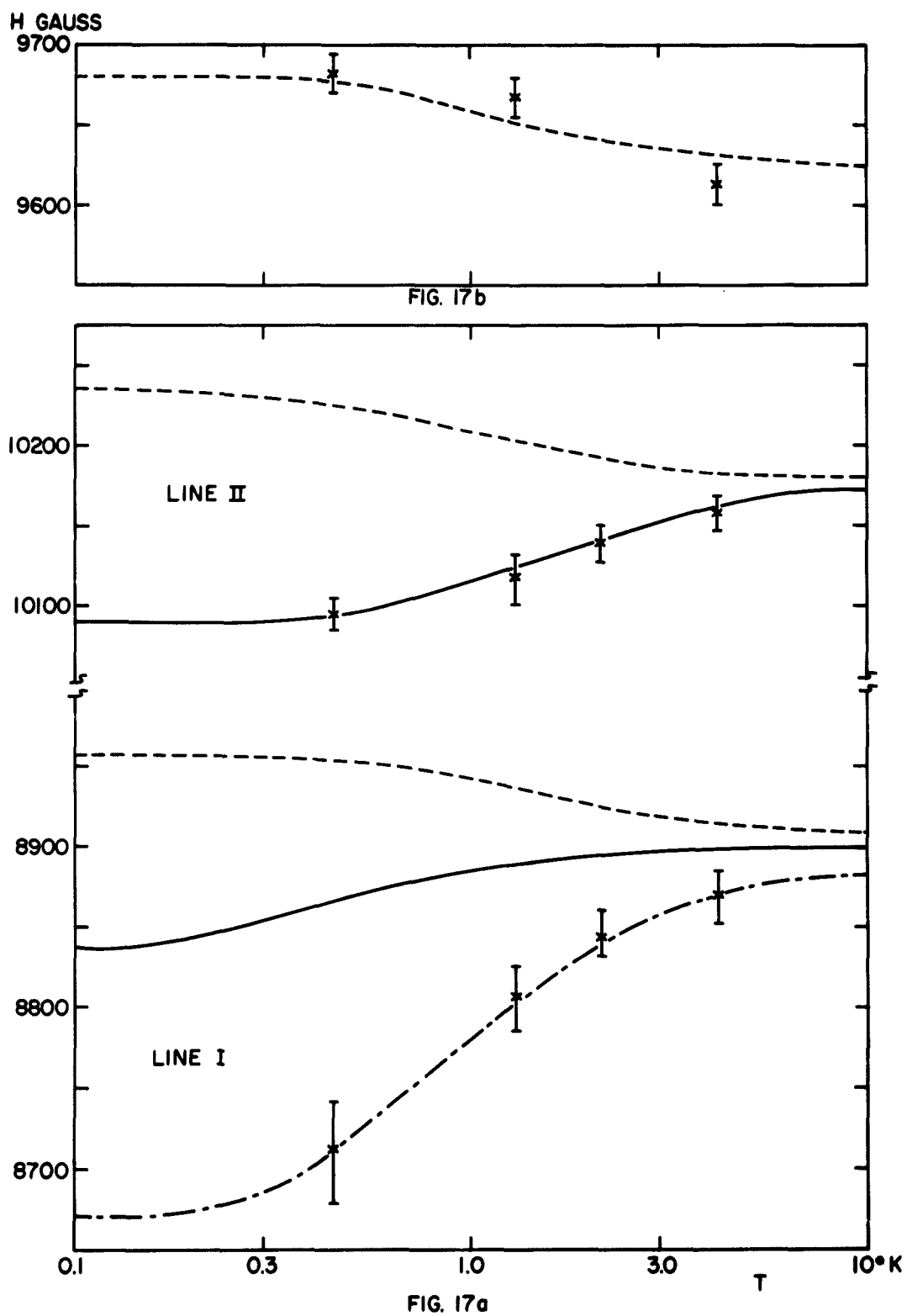


Fig. 17 First Moment Shift of Resonance in $K_2Cu(SO_4)_2 \cdot 6H_2O$.

Fig. 17a. Field Angle 45° With Respect to Crystal Axes a and b.

Fig. 17b Field Parallel to b-Axis.

An exact calculation of the lineshifts from the first moment theory is hardly possible because of the rhombic character of the two g -tensors. We will use formulas (1-24) and (1-43) with the measured g -values and use at first the usual criterion that unseparated lines mean like spins. Different g -values in directions perpendicular to \vec{H}_0 will cause small changes in transition probabilities and possibly in lineshapes, but any such effect will be ignored.

For the field along the b -axis, all spins are like and the lattice sum is found to be

$$\sum_j' (3 \cos^2 \theta - 1) / r_{ij}^3 = -3.7 \cdot 10^{21} \text{ cm}^{-3} \quad (5-3)$$

From (1-24), the first moment shift should then be for $g \approx 2.23$, and $g\beta H = 1 \text{ cm}^{-1}$

T	=	0	0.5	1.0	2.0	4.0	∞ °K
$\langle \Delta H \rangle$	=	57	51	36	19	10	0 gauss

This calculated shift is plotted in Fig. 17b, and we see that the agreement with the experimental values is not too bad.

When we observe two lines, we have to calculate the lattice sums separately for like and unlike neighbors. With \vec{H}_0 in the ab -plane making an angle of 45° with \vec{a} the sums are

$$\left[\sum_j' (3 \cos^2 \theta_{ij} - 1) / r_{ij}^3 \right]_{\text{like}} = -6.6 \cdot 10^{21} \text{ cm}^{-3} \quad (5-4)$$

$$\left[\sum_{k'} (3 \cos^2 \theta_{ik'} - 1) / r_{ik'}^3 \right]_{\text{unlike}} = 5.2 \cdot 10^{21} \text{ cm}^{-3} \quad (5-5)$$

The dipolar shift is from (1-43) ,

$$\begin{aligned} \langle \Delta H \rangle_{\text{dip}} = & - \frac{1}{2} \left\{ \text{Tanh} \left(\frac{g_{\parallel} \beta H_0}{2 kT} \right) \frac{(2g_{\parallel}^2 + g_{\perp}^2)\beta}{2g_{\parallel}} \left[\sum_j \right]_{\text{like}} \right. \\ & \left. + \text{Tanh} \left(\frac{g_{\perp} \beta H_0}{2 kT} \right) g_{\perp} \beta \left[\sum_k \right]_{\text{unlike}} \right\} \quad (5-6) \end{aligned}$$

For line I we find the shift by using $g_{\parallel} = 2.41$, $g_{\perp} = 2.11$ and $g_{\parallel} \beta H_0 = 1 \text{ cm}^{-1}$, and for line II we have to use $g_{\parallel} = 2.11$, $g_{\perp} = 2.41$ and $g_{\parallel} \beta H_0 = 1 \text{ cm}^{-1}$. Some numerical values are :

T	=	0	0.5	1.0	2.0	4.0	$\infty^\circ \text{ K}$
$\langle \Delta H \rangle_{\text{I dip}}$	=	51	47	36	20	11	0 gauss
$\langle \Delta H \rangle_{\text{II dip}}$	=	54	41	28	14	7	0 gauss .

These calculated dipolar shifts are indicated by the broken lines in Fig. 17a . The difference between $\langle \Delta H \rangle_{\text{dip}}$ and the experimental values must be caused by exchange between unlike ions.

The first moment change, because of exchange to z unlike nearest neighbors, is from (1-43).

$$\langle \Delta H \rangle_{\text{ex}} = \frac{1}{2} \text{Tanh} \left(\frac{g_{k'} \beta H_0}{2 kT} \right) \frac{z \tilde{A}_{ik'}}{g_i \beta} \quad (5-7)$$

The dipolar plus exchange shifts give the best fit to the experimental values for line II if we choose $\tilde{A}_{ik} = -1.4 \cdot 10^{-18}$ erg, which is a ferromagnetic exchange. Then we have for $z = 4$, nearest, unlike neighbors

T	=	0	0.5	1.0	2.0	4.0	$^{\circ}\text{K}$
$\langle \Delta H \rangle_{\text{Iex}}$	=	-126	-106	-70	-38	-20	0 gauss
$\langle \Delta H \rangle_{\text{IIex}}$	=	-143	-133	-96	-56	-29	0 gauss .

$\langle \Delta H \rangle_{\text{ex}} + \langle \Delta H \rangle_{\text{dip}}$ are shown in full lines in Fig. 17a, and it is seen that the agreement with the experimental shifts of line I is very poor. Even if we assumed the dipolar sums to be in error, it does not seem possible to explain the first moment shifts of both lines with the same isotropic exchange between unlike spins. Neither will it help to postulate anisotropic exchange, since any reasonable type of this will shift the lines the same way and by about the same amount.

We will now discuss qualitatively a possible explanation for the difference in line shift. Isotropic exchange between the spins resonating in line I will not change the first moment of the line at low temperature if we do not restrict spin-flips. This we would have to do if the hyperfine interaction were so strong that we could see the line split into $2I + 1 = 4$ separate components. We do not observe a split line I in $\text{K}_2\text{Cu}(\text{SO}_4)_2 \cdot 6\text{H}_2\text{O}$. This must mean that spin-flips are allowed at least between neighboring hyperfine components and that a re-arrangement within the spin system can easily take up

the energy difference $(\Delta m = 1) B_z$. But it does not necessarily mean that flips between spins of nuclear quantum number $m = \frac{3}{2}$ and $m = -\frac{3}{2}$ are permitted with the same probability, since this involves an energy difference of $(\Delta m = 3)B_z$.

The idea here is essentially the same as the cross relaxation discussed by Bloembergen and co-workers.⁸⁵ Spin-flips that do not conserve energy are not completely prohibited, but they occur with a probability that decreases exponentially as the energy difference increases. Here our interest is in a case where the probability for spin-flips of $\Delta m = 3$, and perhaps $\Delta m = 2$, is sufficiently reduced so that these processes do not influence the resonance lineshape. But considered as a cross relaxation, these flips may still occur at a very fast rate compared to the spin-lattice relaxation.

If exchange spin-flips between the hyperfine components are to be only partly allowed, we must require the order of magnitude exchange field H_e to be somewhat less than 280 gauss from each of the two like neighbors 6.14 \AA away. This limit is considerably higher than the dipolar interaction between the same spins. From

$$H_e = \frac{\tilde{A} S_{zi} S_{zj}}{S_{zi} g\beta} \quad (5-8)$$

we find $|\tilde{A}| < 12 \cdot 10^{-18} \text{ erg.}$

If we, for example, assume that spin-flips of $\Delta m = 2$ and $\Delta m = 3$ must be excluded, then on the average $3/8$ of the spins of

type I would appear unlike to other spins of type I. The resulting first moment shift $\langle \Delta H \rangle_{\text{Iex}}^*$ is given by (5-7) when we use $z = 2 \cdot \frac{3}{8}$. To get calculated shifts in agreement with the experimental data, we choose $\tilde{A} = -10 \cdot 10^{-18}$ erg and find

T	=	0	0.5	1.0	2.0	4.0	∞° K
$\langle \Delta H \rangle_{\text{Iex}}^*$	=	-168	-150	-105	-57	-28	0 gauss

The sum, $\langle \Delta H \rangle_{\text{Idip}} + \langle \Delta H \rangle_{\text{Iex}} + \langle \Delta H \rangle_{\text{Iex}}^*$ is shown as the dash-dot line in Fig. 17a.

The choice of $\tilde{A} = -10 \cdot 10^{-18}$ erg is in good agreement with the condition derived from (5-8). But it should be stressed that a different restriction on the spin-flips will give a different result.

The hyperfine broadening of line II is much smaller, and all spins of this kind can probably be treated as sufficiently similar so that the exchange between them will not shift this line.

Because of the hyperfine contribution to linewidth, no attempt was made to measure the second moment of the lines or compare it to calculated values.

5.3. Discussion of exchange in $\text{K}_2\text{Cu}(\text{SO}_4)_2 \cdot 6\text{H}_2\text{O}$.

Measurements of first moment shifts of resonance lines will only give information about exchange between non-identical spins. This may be of value in complicated crystals to separate the various exchange interactions. We attempted unsuccessfully to explain the

observed line shift in $\text{K}_2\text{Cu}(\text{SO}_4)_2 \cdot 6\text{H}_2\text{O}$ on the basis of some isotropic exchange between the two ions in the unit cell. However, we could get agreement if we assumed that the hyperfine interaction for spins in line I was strong enough to reduce the probability for the spin-flips within the line, and in this way we could guess the order of magnitude exchange interaction between ions in the same lattice positions. Before we go on to compare these results to other data on the strength of the exchange, we should note that this suggestion of partly hyperfine-hindered spin-flips will also help to explain the observed asymmetry of line I. Some of the spins are free to spin-flip with their like neighbors; their resonance frequency is not shifted, and the line should be exchange-narrowed. This would account for the rather sharp peak seen in Fig. 16 for $T = 0.45^\circ$. Other spins are restricted in their spin-flips; their resonance frequencies are then shifted towards lower fields by the ferromagnetic interaction. The maximum shift would be

$$\Delta H = \frac{z_{\text{like}} \cdot \tilde{A} / 2}{g_{\parallel} \beta} = -450 \text{ gauss} , \quad (5-9)$$

and this is about the length of the line tail we see in Fig. 16 .

The Curie temperature of $\text{K}_2\text{Cu}(\text{SO}_4)_2 \cdot 6\text{H}_2\text{O}$ has been derived from susceptibility and specific heat measurements on powdered samples. DeKlerk⁸⁶ found $\theta = 0.054^\circ\text{K}$; data of Kramers et al.⁸⁷ seemed to be in agreement with this, but Garrett⁸⁸ and Benzie and

Cooke⁷⁶ have found $\theta = 0.034^\circ\text{K}$ and $\theta = 0.035^\circ\text{K}$, respectively. The interaction is ferromagnetic. Dipolar interactions contribute to this Curie temperature, and Daniels⁵⁹ has given a rather complicated formula for θ_{dip} in Tutton salts, taking account of the two different ions in the unit cell. However, the Curie temperature from dipolar interactions will only be of the order 0.001°K , and in view of the variations in the measured θ , it is of little consequence to neglect the dipolar contribution to θ .

We can relate the Curie temperature to the strength of the exchange by the approximate formula (3-24). Since, in this case, we probably have an exchange \tilde{A}_1 to $z_1 = 2$ like nearest neighbors and \tilde{A}_2 to $z_2 = 4$ unlike nearest neighbors, we should write

$$\theta = - \frac{(\tilde{A}_1 z_1 + \tilde{A}_2 z_2) S(S+1)}{3k} \quad (5-10)$$

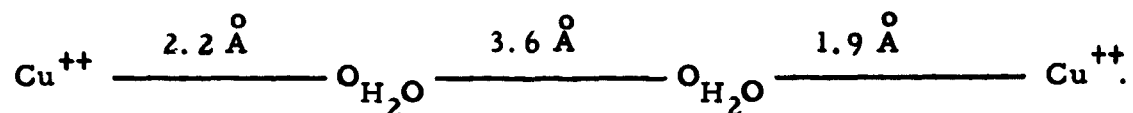
In the previous section we found that the first moment changes could best be explained by assuming $\tilde{A}_2 = -1.4 \cdot 10^{-18}$ erg. Then we can solve (5-10) for \tilde{A}_1 and find

$$\tilde{A}_1 = - \frac{40k}{z_1} - \frac{\tilde{A}_2 z_2}{z_1} = \begin{cases} -7 \cdot 10^{-18} \text{ erg for } \theta = 0.035^\circ\text{K} \\ -12 \cdot 10^{-18} \text{ erg for } \theta = 0.054^\circ\text{K} \end{cases} \quad (5-11)$$

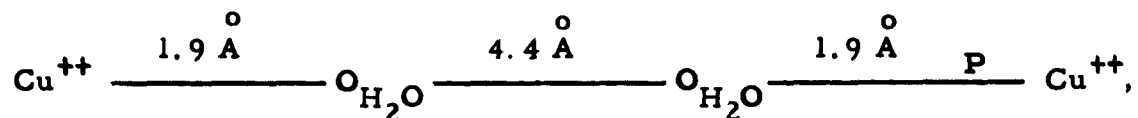
This is surprisingly close to the very speculative value $\tilde{A}_1 = -10 \cdot 10^{-18}$ erg derived on the assumption of some restriction on

spin-flips between hyperfine lines. However, no great faith should be put on this particular value of \tilde{A}_1 ; all that can safely be said is that it appears likely that the exchange between like nearest neighbors in $K_2Cu(SO_4)_2 \cdot 6H_2O$ is somewhat stronger than the exchange between unlike neighbors.

This also appears reasonable from the crystalline structure. From the published atomic positions⁸⁰ (which have been criticized), we find the most likely exchange path between like neighbors as



Unlike neighbors would have to be coupled via the longer path



and one would guess that this interaction is weaker.

5.4. Description of copper sulfate.

The crystal structure of $CuSO_4 \cdot 5H_2O$ has been investigated by Beevers and Lipson.⁸⁹ The unit cell is triclinic and has the following dimensions :

$$\begin{array}{lll} a_o = 6.12 \text{ \AA} & b_o = 10.7 \text{ \AA} & c_o = 5.97 \text{ \AA} \\ a = 82^\circ 16' & \beta = 107^\circ 26' & \gamma = 102^\circ 40' \end{array}$$

There are two inequivalent copper ions in the unit cell on the positions $(0, 0, 0)$ and $(\frac{1}{2}, \frac{1}{2}, 0)$. Each of them is surrounded by an

approximate octahedron of oxygen atoms, belonging to four water molecules and two sulfate ions. We expect the crystalline field to be mainly cubic, but with a tetragonal component along the line joining the two sulfate oxygens. The angle between the tetragonal axis of the two copper ions is about 82° .

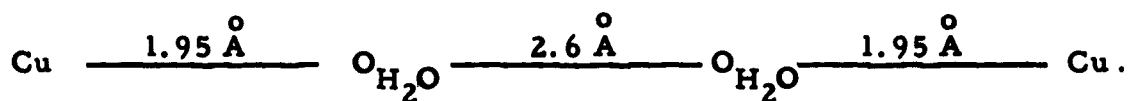
As in $\text{K}_2\text{Cu}(\text{SO}_4)_2 \cdot 6\text{H}_2\text{O}$, the field of tetragonal symmetry will leave a Kramers' doublet with an axial g -tensor as the lowest state of the Cu^{++} ion.

From susceptibility measurements, one can deduce the values $g_{\parallel} = 2.47$ and $g_{\perp} = 2.06$, and the directions of the magnetic axes are in good agreement with what is expected from the crystalline structure.⁹⁰ These g -values have not been checked directly by resonance measurements, since the presence of considerable exchange interaction between the unlike ions tends to broaden the lines and make them overlap. Even with a frequency as high as 35 kMc/s, Bagguley and Griffiths⁹¹ are just barely able to separate the lines associated with the two non-equivalent crystal sites. At room temperature, the apparent g -factors are $g_{\parallel} = 2.37$ and $g_{\perp} = 2.12$. For directions of the field where the two resonances overlap, the line is strongly exchange-narrowed.

No hyperfine lines have been previously reported in $\text{CuSO}_4 \cdot 5\text{H}_2\text{O}$ since this salt cannot be magnetically diluted by Zn, Mg or Cd. However, we expect the hyperfine splitting to be of the same order as in $\text{K}_2\text{Cu}(\text{SO}_4)_2 \cdot 6\text{H}_2\text{O}$ which has similar g -values.

From susceptibility measurements, it has been observed that the exchange leads to an anisotropic Curie temperature of about -0.6°K .⁹² This is supported by specific heat measurements by Geballe and Giaugue⁹³ who found a specific heat maximum around 1°K . But the entropy associated with the integrated specific heat peak turned out to be only $\frac{1}{2} R \ln 2$, half of the expected value for an ensemble of identical spins of $S = \frac{1}{2}$. Geballe and Giaugue then suggested that the ions in the unit cell are different and only ions of one kind couple together to give a Curie temperature $\theta = -0.6^{\circ}$.

This idea has been developed further by Miedema et al.⁹⁴ in a recent paper that arrived only after we had started measurements on $\text{CuSO}_4 \cdot 5\text{H}_2\text{O}$. They measured susceptibility and specific heat of this salt down to 0.03°K and found two Curie temperatures and specific heat anomalies. The relatively strong antiferromagnetic coupling giving rise to $\theta = -0.6^{\circ}$ they associate with the ions on crystalline sites $(\frac{1}{2}, \frac{1}{2}, 0)$ (system I). These spins are linked together in a direction parallel to the c-axis via two water oxygens as follows :



A much weaker ferromagnetic coupling giving another Curie temperature of about 0.02°K they associate with the spins on sites $(0, 0, 0)$ (system II), which are coupled via a minimum of three oxygens between equal Cu^{++} neighbors.

The two systems are coupled together with an exchange strength that is very roughly estimated from the resonance lineshape to be about 0.15 cm^{-1} at room temperature.^{95,96} We find this exchange to increase with decreasing temperature, and it is perhaps 50% stronger at helium temperatures.

The coupling between the spin systems has a consequence for susceptibility measurements not pointed out by Miedema et al.⁹⁴ At a temperature so low that system I already is in the antiferromagnetic state, this coupling between unlike spins will tend to align system II antiferromagnetically. The observed weak ferromagnetic coupling in system II must then be the net effect of a ferromagnetic coupling between like spins almost cancelled by a coupling to the antiferromagnetically ordered system of unlike spins.

5.5. Measurements on copper sulfate and discussion of observed magnetostatic modes.

We have measured an almost perfect sphere of $\text{CuSO}_4 \cdot 5\text{H}_2\text{O}$ in the waveguide spectrometer. However, it was very hard to x-ray orient the sample since we had no clue from external faces to explain the Laue patterns from this triclinic crystal. In the end, we, therefore, looked at the resonance of the sample in the cavity spectrometer at room temperature where it was rather easy to move it around until we saw the two resonances fairly well separated. Then the field had to be almost parallel to one of the tetragonal axes, and this was the orientation we used for the low temperature work.

But at 77°K the two resonances had merged into one broad line.

This might be caused by :

- a) The principal values of the g-tensors change in this temperature range.
- b) The exchange between unlike spins changes.

With kind help from Dr. Foner at M.I.T. we attempted to find out what was happening by measuring the crystal at 105 kMc/s at 300°K and 77°K . At this frequency the resonances were far apart at room temperature, but they broadened and moved somewhat towards each other as the temperature was lowered. Although the evidence is not quite conclusive, the exchange appeared to increase when the sample was cooled. Qualitatively, this is what we expect to happen when the lattice contracts and the atoms move closer together.

If we assume that the effect of the exchange in this case can be approximated by the Markoffian random modulation model developed by Anderson,⁷ we see from his Fig. 2 that ω_e/ω_0 must change from about 0.5 at room temperature to at least 0.7 at 77°K . This increase of 40 % in the exchange is rather more than one might expect from a slight thermal contraction of the lattice.

A similar and even larger increase in the exchange is observed by Abe⁹⁷ in $K_2CuCl_4 \cdot 2H_2O$, and we have confirmed this result. At room temperature one has to measure at a frequency larger than 50 kMc/s to see two separate resonances from the two differently oriented magnetic complexes in the unit cell of this salt.⁹⁸ For a frequency of

30 kMc/s, the composite line is about 1200 gauss wide at 300°K, but at 77°K we find the width narrowed to about 200 gauss. This is the order of magnitude exchange-narrowing we expect from the interaction giving a reported Curie temperature of 0.8°K.¹⁹

Fig. 18 shows the change of the resonance in $\text{CuSO}_4 \cdot 5\text{H}_2\text{O}$ at low temperatures when the field is in a direction where the two resonances are separated at room temperature. The first moment of the line clearly changes as we reduce the temperature, but we will not attempt to explain this quantitatively from spin-spin interaction, since the exchange couplings are complex and the g-values and sample orientation are uncertain. However, the line behavior below 1°K is striking. The line broadens and splits up into a number of separate peaks. A similar behavior of the resonance is seen for other orientations of the magnetic field. We have also observed peaks of the same kind in a good sphere of $\text{K}_2\text{Cu}(\text{SO}_4)_2 \cdot 6\text{H}_2\text{O}$ at 0.5°K when H_0 was in a direction where the two resonances overlap.

We first thought that these were hyperfine lines although their positions did not agree very well with the spin-Hamiltonian (5-1) for $\text{K}_2\text{Cu}(\text{SO}_4)_2 \cdot 6\text{H}_2\text{O}$. From the random modulation model of exchange-narrowing by Anderson and Weiss,⁶ one may be misled to believe that the spin-flips should be frozen out and the modulation cease at $T = 0$. This is not so. If we are to observe the resonance, some spins must be excited by the microwave field and these spins are then free to flip with their neighbors in the ground state provided that the

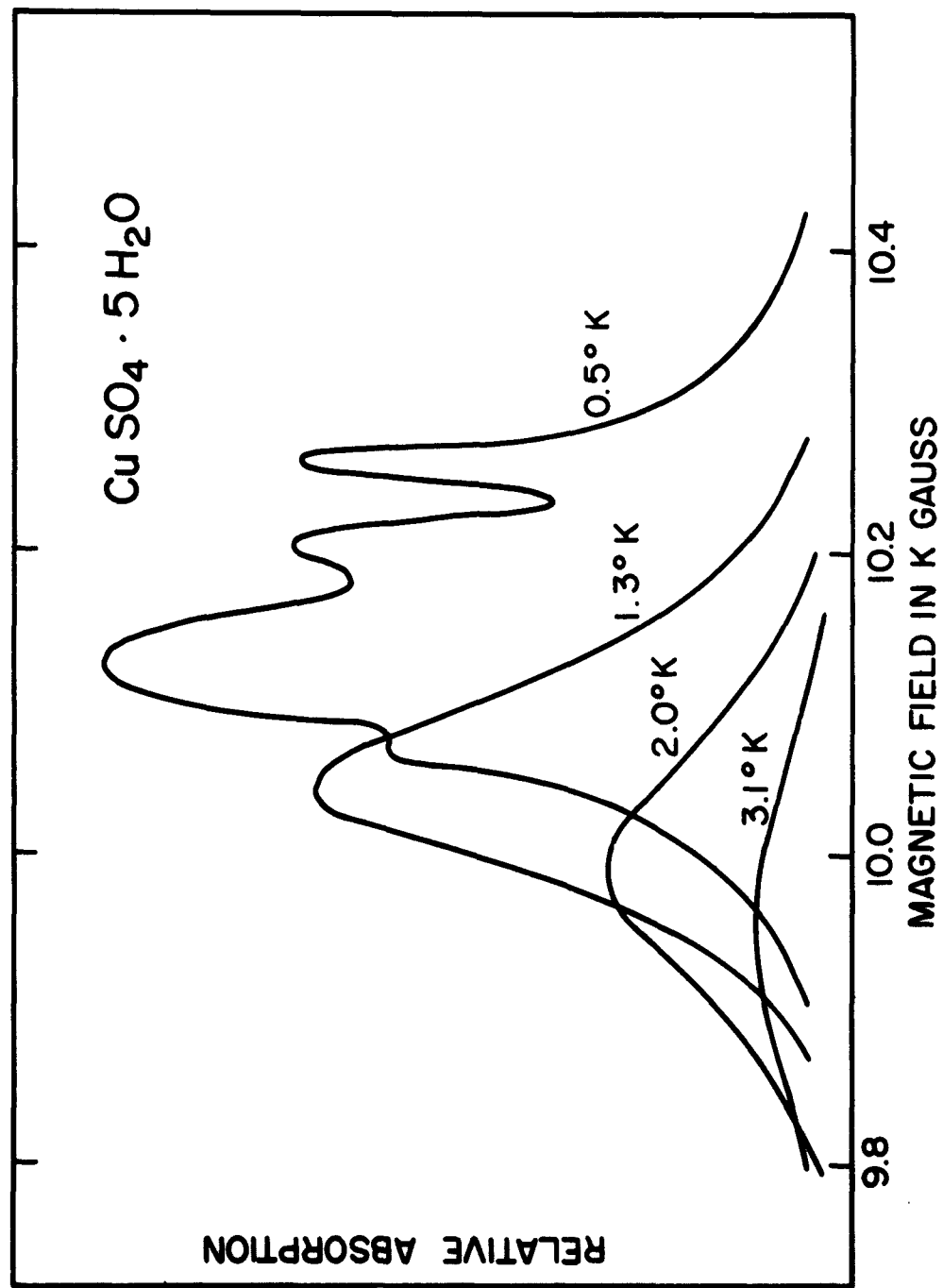


Fig. 18 Shape of Resonance Line in $\text{CuSO}_4 \cdot 5\text{H}_2\text{O}$ as Function of Temperature.

exchange between them is stronger than the possible difference in hyperfine or Zeeman energy. Hyperfine lines masked by spin-spin interaction at high temperature should, therefore, not appear separated when $T \rightarrow 0$, and this cannot explain the observed lineshape.

It is more likely that these peaks are the magnetostatic modes that, in principle, may appear in the resonance of any magnetized body regardless of whether the spin alignment is caused by strong exchange or by low temperature and strong field. In $K_2CuCl_4 \cdot 2H_2O$, such modes have been observed by Abe et al.¹⁹ to branch out from the main resonance below $2.2^\circ K$ when measured at 25 kMc/s. The microwave field in our experiment is probably sufficiently nonuniform to make excitation of magnetostatic modes possible. If so, why should they not then appear around $2^\circ K$ as in $K_2CuCl_4 \cdot 2H_2O$? The saturation magnetization of $CuSO_4 \cdot 5H_2O$ is about 20 % larger than in $K_2CuCl_4 \cdot 2H_2O$, and we also did the work in a stronger field than Abe et al.

This can be explained by the difference between the ferromagnetic coupling in $K_2CuCl_4 \cdot 2H_2O$ that aids the external field in aligning the spins and the antiferromagnetic coupling in spin system I in $CuSO_4 \cdot 5H_2O$ that opposes alignment. The magnetization $p(T)$ relative to the saturation magnetization of $K_2CuCl_4 \cdot 2H_2O$ in a magnetic field H_0 can be found by solving graphically the equation

$$p = \tanh \left(\left(\frac{1}{2} g \beta H_0 + pA \right) / kT \right) . \quad (5-13)$$

The strength of the exchange A is given by the condition that for $H_0 \rightarrow 0$ the equation (5-13) has to give spontaneous magnetization for the Curie temperature $T = 0.8^\circ \text{K}$, so we find $A/k = 0.8$. Then we get for $g \beta H_0 = 25 \text{ kMc/s}$:

T	$=$	2.2	2.0	1.8	1.5	1.0°K
$p = M(T)/M_0$	$=$	0.40	0.45	0.51	0.62	0.86
$P(A = 0)$	$=$	0.265	0.29	0.32	0.38	0.54

Because of the strong exchange, the magnetization is considerably stronger at a given temperature than what it would be in the external field alone, which is given as $P(A = 0)$.

In $\text{CuSO}_4 \cdot 5\text{H}_2\text{O}$, spin system I can give only a small contribution to the magnetization since the antiferromagnetic coupling in this system giving a Curie temperature of -0.60° is comparable to the force of the external field. Then only below 1°K is system II 80-90% aligned for $g \beta H = 30 \text{ kMc/s}$, and only there can this system alone give a magnetization comparable to that of $\text{K}_2\text{CuCl}_4 \cdot 6\text{H}_2\text{O}$ around 2°K .

The maximum separation of modes in $\text{CuSO}_4 \cdot 5\text{H}_2\text{O}$ is about 200 gauss. This is a reasonable splitting since from Walker's theory,²⁰ the maximum separation should be $\Delta H = 2\pi M$. At $T \approx 0.5$, the magnetization in $\text{CuSO}_4 \cdot 5\text{H}_2\text{O}$ is $M \approx \frac{1}{2} M_0 \approx 30 \text{ gauss}$ for $g \beta H_0 = 1 \text{ cm}^{-1}$ so that $2\pi M \approx 200 \text{ gauss}$.

In $\text{K}_2\text{Cu}(\text{SO}_4)_2 \cdot 6\text{H}_2\text{O}$, the saturation magnetization $M_0 = S g \beta N_1$ is only about 32 gauss compared to about 47 gauss in $\text{K}_2\text{Cu Cl}_4 \cdot 2\text{H}_2\text{O}$. Since the exchange in this salt is weak, it also has to be cooled below 1°K before the magnetization becomes comparable to that of $\text{K}_2\text{Cu Cl}_4 \cdot 2\text{H}_2\text{O}$ around 2°K . We tried to measure the position of the modes in $\text{K}_2\text{Cu}(\text{SO}_4)_2 \cdot 6\text{H}_2\text{O}$ as a function of the temperature, but we could not clearly establish that the splitting was proportional to the magnetization as required for Walker modes because the modes were well separated only below 0.5°K .

The conclusion that our observed peaks are magnetostatic modes is also supported by the fact that we see them only in the most spherical samples. In samples of more irregular shape, the modes will be poorly defined, broad and difficult to excite. The use of poor spheres may be the reason why we did not see them in $\text{Nd}(\text{C}_2\text{H}_5\text{SO}_4)_3 \cdot 9\text{H}_2\text{O}$ and $\text{NiSiF}_6 \cdot 6\text{H}_2\text{O}$ where the saturation magnetization is 28 and 86 gauss, respectively. We then have the paradox that a sample of less than perfect shape may actually give the narrowest resonance line when measured below 1°K .

Whether magnetostatic modes can be seen as separate lines obviously also depends upon how wide the uniform resonance is. Excited modes of nearly the same energy will give only one broad line.

CHAPTER 6

RESONANCE LINE BROADENING FROM VARIATION IN CRYSTALLINE FIELD

6.1. Introduction.

The resonance linewidth experiments described in this chapter were undertaken to investigate the practical possibility of a frequency-stable, zero-field maser oscillator suggested by Professor Bloembergen.⁹⁹ His idea is as follows:

A paramagnetic material for a maser oscillator used as a frequency standard should have very narrow resonance lines. Interaction between like spins can be reduced to give negligible line broadening by diluting the crystal with non-magnetic material. But the nuclear moments of protons and other magnetic nuclei will still give a local field variation of a few gauss. This will normally result in a minimum linewidth of the order of 20 Mc/s, and when such a salt is used in a maser oscillator, the resulting frequency will not be particularly stable.

But consider an ion with integral spin in a crystalline field of rhombic or lower symmetry. The $2S + 1$ spin levels are then completely split by the crystalline field, and this makes maser operation possible without an external field.¹⁰⁰ If a weak field H_0 is applied, the magnetic moment operator has no diagonal matrix elements in the representation where the spin-Hamiltonian is diagonalized. The energy levels will then only depend on H_0 in the second order, and

the local field fluctuations from unlike spin neighbors can only cause a negligible broadening of the resonance. Interaction between like ions, however, will broaden the line because of the spin-flips, but this effect can be reduced by diluting the crystal.

An example of a possible zero-field maser system is the Ni^{++} ion of spin $S = 1$ in the rhombic field of hydrated double sulfates. The structure of the monoclinic Tutton salts were described in Section 5.1. There are two ions in the unit cell and their magnetic axes are related by reflection in the symmetry plane ac of the crystal. This is shown schematically in Fig. 19a, where the magnetic axes for each complex are labelled x , y , and z ; the macroscopic susceptibility axes are K_1 , K_2 , and K_3 , and the monoclinic crystal axes are a , b , and c .

The magnetic properties of each complex can be described by a spin-Hamiltonian¹⁰¹

$$\mathcal{H}_0 = g\beta \vec{H}_0 \vec{S} + D(S_z^2 - \frac{2}{3}) + E(S_x^2 - S_y^2). \quad (6-1)$$

When the external field is along the z -axis of one spin, its energy levels are

$$\begin{aligned} \lambda_1 &= \frac{1}{3}D + (E^2 + g^2\beta^2 H_0^2)^{\frac{1}{2}} \xrightarrow{H_0 \rightarrow 0} \frac{1}{3}D + E + g^2\beta^2 H_0^2/2E \\ \lambda_2 &= -\frac{2}{3}D \\ \lambda_3 &= \frac{1}{3}D - (E^2 + g^2\beta^2 H_0^2)^{\frac{1}{2}} \xrightarrow{H_0 \rightarrow 0} \frac{1}{3}D - E - g^2\beta^2 H_0^2/2E. \end{aligned} \quad (6-2)$$

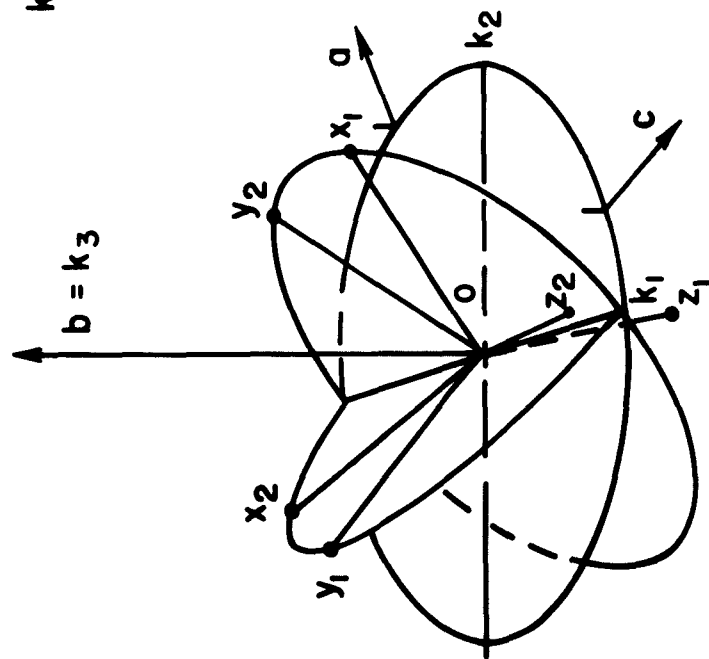


FIG. 19a

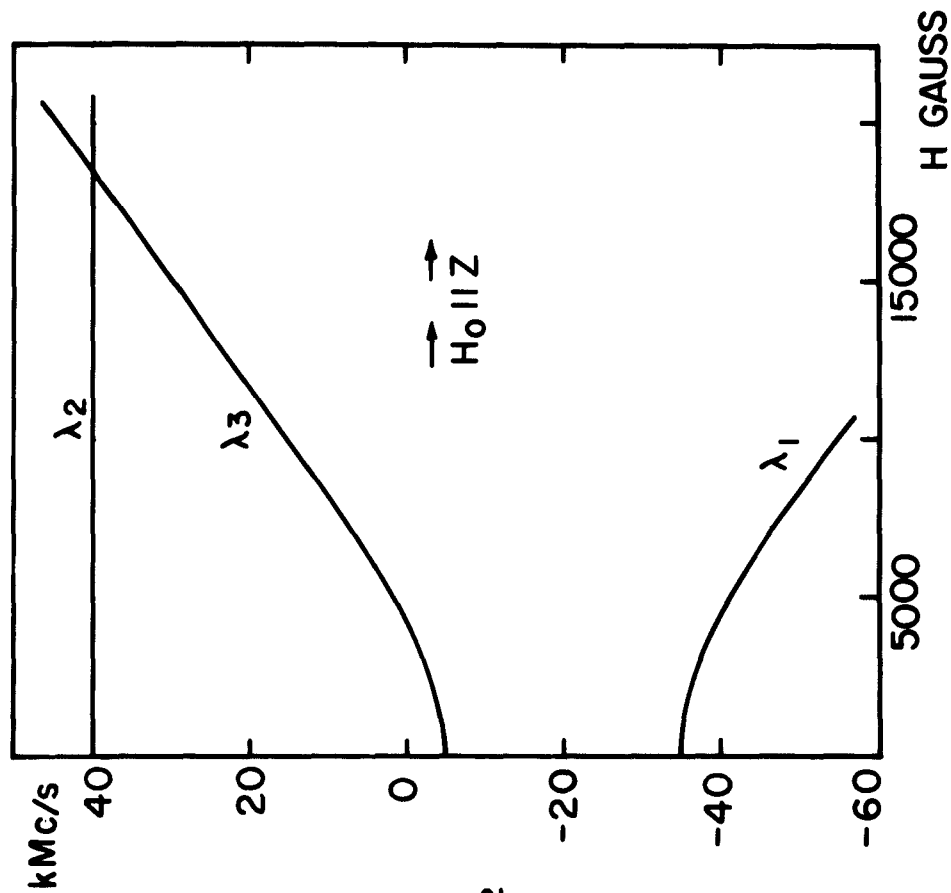


FIG. 19b

Fig. 19a Direction of Magnetic Axes in $\text{Ni}(\text{NH}_4)_2(\text{SO}_4)_2 \cdot 6\text{H}_2\text{O}$.

Fig. 19b Energy Levels in $\text{Ni}(\text{NH}_4)_2(\text{SO}_4)_2 \cdot 6\text{H}_2\text{O}$ when $H_0 \parallel z$

The rhombic field mixes the spin states so that all transitions $\lambda_i \rightarrow \lambda_j$ are allowed.

Griffiths and Owen¹⁰¹ have investigated a number of the Ni - Tutton salts. The crystalline field parameters D and E and the direction of the magnetic axes varies somewhat from salt to salt, and these parameters are also functions of temperature. For $\text{Ni}(\text{NH}_4)_2(\text{SO}_4)_2 \cdot 6\text{H}_2\text{O}$, they find at 90° K

$$g = 2.25 \quad D = -1.99 \text{ cm}^{-1} \quad E = -0.48 \text{ cm}^{-1}.$$

The energy levels (6-2) with these parameters are shown in Fig. 19b as functions of the magnetic field in the z-direction. The z-axes of the two complexes almost coincide in this salt; the angle $z_1 \text{ } 0 \text{ } z_2$ shown in Fig. 19a is 7°.

A zero-field maser using $\text{Ni}(\text{NH}_4)_2(\text{SO}_4)_2 \cdot 6\text{H}_2\text{O}$ would oscillate at about 29 kMc/s ($\lambda_1 \rightarrow \lambda_3$) and it would require a pump frequency of about 75 kMc/s ($\lambda_1 \rightarrow \lambda_2$). The theoretical linewidth of this salt when highly diluted should be comparable to the 4 kc/s width of the NH_3 -transition in the beam maser.¹⁰² However, this would require the crystalline field to be constant to 1 part in 10^7 . Strains and crystal distortions around defects and impurities will probably make such narrow lines impossible. But even for a width of 1 Mc/s, Bloembergen estimated that the frequency stability of such a maser oscillator might compare favorably to the stability of about $1 : 10^{11}$ of the NH_3 beam maser.¹⁰² This is because the solid state maser

oscillates at a higher power level, gives off negligible noise and is little influenced by temperature and pressure variations.

Before it could be decided whether a zero-field maser would be worth building, we needed more information about linewidths in diluted crystals. In the next section some measurements on nickel Tutton salts will be described.

6.2. Measurements.

For the design of a zero-field maser, the resonance linewidth in exactly zero field is of interest. This can, in principle, be measured with a frequency-swept microwave source. However, the microwave path in a low temperature spectrometer has to be very long, a few hundred wavelengths at a frequency of 30 kMc/s. The small reflections at every waveguide joint and bend makes the response of the system vary widely with frequency if not continuously retuned. In practice, only lines narrower than a few Mc/s can be measured directly this way.

We attempted to get around the problem of reflections in the waveguide by changing the frequency step-wise, tuning up the transmission line in which the sample was sitting for each frequency and measuring the difference in transmitted power between periods of no field at the sample and of a field of a few thousand gauss there. Since the measurements were made at liquid helium temperature, we could make the field coil of superconducting niobium wire. A coil of 7650 turns of 0.005" wire wound directly around the stainless steel waveguide was calculated to give

a field of about 2000 gauss for a current of 1 A. This was the maximum field the niobium could stand in the superconducting state. If this field is applied along the magnetic z-axis, we find from (6-2) that it would shift the position of the resonance ($\lambda_1 - \lambda_3$) by 2600 Mc/s. We used a circuit built by Dr. Jeener to switch the field on and off once a second and to integrate the difference between transmitted microwave power during the field "on" and "off" periods.

However, this spectrometer design was not successful. The resonant behavior of the long waveguide and the dispersion effect from the sample resulted in a great number of apparent absorptions. We, therefore, had to give up the attempt to measure linewidths in exactly zero field and began measurements at constant frequencies and small, swept fields. Then the lineshape recorded in field units had to be graphically converted to the more meaningful frequency units, since the resonance shift was not a linear function of the field. The linewidths in zero field could only be found by extrapolating the results in finite fields.

We used a waveguide reflection spectrometer with simple crystal detection similar in principle to the one described in Section 2.1. The fixed cavity version could not be used since we had to measure at a number of frequencies close to the zero-field resonance. For the same reason, we chose a Varian X-12 klystron followed by a crystal harmonic generator as our microwave source. This combination would give a useful output over the frequency ranges 25 - 33 kMc/s and

38 - 43 kMc/s, which is a much wider band than could have been covered directly by any single tube. The magnetfield available was limited by power supply arcing to about 6000 gauss. This field limit restricted the number of resonances that could be observed.

We measured at 4.2°K some nickel ammonia double sulfates with various percentages of dilution by Zn, Mg, and Cd. The crystals were generally cut rectangularly with tapered ends and pressed in place against the waveguide wall by a polyfoam plug. With the crystal \rightarrow b-axis vertical, the magnet was rotated until the field was along the susceptibility axis K_1 . This direction is close to the z-axes of both ions and the two resonances overlap. Around 30 kMc/s, we could observe the resonance $(\lambda_1 - \lambda_3) = 2(E^2 + g^2 \beta^2 H_0^2)^{\frac{1}{2}}$. Working with the third harmonic from the multiplier around 40 kMc/s, we could usually also see the transition $(\lambda_2 - \lambda_3) = D + (E^2 + g^2 \beta^2 H_0^2)^{\frac{1}{2}}$.

In the concentrated $\text{Ni}(\text{NH}_4)_2 \cdot (\text{SO}_4)_2 \cdot 6\text{H}_2\text{O}$, the linewidth was very large, 2300 ± 500 Mc/s. This is more than we expect from dipolar interaction alone and signifies some exchange coupling. In the diluted salts, the linewidth was less, but dilution below about 1% Ni^{++} concentration did not seem to reduce the width any more. The residual linewidth found in salts of nominal Ni^{++} concentration of 0.1% together with measured values of the crystalline field parameters is listed in Table (6-1). Approximate ionic radii¹⁰³ of Ni^{++} and dilutants are included for purpose of comparison.

Dilutant	Ionic Radius	D	E	g^*	Residual Linewidth
Mg ⁺⁺	0.75 Å	1.895 \pm 0.003 cm ⁻¹	0.466 \pm 0.001 cm ⁻¹	2.24 \pm 0.01	70 \pm 20 Mc/s
Zn ⁺⁺	0.83	1.98 \pm 0.01	0.482 \pm 0.001	2.23 \pm 0.01	130 \pm 30
Cd ⁺⁺	0.99	> 2 or < 1	0.385 \pm 0.001	2.16 \pm 0.01	230 \pm 50
Ni ⁺⁺	0.74		0.48	2.25	2300 \pm 500

TABLE (6-1)

The apparent g^* listed here is considerably smaller in the Cd-diluted salt than the usual value 2.25 for Ni⁺⁺. This probably reflects a change in the orientation of the magnetic axis, and the small g^* can be explained if the angle $K_1 0z_1$ in Fig. 19a has increased from the value 3.5° in the undiluted salt. No attempt was made to measure the orientation of magnetic axes in the diluted salts.

The residual linewidth was not field dependent down to the minimum field of about 500 gauss that we could work with. The widths must, therefore, be caused by variations of the crystalline field parameters D and E, rather than by a variation in g or the orientation of the magnetic axes. The transitions $(\lambda_1 \leftrightarrow \lambda_3)$ and $(\lambda_2 \leftrightarrow \lambda_3)$ depend on D and E in different ways. No difference in the widths of these lines was found, and the absolute variations in D and E must, therefore, be approximately the same. The residual linewidth

remained essentially the same when the magnet was rotated so that the resonance frequency was a very strong function of field angle. From this, we find that the possible variation in orientation of the magnetic axes is less than $1/4^\circ$.

6.3. Discussion.

The resonance line moments in undiluted Ni Tutton salt have been calculated by Ollom⁷⁵ and Stevens¹⁰⁴ for the high temperature limit. For $\text{Ni}(\text{NH}_4)_2(\text{SeO}_4) \cdot 6\text{H}_2\text{O}$ in zero field, the limiting value of Stevens' expression for the second moment of the transition $(\lambda_1 - \lambda_2)$ caused by dipolar interaction is

$$\begin{aligned} \langle \Delta E_z^2 \rangle_{H \rightarrow 0} &\longrightarrow [0.252 \cdot 11 + 0.270 + 0.044 \cdot 4] 10^{-4} \text{ cm}^{-2} \\ &= 0.29 (\text{kMc/s})^2. \end{aligned} \quad (6-3)$$

We expect the second moment for $\text{Ni}(\text{NH}_4)_2(\text{SO}_4)_2 \cdot 6\text{H}_2\text{O}$ to be approximately the same. Our experimental value in near zero field for the transition $(\lambda_1 - \lambda_3)$ is $\langle \Delta E^2 \rangle = 1.4 (\text{kMc/s})^2$, however, and this means that most of the observed linewidth must be caused by exchange. Stevens assumes a ferromagnetic exchange of $\tilde{A} = -5 \cdot 10^{-18}$ erg to each of the two nearest like neighbors and finds then agreement with the second moment measurements of Griffiths and Owen.¹⁰¹

The line moments as function of temperature can be found in the way outlined in Chapter 1, but the calculation is complicated by the

two different ions in the unit cell and the rhombic crystal field that mixes the spin states. Accurate comparison between calculated moments and experimental data obtained in low fields is difficult, because of the nonlinear relation between field and resonance frequency and because of the field dependence of the transition probability.

Kittel and Abrahams¹⁰⁵ have considered the lineshape in randomly diluted crystals. They find the second moment from dipolar interaction to be proportional to the spin concentration f

$$\langle \Delta \nu^2 \rangle_{\text{dil}} = f \langle \Delta \nu^2 \rangle_{\text{conc}} \quad (6-4)$$

The fourth moment decreases relatively less with dilution so that the lineshape will change from approximately Gaussian for $f = 1$ to the Lorentzian with cut-off wings for $f < 0.01$.

The exchange contribution to the second moment in diluted salts will be in the form of satellite lines for the small fraction of spins that happen to have another spin as nearest neighbor. The resonance of all the other spins will not be influenced by the exchange.

For Ni-Tutton salt diluted to $f = 0.001$, the theoretical second moment in zero field is from (6-3) and (6-4)

$$[\langle \Delta \nu^2 \rangle_{\text{dil}}]^{1/2} \approx 17 \text{ Mc/s}.$$

Most of the contribution to the second moment comes from the wings of the line, and the theoretical half-width is considerably less than 17 Mc/s. We observed a minimum of about 100 Mc/s for the linewidth and the second moment. The resonance lines in diluted salts must, therefore, be broadened by a variation in the crystalline field.

We see in Table (6-1) that the minimum linewidths observed vary with the dilutant. It is noted⁸⁰ that increased size of the divalent metallic ion will reduce the stability of the Tutton salt. We found that the cadmium salt disintegrated after a few weeks at room temperature. The trend to reduced stability is reflected in greater variation in crystal field as seen from the table.

Other experiments might have been undertaken to find the effect on linewidth if K^+ or Tl^+ is substituted for $(NH_4)^+$, $(SeO_4)^{--}$ for $(SO_4)^{--}$ or D_2O for H_2O . But it is very unlikely that lines anywhere narrow enough for the ultrastable maser oscillator can be found in hydrated nickel salts. This view is supported by the minimum linewidth of 30 gauss \approx 95 Mc/s found by Hoskins, Pastor and Trigger⁷² in 1000 : 1 Zn-diluted $NiSiF_6 \cdot 6H_2O$. Similar linewidths are found in diluted nickel double nitrates.¹⁰⁶

In the crudest calculation of the spin-Hamiltonian parameters from first principles, the water dipoles surrounding the nickel ion is replaced by point charges.¹⁰⁷ This will give an electric field of known symmetry at the position of the magnetic ion, and the stark splitting of its orbital levels can be calculated as a function of point charge strength. Since the polarization of the water molecules in the crystal is unknown, the static field must be found by fitting the orbital levels to spectroscopic data. The spin-orbit coupling is then applied as a perturbation. In this way, one can, in principle, relate the constants D and E and their variations to certain rhombic distortions of the point charge model. This will not be attempted here.

Qualitatively, the variation in D and E and, therefore, in the low-symmetry part of the crystalline field, is about 1 part in 300. In the point-charge model these field components will vary with at least the third power of the interatomic distance. Thus, a variation of this distance of only 1 part in 1000 will result in the observed spread in the values of D and E . A similar displacement of the point charge in the perpendicular direction will only give a variation in the orientation of the magnetic axes of about 0.001 radian $\approx (1/20)^\circ$. Such an angular variation would have a negligible effect on the width of the resonance line, and so the observed broadening is caused by a variation in the crystalline field parameters D and E .

In the first five chapters of this report, a number of paramagnetic resonance lineshapes observed under conditions where $h\nu \geq kT$ have been analyzed and explained in terms of spin-spin interaction. It is shown that this technique may be an important supplement to other methods of investigating interaction in paramagnetic salts. The advantages of the line moment method at low temperature are:

a) The exchange interaction can be found in sign and magnitude. Possible anisotropy of the exchange can be detected.

b) Exchange interaction between unlike neighbors only can be measured. If the total exchange is known from other data, the exchange between like neighbors can be separated out.

c) The method works best at rather weak interactions where specific heat and susceptibility experiments are difficult to perform with sufficient accuracy.

It should be stressed, however, that the lineshapes can only be completely analyzed in relatively simple systems, preferably the ones with only one magnetic ion per unit cell.

The disadvantages of the method are:

a) A complex ^3He cryostat is needed and it is difficult to mount the sample inside the cavity in good heat contact with the ^3He reservoir.

b) Spherical samples are needed to avoid demagnetizing effects. However, magnetostatic modes are easily excited in spheres, and this may obscure the true lineshape.

The experiments described in Chapter 6 were unsuccessful in the sense that we did not find lines narrow enough for the ultra-stable zero-field maser proposed by Professor Bloembergen. It is difficult to relate the observed small variation in crystalline field to definite distortions of the crystal lattice.

ACKNOWLEDGMENTS

We are especially grateful to Professor N. Bloembergen for his helpful advice and criticism throughout the course of this work. We also profited from discussions with Professor W. Opechowski, Dr. M. McMillan, and Dr. Y. Obata. Mr. J. van der Ziel kindly assisted us with some of the measurements described in Chapter 3, while Mr. E. Royce helped with those mentioned in Chapter 6.

One of us (Ivar Svarre) is indebted to the Norwegian Institute of Technology, Trondheim, for a leave of absence to study at Harvard University.

APPENDIX I

THE MOMENT FORMULAS OF McMILLAN AND OPECHOWSKI FOR INTERACTION BETWEEN LIKE NEIGHBORS^{5,18}

Following Pryce and Stevens,³ McMillan and Opechowski introduce the projection operators P_a and P_β that describe the manifolds of unperturbed energy states E_a and E_β for the spin system. Such operators are defined by

$$P_\lambda |\mu, k\rangle = \delta_{\lambda\mu} |\lambda, k\rangle \quad (A-1)$$

where $|\mu, k\rangle$ satisfies $\mathcal{K}^{(0)} |\mu, k\rangle = E_\mu |\mu, k\rangle$. We can then write

$$\overline{\mathcal{K}} = \sum_{\mu} P_{\mu} \mathcal{K} P_{\mu} \quad (A-2)$$

and when the perturbation is small,

$$\hat{M}_+ = \sum_{a,\beta} P_{\beta} M P_a \quad (A-3)$$

$$\hat{M}_- = \sum_{a,\beta} P_a M P_{\beta} \quad (A-4)$$

where $\sum_{a,\beta}$ means summation over all values of a and β such that $E_{\beta} - E_a = h\nu^*$ where ν^* is the unperturbed frequency.

Expansion of the density matrix gives

$$P_a \mathcal{K} P_a = \frac{E_a P_a}{kT} \left[1 - \frac{P_a \mathcal{K}^{(1)} P_a}{kT} + \dots \right] \quad (A-5)$$

In the first approximation, only the first term in the bracket is kept, and this approximation is identical to our Equation (1-14). The commutator expressions (1-11) and (1-12) for the moments around v^* then become

$$h \langle \Delta v \rangle_1 = B_1^{-1} \sum_{\alpha, \beta} b^E_{\alpha} \text{Trace} (P_{\beta} \kappa^{(1)} P_{\beta} M P_{\alpha} M - P_{\alpha} \kappa^{(1)} P_{\alpha} M P_{\beta} M) \quad (A-6)$$

$$h^2 \langle \Delta v^2 \rangle_1 = B_1^{-1} \sum_{\alpha, \beta} b^E_{\alpha} \text{Trace} (P_{\beta} \kappa^{(1)} P_{\beta} \kappa^{(1)} P_{\beta} M P_{\alpha} M - 2P_{\alpha} \kappa^{(1)} P_{\alpha} M P_{\beta} \kappa^{(1)} P_{\beta} M + P_{\alpha} \kappa^{(1)} P_{\alpha} \kappa^{(1)} P_{\alpha} M P_{\beta} M), \quad (A-7)$$

where

$$B_1 = \sum_{\alpha, \beta} \text{Trace} P_{\alpha} M P_{\beta} M. \quad (A-8)$$

As in Section 1.2, these operators have to be evaluated with respect to the eigenfunctions $|a\rangle_1 |b\rangle_2 \dots |d\rangle_N$ where $|c\rangle_i$ satisfies

$$\kappa_i^{(0)} |c\rangle_i = a_c |c\rangle_i.$$

How this can be done has been indicated by Pryce and Stevens,³ but the detailed calculation takes about 20 pages in McMillan's M. Sc. Thesis¹⁸ and it will not be repeated here.

McMillan and Opechowski apply (A-6) and (A-7) to the case when each unperturbed spin has R nondegenerate energy values a_1, a_2, \dots, a_R . Q pairs of these levels have a separation $h\nu^*$, and the lower levels of each of these pairs form a set G .

Their general formulas for the first two moments in the first approximation are then

$$h \langle \Delta \nu \rangle_1 = (NZ\Gamma)^{-1} \left\{ \sum_{e,f} S S b^{a_f} (b^{a_e} - b^{a_{e'}}) \Lambda_{11}(ef) + \sum_e S \sum_f b^{a_e + a_f} \Lambda_{12}(ef) \right\} \quad (A-9)$$

$$\begin{aligned} h^2 \langle \Delta \nu^2 \rangle_1 = (NZ\Gamma)^{-1} & \left\{ \sum_{e,f} S S b^{a_f} (b^{a_e} + b^{a_{e'}}) \Lambda_{21}(ef) + \sum_e S \sum_f b^{a_e + a_f} \Lambda_{22}(ef) \right. \\ & + (N\Gamma)^{-1} Z^{-2} \left\{ \sum_{e,f,g} S S S b^{a_f} (b^{a_e} - b^{a_{e'}}) (b^{a_g} - b^{a_{g'}}) \right. \\ & \Lambda_{23}(efg) \\ & + \sum_{e,f} S S \sum_g b^{a_f + a_g} (b^{a_e} - b^{a_{e'}}) \Lambda_{24}(efg) \\ & \left. \left. + \sum_e S \sum_f \sum_g b^{a_e + a_f + a_g} \Lambda_{25}(efg) \right\} \right\} \quad (A-10) \end{aligned}$$

where

$$Z = \sum_e b^a e$$

$$\Gamma = \sum_e b^a e |(e|m|e')|^2$$

$$\Lambda_{11}(ef) = (e|m|e') (f'|m|f) \sum_{ij} (e'f|\mathcal{K}_{ij}^{(1)}|ef')$$

$$\Lambda_{12}(ef) = |(e|m|e')|^2 \sum_{ij} [(e'f|\mathcal{K}_{ij}^{(1)}|e'f) - (ef|\mathcal{K}_{ij}^{(1)}|ef)]$$

$$\Lambda_{21}(ef) = (e|m|e') (f'|m|f) \sum_{ij} \sum_{ab}^* (e'f|\mathcal{K}_{ij}^{(1)}|ab) \\ (ab|\mathcal{K}_{ij}^{(1)}|ef')$$

$$\Lambda_{22}(ef) = |(e|m|e')|^2 \sum_{ij} \left[\sum_{ab} |(ef|\mathcal{K}_{ij}^{(1)}|ab)|^2 \right. \\ \left. + \sum_{ab}^* |(e'f|\mathcal{K}_{ij}^{(1)}|ab)|^2 \right] \\ - 2 \sum_{ij} \sum_{ab} [(a|m|a') (e'|m|e) (ef|\mathcal{K}_{ij}^{(1)}|ab) \\ (a'b|\mathcal{K}_{ij}^{(1)}|e'f) + (a|m|a') (e'|m|e) (ef|\mathcal{K}_{ij}^{(1)}|ba) \\ (ba'|\mathcal{K}_{ij}^{(1)}|e'f)]$$

$$\Lambda_{23}(efg) = (e|m|e') (f'|m|f) \sum_{ijk} (e'g|\mathcal{K}_{ij}^{(1)}|eg')$$

$$(fg'|\mathcal{K}_{jk}^{(1)}|f'g)$$

$$\Lambda_{24}(efg) = (e|m|e') (f'|m|f) \sum_{ijk} (e'f|\mathcal{K}_{ij}^{(1)}|ef')$$

$$[(e'g|\mathcal{K}_{jk}^{(1)}|e'g) + (f'g|\mathcal{K}_{jk}^{(1)}|f'g) - (eg|\mathcal{K}_{jk}^{(1)}|eg)$$

$$-(fg|\mathcal{K}_{jk}^{(1)}|fg)]$$

$$\Lambda_{25}(efg) = |(e|m|e')|^2 \sum_{ijk} [(e'f|\mathcal{K}_{ij}^{(1)}|e'f) - (ef|\mathcal{K}_{ij}^{(1)}|ef)]$$

$$[(e'g|\mathcal{K}_{jk}^{(1)}|e'g) - (eg|\mathcal{K}_{jk}^{(1)}|eg)]$$

where the notation used is :

$|e'\rangle$ denotes the single spin state of energy $a_{e'} = a_e + h\nu^*$,

$(e'|m|e)$ denotes the matrix element between states $|e\rangle$ and $|e'\rangle$ of the microwave field,

$(ef|\mathcal{K}_{ij}|ab)$ denotes the interaction matrix element between states $|e\rangle_i|f\rangle_j$ and $|a\rangle_i|b\rangle_j$,

\sum_e means summation over all R states $|e\rangle$ of a single spin,

\sum_G means summation over the states in the set G,

\sum_{ab} means summation over all a and b so that $a_a + a_b = a_e + a_f$.

\sum_{ab} means summation over all a and b so that $a_a + a_b = a_e + a_f$ and a is in the set G ,

\sum_{ab}^* means summation over all a and b so that $a_a + a_b = a_e + a_f = a_e + a_f + h\nu^*$.

The summations \sum_{ijk}' can be simplified by remembering

$$\sum_{ijk}' B_{ij} B_{jk} = \sum_{ij}' B_{ij} \left(\sum_j' B_{ij} - B_{ij} \right) \quad (A-11)$$

It is not immediately clear how these formulas can be modified to include also the interaction between nonequal neighbors, since this requires a change in the Boltzmann factors as well as the matrix elements.

APPENDIX II

McMILLAN'S FORMULA FOR THE FIRST MOMENT

IN THE SECOND APPROXIMATION¹⁸

McMillan also calculated the first moment to a higher approximation by keeping the term $P_a \mathcal{K}^{(1)} P_a / kT$ in (A-5). His result is

$$h < \Delta \nu >_2 = X/Y \quad (A-12)$$

where

$$\begin{aligned} X = & Z^{-1} \sum_e \sum_f (b^{a_e} - b^{a_{e'}}) (b^{a_f} - b^{a_{f'}}) \Lambda_{11}(ef) \\ & + Z^{-1} \sum_e \sum_f (b^{a_e} - b^{a_{e'}}) b^{a_f} \Lambda_{12}(ef) \\ & + \frac{1}{kT} \left\{ Z^{-1} \sum_e \sum_f b^{a_{e'} + a_f} \Lambda_{41}(ef) \right. \\ & + Z^{-1} \sum_e \sum_f [b^{a_e + a_f} \Lambda_{42}(ef) + e^{a_{e'} + a_f} \Lambda_{43}(ef)] \\ & + Z^{-2} \sum_e \sum_f \sum_g [(b^{a_{e'}} - b^{a_e}) b^{a_f + a_g} \Lambda_{44}(efg) \\ & \quad + (b^{a_e} - b^{a_{e'}}) b^{a_{f'} + a_g} \Lambda_{45}(efg)] \\ & + Z^{-2} \sum_e \sum_f \sum_g [(b^{a_{e'}} \Lambda_{46}(efg) - b^{a_e} \Lambda_{47}(efg)) b^{a_f + a_g} \end{aligned}$$

$$\begin{aligned}
& + Z^{-3} S_e S_f \sum_g \sum_h (2b^{a_{e'} + a_f} - b^{a_{e'} + a_{f'}} - b^{a_e + a_f}) b^{a_g + a_h} \Lambda_{48}(efgh) \\
& + Z^{-3} S_e \sum_f \sum_g \sum_h (b^{a_e} - b^{a_{e'}}) b^{a_f + a_g + a_h} \Lambda_{49}(efgh) \Big\}
\end{aligned}$$

$$Y = N S_e (b^{a_e} - b^{a_{e'}}) \Lambda_0(e)$$

$$\begin{aligned}
& + \frac{1}{KT} \left\{ Z^{-1} S_e \sum_f (b^{a_{e'}} \Lambda_{31}(ef) + b^{a_e} \Lambda_{32}(ef)) b^{a_f} \right. \\
& \left. + Z^{-2} S_e \sum_f \sum_g (b^{a_{e'}} - b^{a_e}) b^{a_f + a_g} \Lambda_{33}(efg) \right\}
\end{aligned}$$

Here, Λ_{11} and Λ_{12} are given in Appendix I, and

$$\Lambda_0(e) = |(e|m|e')|^2$$

$$\Lambda_{31}(ef) = \sum_{ij} |(e|m|e')|^2 (e'f|\mathcal{K}_{ij}^{(1)}|e'f)$$

$$\Lambda_{32}(ef) = - \sum_{ij} |(e|m|e')|^2 (ef|\mathcal{K}_{ij}^{(1)}|ef)$$

$$\begin{aligned}
\Lambda_{33}(efg) &= \sum_{ijk} |(e|m_k|e')|^2 (fg|\mathcal{K}_{ij}^{(1)}|fg) \\
&= (N-2) \sum_{ij} |(e|m|e')|^2 (fg|\mathcal{K}_{ij}^{(1)}|fg)
\end{aligned}$$

$$\Lambda_{41}(ef) = 2 \sum_{ij} (e|m|e')(f'|m|f) \sum_{\substack{a+b \\ =e+f+1}} (e'f|\mathcal{K}_{ij}^{(1)}|ab) \\ (ab|\mathcal{K}_{ij}^{(1)}|ef')$$

$$\Lambda_{42}(ef) = \sum_{ij} \left\{ |(e|m|e')|^2 \sum_{\substack{a+b \\ =e+f}} |(ef|\mathcal{K}_{ij}^{(1)}|ab)|^2 \right. \\ \left. - \left[\sum_{\substack{a \\ b=e+f-a}} \left\{ (ef|\mathcal{K}_{ij}^{(1)}|ab)(a'b|\mathcal{K}_{ij}^{(1)}|e'f)(a|m|a')(e'|m|e) \right. \right. \right. \\ \left. \left. \left. + (ef|\mathcal{K}_{ij}^{(1)}|ba)(ba'|\mathcal{K}_{ij}^{(1)}|e'f)(a|m|a')(e'|m|e) \right\} \right] \right\}$$

$$\Lambda_{43}(ef) = \sum_{ij} \left\{ |(e|m|e')|^2 \sum_{\substack{a+b \\ =e+f+1}} |(e'f|\mathcal{K}_{ij}^{(1)}|ab)|^2 \right. \\ \left. - \left[\sum_{\substack{a \\ b=e+f-a}} \left\{ (ef|\mathcal{K}_{ij}^{(1)}|ab)(a'b|\mathcal{K}_{ij}^{(1)}|e'f)(a|m|a')(e'|m|e) \right. \right. \right. \\ \left. \left. \left. + (ef|\mathcal{K}_{ij}^{(1)}|ba)(ba'|\mathcal{K}_{ij}^{(1)}|e'f)(a|m|a')(e'|m|e) \right\} \right] \right\}$$

$$\Lambda_{44}(efg) = \sum_{ijk} (e|m|e')(f'|m|f)(e'f|\mathcal{K}_{ij}^{(1)}|ef') \\ [(eg|\mathcal{K}_{jk}^{(1)}|eg) + (fg|\mathcal{K}_{jk}^{(1)}|fg)]$$

$$\Lambda_{45}(efg) = \sum_{ijk} (e|m|e') (f'|m|f) (e'f|\mathcal{K}_{ij}^{(1)}|ef')$$

$$[(e'g|\mathcal{K}_{jk}^{(1)}|e'g) + (f'g|\mathcal{K}_{jk}^{(1)}|f'g)]$$

$$\Lambda_{46}(efg) = \sum_{ijk} |(e|m|e')|^2 [(e'f|\mathcal{K}_{ij}^{(1)}|e'f)$$

$$-(ef|\mathcal{K}_{ij}^{(1)}|ef)] [(e'g|\mathcal{K}_{ik}^{(1)}|e'g) + (fg|\mathcal{K}_{jk}^{(1)}|fg)]$$

$$\Lambda_{47}(efg) = -\sum_{ijk} |(e|m|e')|^2 [(e'f|\mathcal{K}_{ij}^{(1)}|e'f)$$

$$-(ef|\mathcal{K}_{ij}^{(1)}|ef)] [(eg|\mathcal{K}_{ik}^{(1)}|eg) + (fg|\mathcal{K}_{jk}^{(1)}|fg)]$$

$$\Lambda_{48}(efgh) = \sum_{ijkl} (e|m|e') (f'|m|f) (e'f|\mathcal{K}_{ij}^{(1)}|ef') (gh|\mathcal{K}_{kl}^{(1)}|gh)$$

$$\Lambda_{49}(efgh) = \sum_{ijkl} |(e|m|e')|^2 [(ef|\mathcal{K}_{ij}^{(1)}|ef)$$

$$-(ef|\mathcal{K}_{ij}^{(1)}|ef)] (gh|\mathcal{K}_{kl}^{(1)}|gh)$$

The summations in Λ_{48} and Λ_{49} appear to be troublesome, since they have terms of the form $\sum_{ijkl} \tilde{A}_{ij} \tilde{A}_{kl}$, which will give contributions of order N^2 . The same is the case for the term Λ_{33} .

If these terms remained in the end result, it would mean that the

correction from the second approximation depended on N , that is, the size of the crystal. However, these terms will cancel if we expand

$$\begin{aligned} h \langle \Delta \nu \rangle_2 &= \frac{a + b/kT}{c + d/kT} \approx \frac{a}{c} + \frac{1}{ckT} \left(b - \frac{ad}{c} \right) \\ &= h \langle \Delta \nu \rangle_1 + \frac{1}{ckT} \left(b - \frac{ad}{c} \right) . \end{aligned} \quad (\text{A-13})$$

Even if b and d contain terms in N^2 that are very large compared to the terms in N , we can still choose T so large that $b/kT \ll 1$ and $d/kT \ll 1$, and the expansion is valid.

REFERENCES

1. J. H. Van Vleck: *Phys. Rev.* 74 1168 (1948).
2. N. Bloembergen: *Physica* 16 95 (1950).
3. M.H.L. Pryce and K.W.H. Stevens: *Proc. Phys. Soc. London*
A63 36 (1950).
4. K. Kambe and T. Usui: *Prog. Teor. Phys.* 8 302 (1952).
5. M. McMillan and W. Opechowski: *Can. J. Phys.* 38 1168 (1960).
6. P.W. Anderson and P.R. Weiss: *Rev. Mod. Phys.* 25 269 (1953).
7. P.W. Anderson: *J. Phys. Soc. Japan* 9 316 (1954).
8. R. Kubo and K. Tomita : *J. Phys. Soc. Japan* 9 888 (1954).
9. R. Kubo : *J. Phys. Soc. Japan* 9 935 (1954).
10. R. Kubo: *Suppl. Nuovo Cim.* 6 1063 (1957).
11. T. Moriya and Y. Obata: *J. Phys. Soc. Japan* 13 1333 (1958).
12. N. Bloembergen, E. M. Purcell and R. V. Pound: *Phys. Rev.* 73
679 (1948).
13. See C. Kittel: *Solid State Physics*, 2 ed. Wiley, New York, 1956,
p. 157 ff.
14. F. A. Osborn: *Phys. Rev.* 67 351 (1945).
15. C. Kittel : *Phys. Rev.* 73 155 (1948).
16. J.H. Van Vleck: *Phys. Rev.* 78 266 (1950).
17. E.E. Schneider and T.S. England: *Physica* 17 221 (1951).
18. M. McMillan: *M. Sc. Thesis* (1959) University of British
Columbia, Vancouver, B.C.

19. H. Abe, H. Morigaki and K. Koga: Intern. Conf. Paramag. Resonance, Jerusalem 1962.
20. L.R. Walker: Phys. Rev. 105 390 (1957).
21. L. R. Walker: J. Appl. Phys. 29 318 (1958).
22. P. Fletcher, I.H. Solt, Jr., and R. Bell: Phys. Rev. 114 739 (1959).
23. J. F. Dillon, Jr.: Phys. Rev. 112 59 (1958).
24. B.A. Auld: J. Appl. Phys. 31 1642 (1960).
25. J. E. Mercereau: J. Appl. Phys. 30 184S (1959).
26. A.M. Clogston, H. Suhl, L.R. Walker and P.W. Anderson: Phys. Rev. 101 903 (1956).
27. A.M. Clogston, H. Suhl, L.R. Walker and P.W. Anderson: J. Phys. Chem. Solids 1 129 (1956).
28. R.C. LeCraw, E.G. Spencer and C.S. Porter: Phys. Rev. 110 1311 (1958).
29. H. Suhl : Proc. IRE 44 1270 (1956).
30. E. Schlömann, J. J. Green and U. Milano: J. Appl. Phys. 31 386S (1960).
31. See G. K. White: Experimental Techniques in Low-temperature Physics. Oxford, 1959. p. 204.
32. G. Seidel and P.H. Keesom: Rev. Sci. Instr. 29 606 (1958).
33. See T. Moreno: Microwave Transmission Design Data. Dover, New York, 1958. p. 117 .
34. See J. D. Jackson: Classical Electrodynamics. Wiley, New York, 1962. p. 248 .

35. J. H. Van Vleck: *Quantum Electronics* ed. C.H. Townes, Columbia, New York, 1960. p. 392.
36. H.B.G. Casimir: *Physica* 5 495 (1938).
37. C.G.B. Garrett: *Phil. Mag.* 41 621 (1950).
38. H.S. Carslaw and J. C. Jaeger: *Conduction of Heat in Solids*. Oxford, 1959. p. 232.
39. I.M. Khalatnikov: *J. Expr. Teor. Phys. USSR* 22 687 (1952),
see K. R. Atkins: *Liquid Helium*. Cambridge 1959. p. 203.
40. W.A. Little: *Can. J. Phys.* 37 334 (1959).
41. H.A. Fairbank and J. Wilks: *Proc. Roy. Soc.* A231 545 (1955).
42. K. R. Atkins: *Liquid Helium*. Cambridge, 1959. p. 8 .
43. K. R. Atkins: *Liquid Helium*. Cambridge, 1959. p. 35.
44. H. Van Dijk and M. Durrieux: *Prog. in Low Temp. Physics II*,
ed. C. F. Gorter. North-Holland, Amsterdam, 1957. p. 457.
45. W. H. Keesom: *Helium*. Elsevier, Amsterdam, 1942. p. 113.
46. R. D. Present: *Kinetic Theory of Gases*. McGraw Hill, New York, 1958. p.60.
47. G. K. White: *Experimental Techniques in Low-temperature Physics*. Oxford, 1959. p. 306.
48. R.D. Present: *Kinetic Theory of Gases*. McGraw Hill, New York, 1958. pp. 47, 63.
49. J. de Boer: *Prog. in Low Temp. Phys. I*, ed. C. J. Gorter, North-Holland, Amsterdam, 1955. p. 398.
50. See K. R. Atkins: *Liquid Helium*. Cambridge, 1959, p. 174.

51. G. Feher: Bell Syst. T.J. 36 449 (1957).
52. J.A.A. Ketelaar: Physica 4 619 (1937).
53. R. J. Elliott and K. W. H. Stevens: Proc. Roy. Soc. A219 387 (1953).
54. B. Bleaney, H. E. D. Scovil and R. S. Trenam: Proc. Roy. Soc.
A223 15 (1953).
55. B. Bleaney, R. J. Elliott, H. E. D. Scovil: Proc. Phys. Soc.
London A64 933 (1951).
56. V. Y. Kurenev and S. G. Salikhow: Zh. Expr. Teor. Fiz. 21
864 (1951). See Sci. Abs. 55 5194 (1952).
57. V. I. Iveronova, V. P. Tarasova and M. M. Uruanskii: Invest.
Acad. Nauk USSR. Ser. Fiz. 15 164 (1951).
58. Y. Y. Lee: Can. J. Phys. 39 1733 (1961).
59. M. Daniels: Proc. Phys. Soc. London A66 673 (1953).
60. See C. Kittel : Solid State Physics, 2 ed. Wiley, New York
1956. p. 404.
61. L. D. Roberts, C. C. Sartain and B. Borie: Rev. Mod. Phys. 25
170 (1953).
62. A. H. Cooke, S. Whitley and W. P. Wolf: Proc. Phys. Soc.
London B68 415 (1955).
63. R. Finkelstein and A. Mencher: J. Chem. Phys. 21 472 (1953)
64. L. Pauling: Z. Krist. 72 482 (1930).
65. O. Hassel and J. R. Salvesen: Z. Phys. Chem. 128 345 (1927).
66. E. Ishiguro, K. Kambe and T. Usui: Physica 17 310 (1951).

67. W. M. Walsh : Phys. Rev. 114 1473 (1959).
68. R. Schlapp and W. G. Penney: Phys. Rev. 42 666 (1932).
69. J. Bequerel and W. Opechowski: Physica 6 1039 (1939).
70. P. R. Penrose and K. W. H. Stevens: Proc. Roy. Soc. London A63 29 (1950).
71. A. N. Holden, C. Kittel and W. A. Yager: Phys. Rev. 75 1443 (1949).
72. R. H. Hoskins, R. C. Pastor and K. R. Trigger: J. Chem. Phys. 30 601 (1959).
73. G. E. Pake and E. M. Purcell: Phys. Rev. 74 1184 (1948).
74. M. McMillan and W. Opechowski: Can. J. Phys. 39 1369 (1961).
75. J. F. Ollom: Thesis, Harvard, 1952. (Unpublished).
76. R. J. Benzie and A. W. Cooke: Proc. Phys. Soc. London A63 213 (1950).
77. J. F. Ollom and J. H. Van Vleck: Physica 17 205 (1951).
78. C. F. Hempstead, Bell Labs. Unpublished data given to W. Opechowski.
79. A. E. H. Tutton: Proc. Roy. Soc. A118 367 (1928).
80. W. Hofmann: Z. Krist. 78 279 (1931).
81. R. W. G. Wyckoff: Crystal Structure vol. III, Interscience, New York 1948.
82. D. Polder: Physica 9 709 (1942).
83. B. Bleaney, K. D. Bowers and D. J. E. Ingram: Proc. Roy. Soc. A228 147 (1955).

84. B. Bleaney, R. P. Penrose and B. I. Plumptre: Proc. Roy. Soc.
A198 406 (1949).
85. N. Bloembergen, S. Shapiro, P. S. Pershan and J. O. Artman:
Phys. Rev. 114 445 (1959).
86. D. de Klerk: Physica 12 513 (1946).
87. H. C. Kramers, J. D. Wasscher and C. J. Gorter: Physica 18
329 (1952).
88. C. G. B. Garrett: Proc. Roy. Soc. A203 375 (1950).
89. C. A. Beevers and H. Lipson: Proc. Roy. Soc. A146 570 (1934).
90. K. S. Krishnan and A. Mookherji: Phys. Rev. 54 533 and 841
(1938).
91. D. M. S. Bagguley and J. H. E. Griffiths: Proc. Roy. Soc. A201
366 (1950).
92. R. J. Benzie and A. H. Cooke: Proc. Phys. Soc. London
A64 124 (1951).
93. T. H. Geballe and W. F. Glauque: J. Amer. Chem. Soc. 74
3513 (1952).
94. A. R. Miedema, H. Van Kempen, T. Haseda and W. J. Huiskamp:
Physica 28 119 (1962).
95. M. H. L. Pryce: Nature 162 539 (1948).
96. M. Yokota and S. Koide: J. Phys. Soc. Japan 9 953 (1954).
97. H. Abe: J. Phys. Soc. Japan 16 836 (1961).
98. H. Abe, K. [^]Ono, I. Hayashi, J. Shimada and K. Iwanaga :
J. Phys. Soc. Japan 9 814 (1954).

99. N. Bloembergen: Quantum Electronics, ed. Townes, Columbia, New York 1960. p. 160.
100. G. S. Bogle and H. F. Symmons, Austr. J. of Phys. 12 1 (1959).
101. J. H. E. Griffiths and J. Owen: Proc. Roy. Soc. A213 459 (1952).
102. J. P. Gordon, H. J. Zeiger and C. H. Townes: Phys. Rev. 99 1264 (1955).
103. R. W. G. Wyckoff: Crystal Structures, Interscience, New York 1948, Vol. I, Chap. III, p. 15.
104. K. W. H. Stevens: Proc. Roy. Soc. A214 237 (1952).
105. C. Kittel and E. Abrahams: Phys. Rev. 90 238 (1953).
106. R. H. Hoskins, R. C. Pastor and K. R. Trigger: J. Chem. Phys. 30 1630 (1959).
107. W. Low: Paramagnetic Resonance in Solids, Academic Press, New York 1960, pp. 11 ff.

